V. PHYSICS AND SIMULATIONS

V.1 INTRODUCTION

We have performed detailed Monte Carlo simulations to determine the sensitivity of E889 with a few assumptions about the detectors and for several different channels of analysis. We have included both the beam and detector related systematic errors and the effects of backgrounds in a unified manner. These effects have been estimated by Monte Carlo calculations using the proposed geometry of E889 or by using published data from previous experiments.

We estimate our sensitivity for neutrino oscillations in the three most important *analysis* channels. They are (1) direct ν_μ disappearance, (2) ν_μ disappearance using the neutral current π^0 events as normalization, and (3) ν_e appearance. The actual *oscillation* channel ($\nu_\mu \rightarrow \nu_\tau$, $\nu_\mu \rightarrow \nu_e$, or $\nu_\mu \rightarrow \nu_s$, where ν_s is sterile) can be uniquely determined over most of the parameter range with the above three analysis channels. Identification of the oscillation channel is performed by counting quasi-elastic muon, quasi-elastic electron, and neutral current π^0 events. At the AGS energies quasi-elastic muon neutrino events account for about 60% of the total neutrino cross section. About 12% of all events will be from neutral current π^0 production. Only about 1% of the events will be quasi-elastic electron neutrino events from the electron neutrino contamination in the beam. Depletion of muons will be seen in the far detectors for all three oscillation channels. Oscillation into electron neutrinos will cause an increase of electrons, while in the unlikely case that oscillations are into a sterile neutrino with no weak interactions a depletion of neutral current π^0 events will be seen. In all analysis channels the observations in the near detectors are used to predict the event rates and the spectrum in the far detectors assuming no oscillations. The important issues of pattern recognition and event reconstruction for a water Cherenkov detector are addressed in Chapter IV.

Most of the studies in this chapter assume two near detector tanks on the BNL site, one at 1 km and one at 3 km, and one far detector tank at the 24 km Northville site and another far detector tank at the 68 km Plum Island site. Each tank is 18 m in diameter and 18 m high. There are 2195 photomultiplier tubes with 20 cm diameter photocathodes facing inside placed about 68 cm apart on a cylinder 15 m in diameter and 15 m high (the active or inner volume) centered inside the tank. The active veto volume, 1.5 m of water between the two cylinders, is viewed by 400 photomultiplier tubes facing outside. The PMTs facing inside are equipped with light collectors that increase the coverage by a factor of 1.6; the veto PMTs do not have the light collectors. The nominal fiducial volume is 13 m diameter $\times$ 13 m high,

but, of course, in the actual experiment we will vary the fiducial cuts for different samples of events and studies. We have assumed actual running time of 16 months with 20 hrs of fast extracted beam every day at an intensity of 4×10^{13} protons on target per 1.6 s. This corresponds to 8.8×10^{20} protons on target (POT); we will also comment on the first two runs of 4 months duration or 2.2×10^{20} protons on target each. It should be noted that the AGS has already exceeded this assumed intensity and more improvement is planned.

V.2 DIRECT MEASUREMENT of ν_μ DISAPPEARANCE

V.2.1 FORMALISM

The disappearance of muon neutrinos is signaled by a reduction of the weak charged current quasi-elastic muon neutrino reactions ($\nu_\mu + n \rightarrow \mu^- + p$) at a detector located far from the source of the neutrinos. The following expression approximates the number of events classified as quasi-elastic muon neutrino interactions, f, induced by neutrinos within a single energy bin.

$$f = \frac{A}{(r - r_0)^2}[1 - \sin^2(2\theta)\sin^2(\frac{1.27\Delta m^2(r - r_0)}{E}) + B] + C_B \qquad (1)$$

Here r is the distance of the detector in km from the production target, while r_0 is an effective distance of the mean origin of neutrinos. A, the number of events without oscillations at 1 km, is a normalization constant. Δm^2, mass difference squared in units of eV^2 and θ, the mixing angle, are the usual oscillation parameters. E is the neutrino energy in GeV. B quantifies the fraction of events that are background from two sources: neutral current events that are misidentified as quasi-elastics and misidentified multiparticle background due to neutrinos in the high energy tail of the neutrino spectrum (without appreciable oscillation probability). C_B is the number of cosmic ray events that cause background to the quasi-elastic sample. Two main approximations in this formula are as follows: Although the neutrinos are generated over the entire tunnel length with a distribution based on the momentum distributions of both pions and kaons, we have approximated the effect of the tunnel as an average position (r_0) within the tunnel. Secondly, we have ignored the effects of placing detectors at a small angle with respect to the tunnel axis. For large angles, one must replace $(r - r_0)$ by the vector equivalent $|\vec{r} - \vec{r}_0|$, but in our case $(r - r_0)$ and $|\vec{r} - \vec{r}_0|$ are close enough to be considered indistinguishable.

We denote the counts measured at three different sites as f_a, f_b, and f_c where a, b, and

c are the designations of the near and the middle sites (both on the BNL site), and the far site (at 24 or 68 km), respectively. The sites are also sometimes referred to as D1, D3, D24, and D68. We will denote the flux predicted at the far sites using the observations at a and b under the assumption of no oscillations as f_p. An oscillation signal results when f_c (at 24 or 68 km) is observed to be significantly different from f_p. The significance of the oscillation result will clearly depend on the systematic errors in calculating f_p from f_a and f_b, the effects of oscillations on the near site counting rate, the background and cosmic ray level, and most importantly the statistics at the far site.

There are several important features of Equation 1: For small oscillations ($\frac{\Delta m^2(r-r_0)}{E} << 1$) the number of events missing is independent of distance. Then using the inverse square law (a good approximation when $r >> r_0$) for the number of expected events one calculates that the significance of oscillations increases linearly with distance if one considers only the statistical error at the far site, while $\sin^2(2\theta)$ reduces the significance linearly. Not subtracting the neutrino induced background fraction, B, from the rates observed in both the near and the far detectors then reduces the significance by an amount $\frac{1}{(1+B)}$. Lastly, the cosmic ray background, C_B, is independent of the distance and therefore increases in importance relative to signals with distance of the far detectors. Since the loss of events due to small oscillations is independent of distance a small cosmic ray background could limit the sensitivity. Therefore we have placed much emphasis on understanding and eliminating any cosmic ray backgrounds.

V.2.2 QUASI-ELASTIC MUON NEUTRINO EVENTS

Before deriving the expected size of the disappearance signal, we will describe the nature of the quasi-elastic events in the detectors. At the neutrino energies at the AGS ($E_\nu > 300$ MeV) the cross sections for the quasi-elastic reactions on light nuclei may be calculated to good approximation using a relativistic Fermi gas nuclear model with a semiempirical nucleon binding energy value [1]. Above 300 MeV, in this model the bound and free neutron cross sections differ by less than 20%, and the ν_e and ν_μ quasi-elastic cross sections are approximately equal despite the muon-electron mass difference. Both the total cross section as a function of energy and the differential cross section have been measured in previous experiments [2,3] (Figure 1 and 2).

We have performed detailed simulations of the quasi-elastic events and backgrounds in our water Cherenkov detectors. For these simulations, rays of neutrinos were generated from the decay tunnel according to our GEANT based beam simulation program. If a neutrino ray was found to intercept one of the four detector tanks located at the correct distance and

	1 km	3 km	24 km	68 km
Events in Detector	10.3×10^6	11.5×10^5	17916	2232
Events in Fiducial	6.80×10^6	7.54×10^5	11820	1473
Contained	5.21×10^6	5.80×10^5	9102	1136

Table 1: *The number of quasi-elastic muon events after 16 months of running at the four detector sites with one detector tank each. The uncertainty on the absolute normalization is about 15%.*

offset from the beam axis, then a neutrino event was generated after appropriate weighting for the cross section as a function of energy and the path-length through the detector. Using the 1.5 degree offset spectrum (Figure 3) computed in Chapter III.A we compute the integral $\int dE\phi(E)\sigma(E)$ over the interval $0 < E_\nu < 5$ GeV to be 1.78×10^{-47} per proton on target at 1 km. There is an additional correction that suppresses the total cross section by 0.93 due to Pauli exclusion effects in the nucleus. Thus the number of events in water at 1 km is given by 4.43×10^{-15}/kTon/POT. In Table 1 the event counts in each of the detectors is shown as a function of several cuts after 8.8×10^{20} POT. The first row is the number of events in the entire inner volume viewed by the PMTs (15 m diameter and 15 m height), and the last row is with both fiducial (vertex within 13 m diameter and 13 m height) and containment (muon stop within 15 m diameter and 15 m height) cuts. There is an uncertainty of about 15% on the absolute neutrino flux, most of which is due to the uncertainties in the simulation of the hadronic showers in the horn-target system. The spectrum of neutrinos, however, has much less uncertainty because we have checked our simulation against the results from a previous AGS experiment in a similar neutrino beam, E734 (Figures 2 and 4).

Most of the contained events with the vertex in the fiducial volume will have a single clear ring with a sharp edge characteristic of a muon. We can decide if the muon is contained by two separate methods. We can look at the pattern and the pulse height of the photomultiplier hits at the center of the ring. For an exiting muon the ring does not have a hole and the photomultipliers in the center have very large pulse heights. For the second method we can make cuts on the pulse height in the veto volume that corresponds to the center of the ring in the inner detector. The first method causes a small loss of events because some events will be rejected because their tracks end close to the edge of the detector. In any case, we intend to use both methods to check our results. Assuming that a cut on the veto

volume is used, 0.77 of the events in the fiducial volume are contained. Figure 5a shows the muon momentum spectrum of these contained events. Figure 5b shows the spectrum of the neutrinos that produce these muons. Also interesting is the number of photoelectrons (Figure 5c) and the number of hit photomultipliers (Figure 5d) in the detector configuration described at the beginning of this chapter. Two further cuts on the contained events that will be needed to obtain a clean sample of muons with little background are cuts on the number of photoelectrons and on the muon angle. These cuts will be tuned to eliminate low momentum particles that are difficult to classify as muons or electrons and wide angle backgrounds. Figure 6 shows the response of the detector for muons, electrons, and charged pions as a function of momentum. The vertex and angular resolutions are discussed in Chapter IV.

In the next few sections we will show how the effect of oscillations and background modifies the total number of events and the spectrum at the far sites at 24 and 68 km. It can be seen immediately, however, that the statistics at the near detectors will be sufficiently large that we will be able to predict the spectrum and the number of events at the far sites with minimal statistical error and a small systematic error. The systematic error will be due to the beam and detector effects discussed in detail below. The statistical error at D24 will be about 1%, and therefore the oscillation sensitivity at D24 will depend on whether we can control the systematic errors to be less than or equal to that value. The statistical error at D68 will about 3%, and therefore the oscillation sensitivity will likely not depend on the systematic error. Thus we will be able to pursue two approaches to this oscillation experiment: high statistics with low systematic error, and statistics-limited with a larger oscillation signal.

V.2.3 BACKGROUNDS

V.2.3.1 NEUTRINO INDUCED BACKGROUNDS

WEAK CHARGED CURRENT BACKGROUNDS

The WCC background event information, listed in Table 2, contains data obtained in the ANL 12 foot H_2/D_2 bubble chamber with the neutrino beam shown in Figure 7 and compares them with the results of a calculation based on the Monte Carlo simulation for the Kamiokande detector [4]. Normalization of the calculation is done by adjusting the calculated quasi-elastic total to the measured. We utilize these results because the 1.5 degree neutrino spectrum is similar to the spectrum with which the 12 foot chamber results were obtained. The results show the agreement of the simulation with the data and with earlier theoretical estimates in Ref. 5.

Interaction	Argonne	ν Monte Carlo
$\nu p \to \mu^- p\pi^+$	308 ± 24	301
$\nu p \to \mu^- p\pi^+ (m\pi^0) m \geq 1$	20 ± 5	22.3
$\nu p \to \mu^- n\pi^+\pi^+ (m\pi^0) m \geq 0$	15 ± 5	12.2
$\nu p \to \mu^- p\pi^+\pi^+\pi^-$	10 ± 3	2.5
$\nu p \to \mu^- p\pi^+\pi^+\pi^-\pi^0$	-	1.3
$\nu p \to \mu^- n\pi^+\pi^+\pi^+\pi^-$	1 ± 1	0.5
$\nu p \to \mu^-$ strange particle	1 ± 1	-
$\nu n \to \mu^- p$	833 ± 41	833
$\nu n \to \mu^- p\pi^0$	124 ± 14	129
$\nu n \to \mu^- n\pi^+$	90 ± 11	89.0
$\nu n \to \mu^- p (m\pi^0) m \geq 2$	31 ± 13	13.1
$\nu n \to \mu^- n\pi^+ (m\pi^0) m \geq 1$	29 ± 12	24.6
$\nu n \to \mu^- p\pi^+\pi^-$	20 ± 5	21.1
$\nu n \to \mu^- p\pi^+\pi^- (m\pi^0) m \geq 1$	8 ± 4	9.1
$\nu n \to \mu^- n\pi^+\pi^+\pi^- (m\pi^0) m \geq 0$	3 ± 2	6.1
$\nu n \to \mu^- p\pi^+\pi^+\pi - \pi -$	0	1.5
$\nu n \to \mu^-$ strange particle	12 ± 4	-

Table 2: *The event rate of each exclusive interaction in the Argonne data compared with the results of the Kamioka Monte Carlo calculation. The calculation is normalized to the* $\nu_\mu n \to \mu^- p$ *event rate. Taken from Ref. 4.*

Even if there is no discrimination whatsoever against weak charged current backgrounds to the direct ν_μ disappearance measurement, this experiment will detect neutrino oscillations because these backgrounds come from neutrinos that also oscillate. Since their energy distribution will not be as well known as that of the quasi-elastic signal, weak charged current backgrounds could lead to errors in measuring the oscillation parameters using the spectrum shape, but they will not fake a statistically significant oscillation signal. Furthermore, from Table 2 we see that because of the low beam energy, all such backgrounds combined are only about 2/3 of the quasi-elastic signal. To improve the accuracy of the measurement, we shall use several methods to exclude backgrounds. Some characteristics that permit exclusion are: (1) Backgrounds tend to have extra Cherenkov rings. (2) Single ring background events usually have low visible energy. (3) As is discussed in the Pattern Recognition section, electromagnetic showers produce Cherenkov rings that are quite different from rings produced by fast muons. Any $\pi^0 \to \gamma\gamma$ in a background will in general produce two electromagnetic showers that will mimic a single muon less than 0.2% of the times. (4) Muons and π^+ both lead to Michel electron production, typically a few microseconds after the initial event. If two Michel decays are detected near the origin of a quasi-elastic candidate event in both space and time, that candidate is likely to be a background. Because of the cosmic muon rate, this last method requires some care to avoid losing real quasi-elastic events; in what follows we discuss how well we can do without its use.

(a) MULTIPIONS

The multipion event total in Table 2 is 17% of the quasi-elastic event total. In general, WCC multipion events are contained and will exhibit two, three, or sometimes four Cherenkov rings and two or more muon decays. Most events have a final state π^0. Where rings overlap, the complex PMT hit pattern serves as convincing evidence of a multiring event. Figures 8, 9, and 10 show typical quasi-elastic muon, quasi-elastic electron, and multiring pion events, respectively.

As an illustration of the discrimination against multipion backgrounds in the $QE(\mu^-)$ sample, we consider in detail the reaction $\nu_\mu n \to \mu^- p\pi^+\pi^-$ with a rate 0.024 of the quasi-elastic rate. Neglecting the proton, there are 3 charged particles in the final state and 2 muon decays. From the calculated momentum distributions of the μ^-, π^+ and π^- [4] which give the fractions above detection threshold, one has the normalized probabilities: 45% of all events exhibit 3 rings, 42% exhibit 2 and only 2 rings, 12% show 1 and only 1 ring, and 1% show no rings. Thus such events could contribute a background that is only 0.3% as large as the expected quasi-elastic signal. If we apply the same reduction factor of 12% to

all the multipion events we calculate that the maximum possible background is about 2%. One must keep in mind that additional cuts to reduce this small background are possible. In particular, most of the multipion events will have very low visible energy, wide angles, and several muon decay electrons. In our case with cosmic ray muons within the detector the detection of muon decays may not be as effective a rejection tool as in the case of Kamioka. Nevertheless, with these additional cuts the contamination in the quasi-elastic signal events from charged current multipion events should be reduced to less than 1%.

(b) SINGLE CHARGED PION

The two single charged pion reactions $\nu_\mu p \rightarrow \mu^- p\pi^+$ and $\nu_\mu n \rightarrow \mu^- n\pi^+$ produce a signal which is 48% of the quasi-elastic total in Table 2. The momentum distributions of the π^+ and μ^- are shown in Figure 11. We have visually scanned these events and found that if both the muon and the pion produce more than 50 photoelectrons each the event can be easily identified as a two ring event. 50 photoelectrons corresponds to about 170 MeV/c (250 MeV/c) for muons (pions). With such a cut we find that 40% of the events will show one ring (principally the μ^-). Figure 12 shows the photoelectron spectrum of these events. We see that 0.65 of these single ring events are above 300 photoelectrons while 93% of the quasi-elastic muons will be above 300 photoelectrons (Figure 5). Therefore about 0.12 ($0.48 \times 0.40 \times 0.65$) of the events identified as quasi-elastic muons could be from charged current single pion channels. The detection of two muon decays could be used to further suppress this background. However, as we stated earlier these background events do not affect the sensitivity very much because the spectrum of neutrinos that produce these events (Figure 12) is very similar to the spectrum that produces the quasi-elastic muons events.

Only 0.20 of the single ring charged current pion events with more than 300 photoelectrons will come from neutrinos above 1.5 GeV where the oscillation probability is small in the parameter range of interest. This low level of background from high energy neutrinos is one of the advantages of the narrow off-axis (1.5 degree) neutrino spectrum (Figure 3). This background would be higher by a factor of about 2.5 in the 0 degree beam. Other multiparticle backgrounds would also increase and the event patterns would not remain simple.

(c) SINGLE NEUTRAL PION

The reaction $\nu_\mu n \rightarrow \mu^- p\pi^0$ (the only allowed WCC-π^0 reaction) is 15% of the total quasi-elastic rate. The momentum distribution of μ^- and π^0 are essentially the same as those in Figure 11. We have visually scanned Monte Carlo events of this type (see Chapter IV for complete details) for single rings with clear muon like patterns. Only 0.5% of the WCC-

π^0 events will look like quasi-elastic muon events because at least one of the gamma rays from the π^0 decay is usually visible. Thus this background is negligible in the quasi-elastic sample. If, however, both the μ^- track and the μ decay are missed, the event might be misidentified as WNC-π^0. This is addressed in the section on the oscillation analysis using the ratio $QE(\mu)/NC(\pi^0)$.

In summary, the WCC backgrounds in the $QE(\mu^-)$ sample are expected to be less than 13% of the $QE(\mu^-)$ sample in any of the four detectors. We expect to eliminate half of these by looking for events that show more than one muon decays close in both space and time to the event vertex. Since these backgrounds are ν_μ–induced they will respond to a ν_μ–disappearance resulting from neutrino oscillations in the same way as the $QE(\mu^-)$ events. Less than 3% of the $QE(\mu^-)$ sample will consist of WCC-multiparticle events from high energy neutrinos (> 1.5 GeV) with small oscillation probability. Furthermore, the treatment of systematic errors will show that these background will be the same in all the detectors to first order. Therefore the distortion of the measured muon spectrum and the E_ν distribution produced by the WCC backgrounds can be simulated and subtracted with a small systematic error.

WEAK NEUTRAL CURRENT BACKGROUNDS

(a) MULTIPIONS

The WNC multipion reactions total 5% of the $QE(\mu^-)$ rate at low ν_μ energies, and produce final states with 2, 3, or 4 Cherenkov rings, counting only events with three or fewer pions. Of the eight such final states, four have a π^0, and all final states except one (which has a π^0) have at least one π^+. Detailed reasoning similar to that for the WCC multipion background reactions indicates that the principal background sources are the final states $\nu n\pi^+\pi^-$ and $\nu p\pi^+\pi^-$. For these, the probability of showing 1 and only 1 track is 0.32 which yields a background in the $QE(\mu^-)$ sample less than 1.6%.

(b) SINGLE CHARGED PION

The WNC single charged pion reactions, $\nu p \rightarrow \nu n\pi^+$ and $\nu n \rightarrow \nu p\pi^-$, each have a rate 7.3% of the $QE(\mu^-)$ rate. These reactions will produce single ring events that are not distinguishable from quasi-elastic events from the pattern alone. The momentum distribution of the final state pion is shown in Figure 13. The shape of the pion momentum distribution and the spectrum of photoelectrons are very different from those of the $QE(\mu^-)$. A cut at 300 photoelectrons eliminates 94.5% of these events while keeping more than 93% of the quasi-elastic signal. Therefore the amount of background from this source in the quasi-elastic

sample will be about 0.8% ($2 \times 0.073 \times 0.055$).

In summary, WNC events will cause less than 2.4% background in the $QE(\mu^-)$ sample. If left unsubtracted this background will dilute any oscillation effect by a small amount since the background will be the same fraction in all four detectors.

V.2.3.2 COSMIC RAY BACKGROUNDS

COSMIC RAY MUONS

The cosmic ray muon flux at the surface of earth at sea level is given by the following equation [6].

$$j(\theta,\phi) = \frac{360}{\pi}\cos^2(\theta) m^{-2} s^{-1} str^{-1} \tag{2}$$

Here θ is the angle with respect to the zenith or the vertical axis and ϕ is the azimuthal angle, and the flux is the number of particles incident on a sphere of unit cross sectional area per unit time per unit solid angle. To convert this quantity into the number of particles crossing a horizontal surface area we evaluate the following integral.

$$\int_A \int_{\theta<\pi/2} j(\theta,\phi)\cos(\theta) d\Omega dA \tag{3}$$

where the first integral is over the surface area and the second integral is over the upper hemisphere. Similarly for the vertical surface of the tank we have the following integral.

$$\frac{1}{2}\int_A \int_{\theta<\pi/2} j(\theta,\phi)\sin(\theta) d\Omega dA \tag{4}$$

where the extra factor of 1/2 takes into account that only the muons crossing from outside the tank wall are relevant. We use Equations 3 and 4 to calculate the muon rates in both the veto counter and the inner detector entering from the top and the side (Table 3). The surface area for the veto counter is calculated by assuming a diameter of 18 m and height of 18 m whereas the inner detector has a diameter of 15 m and a height of 15 m. The total muon rate in the inner detector of some 80 kHz might be considered high, especially for the far detectors where the neutrino event rates are low. However, the rejection obtained with the use of an active veto counter, the time structure of the beam, and the characteristics of the events themselves is quite adequate. The high cosmic rate is not a problem, but a source to test and calibrate the detectors in an identical fashion before and during the neutrino data runs.

	Into the Veto	Into the Inner
Muons from the Top	45780 Hz	31790 Hz
Muons from the Sides	71860 Hz	49900 Hz
Total Muons	117640 Hz	81690 Hz
Stopping Muons	-	43132 Hz

Table 3: *Cosmic ray muons entering the veto volume of the detector and then the inner volume per second. The spectrum of muons from Ref. 10 is used to calculate the number that stop in the inner detector.*

NEUTRAL COSMIC RADIATION

The rates in the inner volume due to muons should be somewhat lower than our calculation because of the passive shielding effect of the veto volume. This passive shielding effect will be more effective for neutral cosmic radiation of neutrons and photons. The high energy neutron intensity at sea level is approximately 1/30 the intensity of muons [7–10]. The minimum 1.5 m thickness of water in the veto volume corresponds to 1.74 absorption lengths (the Fe tank structures and the insulation are not considered but should also help); therefore the rate of neutron induced interactions in the inner detector should be less than 6×10^{-3} times the rate of muon interactions. We do not expect much background from photon induced interactions because high energy photons from the atmosphere are normally associated with electromagnetic showers that contain charged particles, electrons and positrons. These will produce hits in the active veto, and in the extremely rare case that a single high energy photon enters the detector it must pass through 4.17 radiation lengths in the active veto without interacting to enter the inner detector.

ACTIVE VETO

We plan on rejecting the muons at an early stage using the active veto. The exact geometry of the photo-multiplier tubes in the active veto volume has not yet been finalized. We are looking at two different options: 1) Photomultipliers on the inner cylinder facing outwards with enough density to have at least one hit for any high energy charged particle no matter what the entry angle. Reflective coating on the walls will increase the light yield, but also cause many more PMTs to be hit over a longer period of time. 2) Photomultipliers isolated from each other by enclosed cells with reflective coating on the inside.

In the past veto inefficiency of similar veto shields has been found to be much less than

10^{-3} (See References in Chapter IV). The number of photoelectrons collected from the veto will depend on the efficiency of the reflective coating as described in Ref. 12. Assuming 400 PMTs in the veto volume and a reflection efficiency of 60%, we calculate that we will collect more than 150 photoelectrons for a cosmic ray muon entering the tank at right angles. The main reason for any veto inefficiency will then be dead PMTs or electronics deadtime. We estimate that 10^{-3} is a very conservative number.

THE TIME STRUCTURE

The most important tool in eliminating cosmic events from the neutrino data is the use of the accelerator time structure. The AGS fast extracted beam will be delivered every 1.6 s to the neutrino production target in 8 buckets with a width of 20-30 ns each. The buckets will be 335 ns apart. We intend to measure the absolute time of both the AGS beam buckets at the beam stop and the neutrino events at the detectors with synchronized clocks. As explained in Chapter III.C, we will be able to synchronize the clocks to within 10 ns of each other. The 10 ns error in the synchronization will most likely be the maximum possible error, rather than a Gaussian distributed error. The error in the reconstructed time of the event (about 1.5 ns) from the PMT hits will be negligible on this scale. Thus the effective duty factor associated with the timing cuts will be less than $2.5 \times 10^{-7} = \frac{8\times(10+30+10)\text{ ns}}{1.6\text{ s}}$. Figure 14 shows the reconstructed time of neutrino events in experiment E734 which was in a similar AGS neutrino beam. We see no difficulty in finding the neutrino events in E889 by using this type of timing.

RECONSTRUCTION

To gain additional discrimination with respect to cosmic rays we have performed GEANT Monte Carlo simulations of both muons and neutrons in the detectors using the experimentally measured and parameterized spectra in Figures 15 and 16 [7,10]. The muon spectrum has considerable dependence on zenith angle; we have parameterized this dependence as an angle dependent inflexion point at which the momentum spectrum changes from a flat to a power law spectrum. The neutron spectrum is somewhat softer than the muon spectrum. The neutron zenith angle dependence is not well known; we assumed it to be the same as for muons. The spectrum of photo-electrons and the total number of photomultipliers is shown in Figure 17. The character of the cosmic events can be seen to be quite different from the quasi-elastic neutrino events in Figure 5. If we require that the number of photo-electrons be greater than 300 ($P_\mu > 300$ MeV) and less than 3500 ($P_\mu < 4.0$ GeV) then we reduce the signal quasi-elastic events by about 7%, but the same cut retains only 47% of the muon and

	Muons	Neutrons
Raw rate kHz	81.7	2.7
Reduction factors		
Beam time structure	2.5×10^{-7}	2.5×10^{-7}
Passive/active shielding	10^{-3}	0.18
Energy cuts	0.47	0.26
Vertex and Direction	3.3×10^{-3}	6.2×10^{-2}
Total reduction	3.9×10^{-13}	7.2×10^{-10}
Background in 16 months	1.1 events	68 events

Table 4: *Cosmic ray background to quasi-elastic muon neutrino events in each detector tank after 16 months of running. Over 1100 quasi-elastic muon events are expected in D68 over the same period.*

26% of the neutron cosmic events.

We have applied our reconstruction algorithm to a sample of the remaining muon cosmic events. Figure 18 shows the reconstructed vertex position for a sample of muon cosmics entering the inner detector within the above energy cuts. A fiducial cut to restrict the reconstructed vertex to be within a cylinder of 13 m diameter and 13 m height leaves a background of only 4 events out of 306 events. Requiring that the muon be within 90 degrees of the neutrino beam direction keeps only 1/4 of these remaining events.

An eye-scan of the neutron induced events simulated by GEANT that passed the energy cuts was performed. Since typical high energy neutron interactions produce several particles, we found that only 1/8 of the remaining neutron events looked like single ring muon-like events that could be a background to the quasi-elastic signal. The number of single ring showering events that could be background for the electron neutrino appearance search was found to be negligible. These single tracks are approximately isotropically distributed, and therefore a requirement that the track point within 90 degrees of the neutrino beam direction reduces this background further by a factor of 2.

In Table 4 we have collected all of these reduction factors to compute an estimate of the cosmic ray contamination to neutrino events after 16 months of running. We see that the background is small even at the far distance of 68 km where over 1100 quasi-elastics are expected over the same running period. We also note that most of the reduction depends on

the time structure and the active/passive veto shield, which are relatively simple systems. We need not perform complete analysis and reconstruction of the data to have confidence in the detector at an early stage of the experiment.

COSMIC BACKGROUND SUBTRACTION

The data acquisition electronics and the trigger of the experiment will be quite flexible so that events can be collected continuously for 10-15 μs after the AGS beam gate (to search for muon decay electrons, for instance). The trigger can also be enabled outside the beam gate. In this manner we intend to collect large amounts of cosmic ray data for background studies and calibration. We will use these data to subtract the cosmic ray background from each detector before comparing the event rate. The procedure will introduce a small systematic error which will depend on knowing the time windows over which the subtraction must occur at each of the detectors. Since the correction is of the order of 6% at the 68 km site, an error of 5% (from possible jitter in the *BEAM-ENABLE* signal) in subtraction will cause a systematic error of 0.3% at that farthest site. In the present analysis, however, we prefer to show our sensitivity without this subtraction.

V.2.4 SYSTEMATIC ERRORS

The systematic errors for the experiment fall in two broad somewhat overlapping categories: 1) beam related and 2) detector related. In the following we describe our experimental design which will minimize effects that cause spurious oscillation signals to arise. In the past most neutrino oscillation experiments have reported oscillation type effects at an early stage of the experiments, always at the edge of their sensitivity. We want to avoid these difficulties by having redundant measurements and very little reliance on Monte Carlo simulations to detect oscillations over most of our sensitivity range.

In the following we will discuss the systematic errors in the context of the direct muon disappearance experiment. The same results with small modifications will also be true for the systematic error on the background for the ν_e appearance analysis. The systematic error on the indirect ν_μ disappearance search using the ratio of quasi-elastic muons to neutral current π^0s ($QE(\mu^-)/NC(\pi^0)$) will not have many of the contributions discussed below. In any case, the systematic error will not be important to either the ν_e appearance or the $QE(\mu)/NC(\pi^0)$ technique at small values of Δm^2 because the statistical errors will dominate. Similarly, the systematic error will not be important at D68 compared to the expected statistical error of 3% for the direct ν_μ disappearance analysis.

V.2.4.1 BEAM SYSTEMATIC ERROR

BEAM PARAMETERS

Before a complete discussion of the systematic errors due to the neutrino beam we will demonstrate the assumption that the neutrino origin can be approximated as some average position within the tunnel. Let $\rho(r')$ be the distribution of neutrino origins in the decay tunnel; r' is the position where a meson decayed and produced a neutrino that caused an interaction in the detector. We normalize $\rho(r')$ so that $\int_0^L dr'\rho(r') = 1$ where L is the length of the decay tunnel. If $F(r)$ is the true count rate due to these neutrinos in a detector located at r then

$$\begin{aligned} F(r) &= \int_0^L dr'\rho(r')\frac{A}{(r-r')^2} \\ &= \int_0^L dr'\rho(r')\frac{A}{r^2}(1+2\frac{r'}{r}+3\frac{r'^2}{r^2}+...) \\ &= \frac{A}{r^2}(1+2\frac{<r'>}{r}+3\frac{<r'^2>}{r^2}+...) \end{aligned} \tag{5}$$

If we make the approximation that the neutrino origin is some average position inside the decay tunnel, $r_0 =< r' >$, then from Section V.2.1

$$\begin{aligned} f(r) &= \frac{A}{(r-<r'>)^2} \\ &= \frac{A}{r^2}(1+2\frac{<r'>}{r}+3\frac{<r'>^2}{r^2}+...) \end{aligned} \tag{6}$$

Therefore the error we make with this approximation to lowest order is given by

$$F(r) - f(r) \approx 3\frac{A}{r^2}(\frac{<r'^2> - <r'>^2}{r^2}) \tag{7}$$

An exponentially decaying distribution of origins inside the tunnel (mostly from decaying pions) has a smaller value of $< r'^2 > -< r' >^2$ than does a flat distribution, for which the fractional error on $f(r)$ is approximately $L^2/4r^2$. For r as small as 1 km, with a 180 m long tunnel, the approximation of all neutrinos from $r_0 =< r' >$ results in a fractional error on the detector rate of less than $L^2/4r^2 = 0.8\%$. Even this error will be mostly eliminated because the actual data analysis will not assume that all neutrinos come from the same point. In effect it will correct for the error described by Equation 7; so the systematic error from the

fact that the neutrino origin has a spread in positions will come from the Monte Carlo error in a correction whose full size is less than 0.8%. The systematic error from this effect will therefore be negligible. What will not necessarily be negligible is the error in our Monte Carlo estimate of $< r' >$. Thus almost all of the beam systematic error will be contained in our determination of $r_0 =< r' >$.

The beam in each energy bin is well defined by two parameters: the overall normalization, A, and the average origin, r_0. These two parameters can either be measured by placing detectors close to the beam origin or they can be calculated. If only one detector (at 3 km) is near the beam origin then we will have to rely on a calculation of r_0 to predict the flux or the number of muons at the far detector. Due to resolution and acceptance effects these muons will come from a range of neutrino energies, and therefore r_0 will be a complicated function of the beam and detector geometry, as well as the analysis cuts and the background contamination. An error in this complex calculation of r_0 will produce a systematic error in f_p given by:

$$\frac{\delta f_p}{f_p} \approx 2\frac{\delta r_0}{(r_a - r_0)} \tag{8}$$

where r_a is the distance to the first detector, f_p is the predicted count rate at the far detectors, and the factor of 2 arises because of the $\frac{1}{(r-r_0)^2}$ dependence.

This systematic error caused by having only one detector near the beam origin could lead to a spurious oscillation signal when the statistical error in the far detectors becomes small after several months of running. Therefore it is desirable to eliminate this source of systematic error. Placing two detectors separated by 1-2 km near the beam origin eliminates the reliance on a Monte Carlo calculation of r_0. The two near detectors allow us to extrapolate the number of events at site a and b to the far sites to obtain f_p and to the origin to obtain r_0. In such a situation the detector at site b serves to monitor the normalization and the detector at site a serves to define the source of the neutrinos.

ERROR IN DETERMINATION OF BEAM PARAMETERS

The above formulation of the beam parameters is based on the assumption that either the beam is isotropic or the detectors are infinitesimal in size; neither of these is true. The neutrino beam is quite strongly focused in the forward direction. In the presence of such anisotropy, r_0 cannot be interpreted as the actual average origin of the neutrinos; nevertheless, it remains a useful parameter to understand the beam properties and the systematic error.

At 0 degrees the flux has a maximum and falls approximately as the square of the angle (or horizontal distance). Therefore event counts in detectors of equal size placed at various

distances at 0 degrees will not follow the $1/(r-r_0)^2$ law. On the other hand, at 1.5 degrees the quadratic term across the detector is small, and a linear fall in intensity dominates the flux shape (Figure 19). This linear fall does not cause a deviation from the $1/(r-r_0)^2$ behavior, since it is an odd function with respect to the center of the detector. Figure 19 also shows the change in spectrum across D1. The mean E_ν changes by about 10% across the fiducial volume. Figure III.10 shows that the average spectrum at D1 is however very close to the spectra at D3 and the far detectors. Below we will show that when combined with the effects of path-length and cross section this change in the spectrum across the detector at D1 does not cause significant deviation from $1/(r-r_0)^2$ law.

Angle	% deviation from linearity
0^0	1.47
0.25^0	1.04
0.5^0	0.27
1.0^0	-0.31
1.5^0	-0.17
2.0^0	-0.12

Table 5: *The deviation from linearity (extrapolated minus calculated divided by the calculated flux at the far site) for* $q = 1/\sqrt{f}$.

In Figure 20 we have plotted $q = \frac{1}{\sqrt{f}}$, where f is the total neutrino flux in a 15 meter diameter circular aperture located at r =1, 3, and 24 km from the target at various angles with respect to the tunnel axis. The calculations of these fluxes were performed using the GEANT based program originated at TRIUMF (see Figure 3). Since q should be linear in r we have drawn a line through the first two points and extrapolated it to the 24 km point. The vertical size of the box at the 24 km point corresponds to the statistical error expected after 16 months of running E889. The deviation of the central value at the 24 km point from the line is an indication of the departure from the $1/(r-r_0)^2$ behavior. This deviation is tabulated in Table 5. We see that the deviation from the $1/(r-r_0)^2$ behavior is strongest at 0 degrees and diminishes rapidly with angle. Although we don't display the results for the 68 km site, the same arguments hold. In the actual analysis we will use a complete simulation involving the observations in D1 and D3 to predict the event counts in D24 and D68. Nevertheless, we want to design a system that obeys simple geometric laws as fully as

possible. This is achieved in our experiment with detectors at 1.5 degrees.

The calculations shown in Figure 20 did not include the actual cylindrical shape of the detector and the neutrino cross section. The cylindrical shape of the detectors causes the path-length of the neutrinos at the centers of the detectors to be largest, and thus reduces the effect of the change in intensity across the detector. The effect of the change in spectrum across the detector (Figure 19) is small because the quasi-elastic cross section is slowly varying around 1 GeV neutrino energies. We have performed detailed Monte Carlo simulations of the neutrino beam and the resulting interactions in the detectors placed at 1, 3, 24 and 68 km locations with the 1.5 degree offset.

Table 6 shows the number of neutrino quasi-elastic events without cuts at the 1, 3, 24 km detector sites calculated by tracing neutrino rays from the decay tunnel to the detectors and properly accounting for path-lengths and cross section on an event by event basis. The apparent origin, r_0, can be calculated with the formula

$$r_0 = \frac{r_a - r_b\sqrt{(f_b/f_a)}}{1 - \sqrt{(f_b/f_a)}}. \tag{9}$$

We have varied the hadron production models (FLUKA [13] and GHEISHA[14]) used for the beam simulations as well as the neutrino cross section model (Kamiokande versus E734). Variations in the Monte Carlo clearly alter both the overall normalization and the parameter r_0 by significant amounts, but the extrapolation to 24 km using results at 1 and 3 km and the $1/(r - r_0)^2$ law remains robust as shown in Figure 21. The results for the 68 km detector are similar. This figure immediately shows the need for the two near detectors; with only one detector the normalization can be fixed, but r_0 will still need to be calculated by simulations, and systematic errors could result because of the uncertainties on the calculations. With two near detectors the experiment becomes a simple counting experiment to first order.

We plan to have two near detectors for the complete experiment, but we intend to evolve the experiment over time to explore the oscillation parameter space with increasing sensitivity. The first run of the experiment will be with only two detectors, one at 3 km and one at 24 km. Therefore we have to consider the systematic error on r_0 from Monte Carlo calculations for this very first run. Table 6 shows that variations in the hadronic shower physics and the neutrino cross sections can vary r_0 by about 9 m. A few additional geometrical systematic errors must also be considered for a two detector experiment; they are the knowledge of the target-horn materials, geometry, the current, and the proton beam steering (angle and position) on the target during the run. Including these effects, we estimate the total systematic error on the calculation of parameter r_0 to be about 20 m. If the near detector is the one at 3 km the

r (km)	MC-1	MC-2	MC-3
1 km	$2749 \pm 5 \times 10^3$	$2490 \pm 5 \times 10^3$	$2575 \pm 9 \times 10^3$
3 km	$293 \pm 1 \times 10^3$	$267 \pm 1 \times 10^3$	$278 \pm 1 \times 10^3$
24 km	$4.52 \pm 0.05 \times 10^3$	$4.05 \pm 0.05 \times 10^3$	$4.33 \pm 0.03 \times 10^3$
24 km pred.	4.50×10^3	4.11×10^3	4.29×10^3
r_0	30.6 ± 2.8 m	26.2 ± 2.8 m	21.3 ± 4.0 m

Table 6: *Quasi-elastic events in the cylindrical detectors placed at 1.5 degrees from the beam axis. Also shown is the prediction at 24 km using a the* $1/(r - r_0)^2$ *law. Figure 21 also shows this extrapolation. MC-1 is FLUKA beam with Kamioka cross sections. MC-2 is GHEISHA beam with Kamioka cross sections. MC-3 is FLUKA beam with E734 cross sections. The 1 and 3 km results were extrapolated to 24 km and to the horizontal axis to obtain* r_0*. The normalization is for* 2.2×10^{20} *POT. The errors are from Monte Carlo statistics.*

beam related systematic error (Equation 8) in predicting the event counts at the 24 km site will be about 1.3%.

In summary, in the direct measurement of muon disappearance it is essential to have two near detectors to reduce beam related systematic errors that result from the extrapolation of event counts to the far detectors by Monte Carlo calculations. If the acceptances and efficiencies of all the detectors are well understood then an experiment with two near detectors can be considered a simple counting experiment that follows the $1/(r - r_0)^2$ law. The error due to beam calculations in predicting the flux at the 24 or the 68 km sites using two near detectors will be negligible compared to the statistical error at those sites after 16 months of running (about 1% and 3% for the D24 and D68, respectively). Moreover, since the two near detectors, which are identical to the far detectors, decouple the beam from the detector response the experiment will not be to a spurious oscillation signal.

Since we envision that the first run of the experiment will have only one near detector the systematic error in the determination of the parameter r_0 by Monte Carlo calculation must be considered. We estimate it to be $\delta r_0 \approx 20$ m. The beam related systematic error on the prediction at the far site for a two detector experiment given by Equation 8 will be 1.3% if the near detector is at 3 km.

Finally, the beam related systematic error is of importance mainly for the result using D24 where the statistical error will be about 1% after 16 months (2% after 4 months); the

statistical error at D68 will be about 3% after 16 months and therefore the results from D68 will not be limited by systematic errors.

V.2.4.2 DETECTOR SYSTEMATIC ERRORS

We may combine the effects of all detector related systematic errors into a single systematic error on the number of events in one of the near detectors, δf_a. Then it can be shown that the error on the predicted number of events at the far site, δf_p, is, in the case of a two detector experiment:

$$\frac{\delta f_p}{f_p} \approx \frac{\delta f_a}{f_a}. \tag{10}$$

In the case of a three detector experiment we use the known distances to the near two detectors to extrapolate the counts to the far site (Figure 21) and if the near two detectors are sufficiently far apart so that $f_a >> f_b$ then

$$\frac{\delta f_p}{f_p} \approx \frac{r_a - r_o}{r_b - r_a} \frac{\delta f_a}{f_a}. \tag{11}$$

Here f_a and f_b are the counts in the near two detectors, and r_a and r_b are the distances to the near detectors. f_p is the prediction for the far detector, and r_0 is the parameter that describes the beam. We have assumed that most of the systematic error is in the nearest detector in either the two or the three detector situation. Now we will estimate the size of the systematic error in the near detectors due to various contributions.

DETECTOR LOCATIONS

We have located the detectors so that they are all close to each other in both polar and azimuthal angles about the beam axis. Table 7 shows the locations in latitude and longitude of the selected sites which are chosen to lie on a great circle. The local elevations of the ground with respect to sea level are also indicated. There are no severe constraints at any of the sites including the Northville and the Plum Island sites on the exact locations of the detectors. There is also freedom to place the tanks below the existing ground elevation by about 4-5 m by excavation. We will place the bottom of the detector tank, D1, 4 m below the ground level. Figure 22 shows the four detectors as viewed from the neutrino production target in polar and azimuthal angular co-ordinates with respect to the beam axis. We have ignored the small angular tilt (0.25^o at D68) in the detector axis due to the earth's curvature at different sites for the purposes of this analysis. The figure shows that all detectors are aligned with respect to their axes and that D1 covers all detectors in solid angle. The beam can be pointed so that both D24 and D68 are at the same polar angle of 1.5^o, but about 10.2^o

Site	Latitude	Longitude	Elevation m
Production Target	$40^o52'34.167''$ N	$72^o52'43.940''$ W	22.9
D1 at 1 km	$40^o52'50.682''$ N	$72^o52'07.189''$ W	18.0
D3 at 3 km	$40^o53'23.704''$ N	$72^o50'53.672''$ W	17.0
D24 at Northville	$40^o58'49.996''$ N	$72^o38'44.573''$ W	35.0
D68 at Plum Isld.	$41^o10'59.184''$ N	$72^o11'17.350''$ W	10.7

Table 7: *Locations of the sites in latitude and longitude. The local ground elevation with respect to sea level is shown in the last column.*

apart in azimuth. Since the detectors are located with their axes precisely at the same polar angle with respect to the beam, we do not need to make corrections to the numbers of events in each of the detectors to compare them to each other. In particular, the linear component in the flux variation across the detectors in Figure 19 is unimportant because the detectors are aligned to within a fraction of a milliradian. With the alignment shown in Figure 22 any corrections will be quite small. The small difference in the azimuth between D24 and D68 is mainly due to the earth's curvature; we have performed Monte Carlo studies of the beam to see if the neutrino flux can vary over this small angular interval. We have found that such effects, mainly due to proton beam misalignments, will be quite small, and in any case, the neutrinos that go to both D68 and D24 will be monitored by D1.

FIDUCIAL VOLUME AND SOLID ANGLE

The far detectors, which are identical in size and photomultiplier coverage to the near ones, subtend smaller solid angles with respect to the beam. The neutrino flux varies with the angle, and the near detectors see neutrinos at both smaller and larger angles than the far ones. We have chosen to separate the systematic errors due to the effects of flux variation across the detectors into two parts: We have already discussed the systematic error on the apparent origin of the neutrinos which must be computed if we have only one near detector. The second source of potential systematic error results after the analysis cuts from each of the detectors are applied to the events. Because the geometry causes the progenitor distribution of the neutrino events to be somewhat different in each detector tank, the acceptances computed in each detector for the analysis cuts – fiducial, containment, and angle or energy – will be somewhat different. Figures 23 and 24 show the distribution of event vertices across the detector tanks in the horizontal coordinate (perpendicular to the neutrino beam axis). The

Cuts	1 km	3 km	24 or 68 km
Fiducial Contained	0.492 ± 0.005	0.494 ± 0.005	0.496 ± 0.005
Muon angle $< 60^o$	0.323 ± 0.005	0.337 ± 0.005	0.329 ± 0.005

Table 8: *Acceptance for quasi-elastic events for fiducial, containment, and angular cuts for detectors at the various locations. The error is from Monte Carlo statistics.*

figures show that the fiducial (1 m in from the PMT surface) and containment cuts combined with the cylindrical geometry of the detectors tend to force the vertex distributions to be similar at all locations. The nearest detector will have a small excess of events on one side of the detector compensated by a small deficit on the other side. The systematic error on the differences in acceptance will affect both types experiments, i.e. that with only one near detector and that with two near detectors. Table 8 shows the acceptance for quasi-elastic events at the different detector sites. There is a small increase (about 0.8%) in acceptance between the detector at 1 km and the far detectors at 24 km or 68 km. We will have to correct for this change in acceptance to get back to raw event counts displayed in Figure 21. At the moment we will consider this entire change as a systematic error.

SPECTRUM

We have examined the spectrum of muons and the neutrinos that generate the muons for each of the four detector sites. Figure 25 shows that the spectrum of photoelectrons observed in the 3 km and the far detectors should be very close to each other in the absence of oscillations. The spectrum at 24 km and 68 km are identical to each other, and so the 68 km spectrum is implicit when we discuss the 24 km spectrum. The spectrum at 1 km is softer by a small amount. The fraction of the spectrum below 750 photoelectrons ($P_\mu \approx 550 MeV/c$) is about 8% higher in the case of the 1 km detector compared to the 24 km detector. We can correct for this by Monte Carlo or by making tighter fiducial cuts in the 1 km detector and then correcting for the different acceptance. For the purposes of an oscillation analysis the spectrum from the 3 km detector can be used with no corrections for comparison with the spectra from the far detectors.

Figure 26 shows the spectrum of neutrinos that produce the events in Figure 25. Both the detector response and the event characteristics could depend on this spectrum which is slightly different for the 1 km, the 3 km , 24 km, and 68 km detectors. The mean energy of the neutrinos is 0.922 GeV in the 1 km detector and 0.956 GeV in the 3, 24, and 68 km

detectors. Most of the systematic error from the change in the spectrum has already been accounted for in the acceptance cuts (Table 8). Any corrections to the detector efficiencies because of the combination of spectrum change and detector resolutions will be smaller than the acceptance change.

CALIBRATION

Small differences in the detectors could be caused by dead photomultiplier tubes, differences in the light attenuation length in water, differences in the calibration constants or the timing signals, etc. These differences will translate into small differences in the efficiencies for detecting signal events and rejection of backgrounds between detectors. As explained in the section on detector construction we intend to test the photomultiplier tubes and associated hardware for reliability and increase the number of photomultipliers by a small factor to compensate for the probability that some of the tubes will not work after several years of running. From previous experiences in the Kamioka and IMB detectors the probability of dead tubes is less than 5% over the course of the running time. One advantage of having the detector tanks on the surface is the ability to continuously monitor the detector calibration with cosmic rays. With careful control of the hardware and calibrations the systematic errors due to differences in the detectors should be small.

DEAD TIME

There are two main causes of deadtime in the experiment: 1) overlapping cosmic ray events, and 2) overlap of two events from the neutrino beam.

As shown in Chapter III the total spill length for the AGS beam is $2.68\mu s$. Within this time there could be 0.2 cosmic ray events. The readout electronics is such that each PMT will remain dead for 60 to 200 ns after a hit. If we assume that no spatial separation between real cosmic rays and neutrino induced events is possible, then for a neutrino event to be deadtimed a cosmic ray event must occur 200 ns before the time of one of the 8 buckets. This corresponds to 1.5% of the neutrino events lost in each of the detectors. We intend to make this loss smaller by adjusting the PMT deadtime to be less than 200 ns. Some spatial separation of the event vertices is also possible but has not been studied in detail yet. In any case, the deadtime due to cosmic rays will be the same in all detectors and monitored closely by having a separate trigger for cosmics with a fixed gate outside the AGS beam gate.

The second type of deadtime could pose a systematic problem since the event rate in the near detectors is much higher than the event rate in the far detectors. In the case of neutrino events we only need to consider the rate of overlapping events in the same time

bucket because the time between buckets (335 ns) is long enough for the PMTs to recover. The total neutrino event rate in the entire inner volume of the nearest detector at 1 km will be about 0.86 events per AGS spill (with 8 buckets). Using Poisson probability function, 0.37 of the events will be accompanied by at least one other event in one of the 8 buckets; therefore 5% of the events will actually have two separate events in the same bucket. We will most likely reject events as multiring events if the event vertices are closer than ± 2 m in all dimensions. Given that the detector volume is 7.5 m in radius and 15 m in height, a correction of about 0.12% will have to be applied to the event rate in the closest detector. The vertex resolution will be much better than 2 m, but light from two widely separated vertices could still fall on the same PMTs depending on the direction of the particles.

Another way to correct for the loss due to deadtime is by taking a few different runs of data at different intensities. The 1 km detector has an approximate rate of about 10^5 $QE(\mu^-)$ events per week at the nominal intensity of 4×10^{13} POT. In two different running periods (2 weeks each) with 1/3, and 2/3 of the full intensity one can gather data to study the deadtime correction with an error of about 10% of the value of the full correction of 5%.

To further illustrate the trade-offs, if we place the nearest detector at 2 km instead of 1 km the deadtime will reduce by a factor of 4 and the change in the spectrum between the nearest and the farthest detector will also be smaller. On the other hand one could argue that we want a near detector that covers a much larger solid angle than the far detectors to study the beam. At the moment we have optimized with a detector at 1 km, but are studying other possibilities. We will assume a systematic error of 0.5% due to the deadtime corrections.

BACKGROUND SUBTRACTION

As shown in Section V.2.3 we expect a contamination of 5.4% from neutral current events and charged current events of high energy (above 1.5 GeV) neutrinos in the quasi-elastic muon sample. The total contamination above 300 photoelectrons including WCC and WNC events from neutrinos below 1.5 GeV will be about 15%. Also we expect a 6% contamination due to cosmic ray events in the 68 km detector after the full running time.

We are confident that the neutrino induced background can be calculated and subtracted; any error in such a subtraction will dilute an existing signal rather than introduce a new one. The main systematic error in the background procedure will be due to the differences in the neutrino spectrum. The change in the mean energy of the neutrinos between D1 and D24 (or D68) is about 3.6%. Since the cross sections for the backgrounds are approximately linear with energy in this region the maximum systematic error due to neutrino background

subtraction will be about 0.5%. The sensitivity of the experiment does not depend on this background subtraction since 2/3 of the background are WCC events from ν_μ of the same energy spectrum as the $QE(\mu^-)$ signal. If left unsubtracted the significance of an oscillation signal will simply reduce by 5.4% which is the background fraction that does not oscillate.

The cosmic ray background will be measured extremely well. But we will assume no background subtraction for the cosmic ray events when calculating the sensitivity. If we were to subtract the cosmic ray background we are confident that it can be done without introducing a systematic error greater than 0.3% as pointed out in the previous discussion on cosmic ray backgrounds.

V.2.5 SUMMARY OF DIRECT ν_μ DISAPPEARANCE ANALYSIS

In summary, consider the size of the total systematic error compared to the statistical error on the event counts at the far sites. The statistical error at D24 and D68 will be about 1.0% and 3.0%, respectively after 16 months of running, using the contained event count in Table 1. In the case of an experiment with only two detectors, one near at 3 km and one at 24 or 68 km, the total systematic error will come from both the beam calculations (1.3%) and the detector corrections (1.1%). (Equations 8 to 10). Therefore the total systematic error in the case of a two detector experiment will be 1.7%.

In the case of an experiment with three detectors, two near at 1 and 3 km and one far at 24 or 68 km, the contribution from the beam calculations will be small. The main systematic error will be from the detector corrections of 1.1% in the nearest detector. Using Equation 11 which accounts for the use of the second near detector for extrapolation, the systematic error on the prediction at the far detector will be 0.6%.

To get maximum sensitivity with a far detector at 24 km one must perform a three detector experiment which reduces the systematic error below the expected statistical error. On the other hand with a far detector at 68 km the maximum possible sensitivity will be determined by the statistics at that far site. Nevertheless, two near detectors will be essential to eliminate the dependence to first order on a Monte Carlo calculation of the beam and to irrefutably establish a signal. With four detectors as shown in Figure 22 we will satisfy all requirements of statistical and systematic precision and perform an experiment with many independent controls. Moreover, in the case of a positive oscillation signal we will measure the oscillation parameters precisely using the count rates in detectors at different oscillation lengths from the neutrino origin. The discussion of the sensitivity of the direct ν_μ disappearance result is

in Section V.5.

V.3 NEUTRAL CURRENT π^0 EVENTS

V.3.1 INTRODUCTION

If a signal for ν_μ disappearance is observed, it will be important to establish it in as many different ways as possible. An independent way to perform the ν_μ oscillation experiment is to compare the ratio of charged current muon neutrino events to neutral current π^0 production interactions ($QE(\mu^-)/NC(\pi^0)$) in the near and far detectors. The analysis for such a measurement is very different from the muon disappearance analysis. In particular, since the number of reconstructed neutral current pion events will always be smaller than the number of muons the sensitivity will be dominated by the pion statistics and will be lower than the direct muon disappearance analysis. The systematic errors will not be as important because first they will be smaller than the statistical error on the pion counts at the far detectors and second most of the beam or detector related systematic errors will cancel out in the ratio. This method of analysis will also be important in the unlikely case that the oscillations are occurring into a sterile neutrino ($\nu_\mu \rightarrow \nu_s$) that does not interact through charged or neutral current interactions. In such a case a deficit of muon events will be accompanied by the same fractional deficit of pion events, and the ratio of muons to neutral current pions will remain the same at all distances from the beam. In the following we show that the measurement of the ratio ($QE(\mu^-)/NC(\pi^0)$) could be performed with sufficient precision in our apparatus to be sensitive to most of the oscillation parameter space as the direct muon disappearance search. The measurement of this ratio will independently establish or rule out the Kamioka signal.

V.3.2 SIGNAL AND BACKGROUND

The two main neutral current single π^0 channels are

$$\nu n \rightarrow \nu n \pi^0 \tag{12}$$

$$\nu p \rightarrow \nu p \pi^0 \tag{13}$$

The ratio of the neutral current single π^0 cross section to the charged current quasi-elastic cross section has been calculated over the energy region of the AGS beam (Figure 27) [5]. When averaged over the flux the ratio of cross sections is 0.10 for each of the above two channels. About 6% additional π^0 are expected from coherent production off oxygen nuclei

	1 km	3 km	24 km	68 km
Events in Detector	20.7×10^5	23.2×10^4	3632	453
Events in Fiducial	13.6×10^5	15.1×10^4	2364	295
2 Ring Events	7.37×10^5	8.17×10^4	1281	160
1 Ring and Extra Energy	2.83×10^5	3.13×10^4	492	61
Total Reconstructed	10.2×10^5	11.3×10^4	1773	221

Table 9: *The number of neutral current π^0 events for 8.8×10^{20} POT or 16 months of running at the four detector sites with one detector tank each. The events are in the fiducial volume and have at least 50 PMTs hit. There will be about 15% background from charged current π^0 production.*

[11]. The cleanest signature of a π^0 is two electromagnetic Cherenkov rings. A sample of Monte Carlo WNC π^0 events were scanned visually to identify event topologies. These events were tagged as to the number of rings and whether extra energy was present indicating the presence of another photon. Further details of the pattern recognition can be found in Chapter IV. The scanning results indicate that 54% of the events inside the fiducial volume produced two rings without extra energy. An additional 21% of the π^0 events have a single ring with extra energy indicating the existence of the other photon. The extra energy can be either an incomplete ring or an accumulation of energy at the edge of the ring. These events could be recovered with a more sophisticated analysis that reconstructs the mass of the π^0 using the energy measurement of the complete and the incomplete photon rings (see Chapter IV). Combining the numbers, the total number of π^0 events with two clean rings will be about 11% (0.2×0.54) of the quasi-elastic muon rate. A 40% gain in the π^0 statistics would result if we also use events with one incomplete ring. Table 9 gives the total number of neutral current π^0 events in the fiducial volume expected in each detector for a 16 month run with 8.8×10^{20} POT.

The principal background comes from the charged current channel $\nu_\mu n \to \mu^- \pi^0 p$ which normally produces three rings. We have visually scanned these events to find the fraction that appears as two showering rings to be 6% (Chapter IV). In most of these remaining events the muon will be below detection threshold. The fraction of events with one complete showering ring and some extra energy is 1.5%. Since the ratio of the $\mu^- \pi^0 p$ cross section to the quasi-elastic cross section is 0.3, the expected background from the charged current

single π^0 in the neutral current single π^0 channels is 16% ($\frac{0.3\times0.06}{0.11}$) using only the two ring sample. The background for the two ring plus one ring with extra energy sample is 15%. However this sample might have some additional contribution from misidentified particles since the incomplete ring may not be recognized as a clean showering particle. We have not yet examined this background and the obvious method of eliminating it by reconstructing the π^0 mass. The charged current background could be subtracted with the introduction of a small systematic error. If it is left unsubtracted it will dilute the oscillation sensitivity. In neither case will it cause a statistically significant spurious oscillation signal.

The methods we intend to employ in reconstructing the events are discussed further in Chapter IV on pattern recognition. The important point that should be repeated here is that the event samples in the far detectors are small enough that a manual scan of the data can be performed. A random sample of events in the near detectors can be manually scanned to obtain the expected ratio of muons to π^0s. If the random sample is chosen to be sufficiently larger than the number of events in the far detectors, the ν_μ disappearance analysis normalized to the neutral current π^0s can be performed without the use of computer pattern recognition.

V.3.3 SYSTEMATIC ERROR ON ($QE(\mu^-)/NC(\pi^0)$)

As shown in Table 9 the statistical error after 16 months of running on the π^0 counts will be about 2.4% at D24 and 6.7% at D68. Most of the systematic errors discussed for the direct muon disappearance analysis are either small compared to the π^0 statistics or cancel out in the ratio $QE(\mu^-)/NC(\pi^0)$. The systematic error that may not cancel will be due to the spectrum change between the near and the far detectors. The change in the mean energy of the spectrum does not affect the muon counts since the quasi-elastic cross section is approximately flat in the 1 GeV energy region. The cross section for π^0s, however, is linear with energy in the 1 GeV energy region; therefore a correction that accounts for the different cross section dependencies on the energy will have to be made when comparing the ratios measured in the near and far detectors.

We showed in Figure 26 that the neutrino spectra in D3, D24, and D68 are nearly identical, therefore the correction to the ratio when comparing the ratio in D3 and the far detectors will be much smaller than the statistical errors on the π^0 counts. The mean energy of the spectrum does change by 3.6% between D1 (0.922 GeV) and D3 (0.956 GeV), and therefore if we use the near detectors, D1 and D3, to look for oscillations at $\Delta m^2 > 0.1$ eV^2 they will most likely be limited by systematic error on the calculation of the correction to the ratio.

We use the cross sections in Figure 27 to estimate this correction to be 2%. For the current analysis we will assume the entire correction to be the worst case systematic error of 2%. The discussion of sensitivity to neutrino oscillations with the ratio method is in Section V.5.

V.4 ν_e APPEARANCE

V.4.1 INTRODUCTION

If a signal of ν_μ disappearance is observed, it will be important to understand its origin, and in particular check whether the deficit of ν_μ flux is accompanied by an excess of ν_e. Any deviation between the expected number of ν_e events at a far detector and the observed number will constitute an electron neutrino appearance signal. We have discussed in detail how backgrounds, systematic and statistical errors affect the muon neutrino disappearance experiment. The concerns for a ν_e appearance experiment are quite different. As explained in Chapter III.A the contamination of electron neutrinos in the beam is quite small; therefore even a small increase of electron neutrino type events will be detectable if the backgrounds from other processes (mainly misidentification of π^0s) can be kept low. Even if some background is present we will show that very good sensitivity to $\nu_\mu \rightarrow \nu_e$ is obtained by using the near detectors as monitors of the background. Unlike the direct muon neutrino disappearance analysis, the beam or detector systematic errors play a minor role.

V.4.2 BACKGROUNDS TO THE ν_e SIGNAL

The principal background contributions to the ν_e appearance signal come from (1) the small contamination of ν_e's in the AGS beam, (2) the misidentification of neutral current π^0s as electrons, and (3) the misidentification of a small number of μ's as electrons, troublesome since the dominant component of the beam is ν_μ.

V.4.2.1 ν_e CONTAMINATION IN THE BEAM

The ν_e contamination in the AGS neutrino beam is well understood. The experimentally measured ratio of flux, $\frac{\nu_e}{\nu_\mu}$, from experiment 734 is shown in Figure 28. The total ν_e contamination in E734 was measured to be $7.3 \pm 1.4 \times 10^{-3}$. The curve in this figure is from the neutrino beam simulation program indicating the reliability of the calculation. Unlike E734, the detectors in E889 are positioned at 1.5^o off the neutrino beam axis. The off-axis geometry causes an increase in the ν_e contamination in the beam because a majority of it comes from kaon decays which tend to emit ν_e's at wider angles than the decays of pions which are the main source of ν_μ. Figure 29 shows the expected ratio of ν_e's to ν_μ's in the 1.5^o beam; the

calculation includes contributions from both charged and neutral kaons, muon decays, and also a tiny contribution from pion decays. The total fraction of ν_e, $\frac{\int \Phi(\nu_e) dE}{\int \Phi(\nu_\mu) dE}$, for this beam is 1.04%. The contamination from $\bar{\nu}_e$ in the beam is much smaller (0.11%), and therefore will be ignored in the rest of the analysis. The contamination ν_e spectrum tends to be somewhat higher energy than the ν_μ spectrum (Figure 3). We should be able to use this difference to statistically separate out the signal ν_e which come from the oscillation of lower energy ν_μ.

V.4.2.2 π^0 MISIDENTIFICATION AS ELECTRONS

Events containing π^0s can appear like ν_e quasi-elastic events if the π^0 is misidentified as an electron and any other charged particles in the event are below detection threshold. A π^0 will generally appear as two Cherenkov rings, but some times only a single ring will appear because either the π^0 distributes its energy between the photons asymmetrically so that only one ring has enough Cherenkov light to be visible or the two photon showers overlap. To establish the fraction of π^0 events that would be identified as electrons, we have visually scanned both neutral and charged current π^0 events (the $\nu n \pi^0$, $\nu p \pi^0$, and $\mu^- p \pi^0$ channels). The generated momentum distribution of these pions is the same as in Figures 11 and 13 with a mean momentum of about 300 MeV/c. The events were classified as to the number of rings that were present and if there was extra energy outside the ring that might indicate the presence of another low energy particle. A more thorough description of the visual scanning results is presented in the pattern recognition section.

We have found that 23% of the neutral current π^0 events in the entire inner volume appear as single ring events. Only 5% of the charged current π^0 events appear as single ring; furthermore when we require that the single ring should not look like a muon only 1% of the charged current π^0 events remain. Therefore charged current π^0 events do not constitute a significant background. We have examined the vertex and energy distribution of the single ring neutral current π^0 events and found that they tend to be preferentially at the edge of detector; this is understandable because both the probability of losing one of the two photons and of overlapping photons is higher if the π^0 is at the edge of the detector. With a fiducial volume cut of 6.5 m in radius and 13.0 m in height the scanning results indicate that 20% of the NC-π^0's within the fiducial volume look like single ring events; with a tighter fiducial cut of 6.0 m in radius and 12.0 m height 17% look like single ring events. Since a fiducial cut also lowers the statistics on the signal there will be some optimum fiducial cut for the highest statistical measure of sensitivity, but for the purposes of this analysis we will assume our standard fiducial volume of 6.5 m in radius and 13.0 m height. A cut on the angle of the showering particle with respect to the neutrino direction of 90 degrees gets rid of another

25% of the pion background since it is at wider angles, but retains more than 94% of the quasielastic electron signal from oscillated ν_μ. When combined with the cross section for neutral current pion production of 10% of the quasi-elastic muon rate for each of the two neutral current channels, we obtain that the single ring showering particle background from π^0s will be about 3.0% ($2 \times 0.10 \times 0.2 \times 0.75$) of the quasi-elastic muon rate.

This low background level from π^0 contamination is one more advantage of the off-axis 1.5 degree low energy beam. If we were to use the on-axis 0 degree beam, the background could be a factor of 2-3 higher because the higher energy neutrinos have a higher cross section for pion production, and the higher energy pions also have a higher probability for producing events with overlapping showering rings.

V.4.2.3 MUON MISIDENTIFICATION

The misidentification of muons as electrons could be a background since ν_μ is the dominant component of the neutrino beam. We have visually scanned many muon quasi-elastic events and found that the muon-electron separation rapidly improves with energy. Above a cut of 500 photoelectrons (corresponding to about 350 MeV in energy for electromagnetic showers and 400 MeV/c for muon momentum) the fraction of muon events misidentified as electrons will be less than 1% while the particle identification efficiency for electrons will remain more than 95%. Previous water Cherenkov experiments, Kamioka and IMB, have developed sophisticated statistical tests for electron-muon separation. Relying on their experience and the recent beam test conducted at KEK in a smaller water Cherenkov tank, the background from μ/e misidentification is expected to be quite small. The results from the beam test and the appropriate references are discussed in Chapter IV on pattern recognition and reconstruction. We continue to improve our methods for shower recognition, but since this particular background will be small, particularly above the 500 photoelectron cut, we do not include it in the analysis for ν_e appearance.

Other sources of background to electron-like events could be neutral current coherent production of π^0 off the oxygen nuclei, π^0 production due to charge exchange interactions of charged pions produced in other interactions, and π^0 production due to cosmic ray neutrons. We have considered all these sources of background and found them to be small either because the cross sections are small or because they are accompanied by other charged particles above detection threshold.

Figure 30 shows the photoelectron spectrum of the single ring electron like event background. Table 10 shows the expected rate of background single ring showering events. As expected the pion contamination, which dominates the distribution, peaks at about 500 pho-

	1 km	3 km	24 km	68 km
Events in Detector	5.77×10^5	6.44×10^4	1003	125
Events in Fiducial	3.40×10^5	3.77×10^4	591	74
Events Angle $< 90^0$	2.72×10^5	3.02×10^4	473	59

Table 10: *The number of single ring showering events expected from electron neutrino contamination and misidentified π^0 in the absence of neutrino oscillations after 8.8×10^{20} POT or 16 months of running.*

toelectrons. Both the ν_e contamination and the signal events from oscillated ν_μ will be more widely distributed in energy. Therefore a cut at 500 photoelectrons should be quite effective in getting rid of half of the pion contamination and selecting events that can be unambiguously identified as electrons.

V.4.3 BACKGROUND SUBTRACTION AND SYSTEMATICS

The contributions to ν_e background from the ν_e contamination and from NC–π^0 misidentification can be well determined from data in the near detectors. The $1/(r - r_0)^2$ law will allow a reliable determination of the expected rate of showering single rings at the far detectors. Because the total rates for these events are quite low (Table 10) at the far detectors the systematic errors on the extrapolation will not be important. However, we also wish to use the near detectors, D1 and D3, to search for oscillations at higher values of Δm^2. The background statistics in the D3 detector will be large enough so that the sensitivity in $\sin^2(2\theta)$ at these values of Δm^2 will be limited by systematic errors after the full running period. The treatment of systematic errors in this case will be very similar to what was discussed for the direct ν_μ disappearance analysis, except that the systematic errors will be on the background which will be 4.0% of the quasi-elastic muon rate; the signal is expected to be much larger than the background at full mixing. If we use a total systematic error of 1.7% including both beam and detector related effects on the background prediction at D3 using observations in D1, then we should be able to reach sensitivity in $\sin^2(2\theta)$ below 0.001 at $\Delta m^2 \approx 0.5$ eV^2. The discussion of the sensitivity of the $(\nu_\mu \rightarrow \nu_e)$ experiment is in Section V.5.

V.5 SENSITIVITY TO NEUTRINO OSCILLATIONS

In this section we will use the results obtained in Sections V.2, V.3, and V.4 on the backgrounds and the systematic errors to estimate the sensitivity to neutrino oscillations in each analysis channel.

V.5.1 DIRECT ν_μ DISAPPEARANCE

The main channel of analysis is the disappearance of muon neutrino quasi-elastic events. The quasi-elastic event counts in the near detectors will be used to predict the counts in the far detectors. The spectrum of the events in the near and far detectors can also be compared. If the number of events in the far detectors is found to be less than the predictions then the significance (the number of sigmas) of the result will depend on the statistical error on the event counts in the far detector and the systematic error on the prediction. We have used Equation 1 and the systematic errors described in the previous sections to perform this calculation with a number of rather conservative and simplifying assumptions. Our main thrust in this analysis is the identification and elimination of effects that could cause spurious oscillation signals.

- We have integrated all the events up to 3.0 GeV. If we use the energy spectrum of the events then the significance of the result will certainly be higher. The neutrino spectrum at 1.5^o is essentially a narrow band spectrum around 1 GeV. This is of great benefit because one can extract an oscillation signal with minimal analysis of the spectrum.

- We have assumed subtraction of the neutrino beam related backgrounds and included a systematic error associated with it. As explained earlier the neutral current backgrounds mainly dilute the effect of the oscillations. If we under-subtract this background then the remaining background events will dilute the signal; if we over-subtract then the statistical power of the event sample will be lessened. The total significance of the oscillation signal will increase with a proper background subtraction with no chance of a spurious signal.

- We have assumed no subtraction of the cosmic ray background events. This background contributes a constant number of events at each of the detector sites, and thus if left unsubtracted works in the opposite direction to the diminution of quasi-elastic events expected from neutrino oscillations. We have shown that cosmic background will contribute about 6% of the quasi-elastic signal events at the 68 km site. The fraction at the

nearer sites is much smaller. We will be able to measure this background very well by using cosmic ray data from outside the AGS beam gate. By subtracting the measured rate of background from the neutrino events we will be able to increase the sensitivity to neutrino oscillations. However, if we over-subtract the cosmic background there is a danger of causing a spurious oscillation signal. Therefore we prefer not to subtract the cosmic ray background.

- We use a simple formula to predict the number of events at the far site assuming a $1/(r - r_0)^2$ behavior:

$$f_p = f_a \frac{(r_a - r_0)^2}{(r_c - r_0)^2} \tag{14}$$

$$r_0 = \frac{r_a - r_b\sqrt{(f_b/f_a)}}{1 - \sqrt{(f_b/f_a)}} \tag{15}$$

Here a and b denote the near sites. f_p is the predicted number of events at the far site c located at r_c, at 24 or 68 km. And r_0 is obtained from the measurements at the near sites. We apply this formula using the number of events at each of the sites including the effects of oscillations, background and efficiencies. We define the significance of the oscillation signal as:

$$\sigma = \frac{f_p - f_c}{\sqrt{({\sigma_p}^2 + {\sigma_c}^2)}} \tag{16}$$

where f_c is the actual number of events at the far site including the effects of oscillations, backgrounds, and efficiencies which have been discussed in the previous sections. σ_p and σ_c are the systematic error on the prediction and the statistical error on the number of events at the far site, respectively. We do not correct for the small oscillation effects between the near sites in Equation 14. A small oscillation effect at 3 km will cause us to predict a smaller number of events at the far site and reduce the significance of the oscillation signal by a small amount with no chance of a spurious signal. In the actual analysis of data, we will, of course, fit the detected number of events at the various locations with the oscillation parameters to get the best sensitivity. But here we wish to show the strength of the experiment by displaying the large unmistakable oscillation signal that will result after a simple analysis.

The most exciting possibility is the discovery that the atmospheric neutrino oscillation signal seen in the Kamioka and IMB data is correct (Figure 31). We have calculated the

	D24	D68
Single ring muon-like expected	12150	1478
Deficit $\Delta m^2 = 0.01$ eV^2	1490	875
Deficit $\Delta m^2 = 0.005$ eV^2	400	329

Table 11: *Event deficit and the expected signal after* 8.8×10^{20} *POT or 16 months of running at both of the far sites. The muon-like event counts include background from neutral current and charged current single pion production and cosmics.* $\sin^2(2\theta) = 1.0$ *for the result in this table.*

spectrum of single ring muon-like events that will be observed in the far detectors. Figure 32 shows the muon spectrum after the full running time of the experiment with and without oscillations using the best fit oscillation parameters from Kamioka ($\Delta m^2 = 0.01$ eV^2 and $\sin^2(2\theta) = 1.0$). We have included the spectrum of the background events and the appropriate amount of systematic error. The oscillation signal will be large and unmistakable, and will not be caused by spurious effects. In Table 11 we show the numbers of muon like events that should disappear at the far sites compared to the predicted numbers of events for two values of Δm^2 at full mixing.

Figure 33 shows the 90% confidence level sensitivity of the full experiment after 16 months of running, and for intermediate steps. As we have stated above, an analysis of the spectrum will clearly push the sensitivity below that shown in Figure 33. We have designed the experiment, so that we need not wait until all the detectors are built and operated to perform much of the physics. We envision that we will be able to do the physics as soon as the beam and two detectors, one near and one far, are ready to take data. The first run (about 4 months long or 2.2×10^{20} POT) of the experiment will have a detector at 3 km and one at 24 km. At both of these sites we will have large event rates to study and perfect our technique, and the oscillation sensitivity will be sufficient to study most of the Kamioka allowed region. We expect to have the 68 km detector ready for the second run of the experiment; the limit obtained with running the 68 km detector for 4 months is also shown in Figure 33. If large effects are detected in the first run then the 68 km detector will confirm them. For the first two runs there will be only one detector on site and so the systematic errors associated with the beam will be larger. We have included these systematic errors in the calculation of Figure 33. In the final stage of the experiment another detector will be added on site at 1 km to

eliminate the beam related systematic errors and the dependence on a beam calculation. This is reflected in the improved final sensitivity with D24 in the region $0.005 < \Delta m^2 < 0.1$ eV^2. We have also included the limit obtained with the use of 1 and 3 km detectors at high values of Δm^2 in the final sensitivity of the experiment. We assume at the moment that the limit at high Δm^2 will be limited by systematic errors in about 4 months of running. We note that after the full running the statistics accumulated in the 24 km detector will be so large that the result from it will most likely be limited by systematic errors. On the other hand the results from the 68 km detector will continue to improve with statistics.

Clearly, observation of a deficit of events at two different locations with the respective statistical and systematic errors can be used to measure the oscillation parameters. In Figure 34 we show the 1 σ confidence level contour that will result if the oscillation parameters are $\Delta m^2 = 0.01$ eV^2 and $\sin^2(2\theta) = 0.5$. A measurement of Δm^2 with about 20% error will result. For higher Δm^2 or mixing the error will be smaller.

V.5.3 NEUTRAL CURRENT π^0 NORMALIZATION

As we have described above, comparison of the ratio ($R = QE(\mu^-)/NC(\pi^0)$) measured in the near and the far detectors is an independent way to establish ν_μ oscillations. Since the number of reconstructed neutral current pion events will always be smaller than the number of muons the statistical sensitivity will be dominated by the pion statistics and will be lower than the muon disappearance analysis. The systematic errors will not be as important because first they will be smaller than the statistical error on the pion counts at the far detectors and second most of the beam or detector related systematics will cancel out in the ratio. This method of analysis is also important in the unlikely case that the oscillations are occurring into a sterile neutrino ($\nu_\mu \rightarrow \nu_s$) which does not interact through charged or neutral current interactions. In such a case a deficit of muon events will be accompanied by the same fractional deficit of pion events, and the ratio of muons to neutral current pions will remain the same at all distances from the beam.

We have assumed that we will be able to use both the clean double ring events and the events with one clean ring and extra energy (Table 9). The limits obtained with the somewhat lower statistics sample of double ring events with two complete rings are not very different. We have assumed that we will subtract the WCCπ^0 background of about 15% from the π^0 sample without introducing a systematic error that is larger than the statistical error. Since the rate of this background will be measured using the WCCπ^0 events with visible muons, this background subtraction will most likely be semi-empirical. If we leave

the background unsubtracted the sensitivity will be diluted by 15%, but in neither case will there be a spurious oscillation signal because the background procedure will be identical in all detectors.

The significance of an oscillation result is defined by:

$$\sigma = \frac{R_{near} - R_{far}}{\sqrt{(\sigma^2_{stat} + \sigma^2_{syst})}} \tag{17}$$

where R_{near} and R_{far} are the ratios measured in the near and the far detectors and the difference is divided by the total error. The error when comparing the ratio between D3 and the far sites D24 and D68 is dominated by the statistical error on π^0 counts at D24 (2.4%) or D68 (6.7%). When comparing the ratio in D1 and D3 to explore the Δm^2 region above 0.1 eV^2 the systematic error will dominate; we presently take this systematic error between D1 and D3 to be 2%. The 90% confidence level limit is obtained when the significance is set equal to 1.6 (Figure 35). Once again we have assumed three different running scenarios: an initial 2.2×10^{20} POT run with D3 and D24, a second 2.2×10^{20} POT run with D68 added, and the complete running, 8.8×10^{20} POT, with all detectors. The sensitivity using the the ratio, $QE(\mu^-)/NC(\pi^0)$, will certainly be less than the sensitivity in the direct muon disappearance method. But this method will be free of the kind of systematic errors that were discussed for the direct muon disappearance method. The sensitivity in the ratio will be limited by the π^0 statistics only. If a signal is found in the direct muon disappearance method, every effort will be made to run for a long time with high proton intensity to get sufficient π^0 statistics to establish the signal beyond any doubt.

V.5.2 ν_e APPEARANCE

In the case of $\nu_\mu \rightarrow \nu_e$ oscillations relevant limits exist from reactor experiments that look for $\bar{\nu}_e$ disappearance. Figure 36 shows the limits from several different reactor experiments in the interesting region of mass and mixing parameters. The allowed region of parameters if the Kamioka result is interpreted as $\nu_\mu \rightarrow \nu_e$ oscillations is also shown. We see that most of the Kamioka parameter space is already eliminated by the reactor experiments [16]. The Kamioka parameters are, however, at the edge of the sensitivity of all the reactor experiments so far. New reactor experiments at Chooz and San-Onofre intend to extend the reach in δm^2 to lower values [17]. None of the reactor experiments, new or old can have sensitivity to small mixing, however. We will show below that with E889 we will be able to definitively eliminate the Kamioka parameter space, and also be sensitive to mixing as small as $\sin^2(2\theta) = 0.001$ in a short period of time.

Δm^2 (eV^2)	energy cut	D24 4 Mo	D68 4 Mo	D68 16 Mo
0.01	no cut	297	188	754
	$>$ 500 pe	252	176	706
	$>$ 800 pe	155	120	480
0.005	no cut	79	69	276
	$>$ 500 pe	66	60	240
	$>$ 800 pe	40	37	150
0.003	no cut	29	27	110
	$>$ 500 pe	23	23	92
	$>$ 800 pe	15	14	57
background	no cut	114	15	58
	$>$ 500 pe	70	9	36
	$>$ 800 pe	36	5	18

Table 12: *The number of ν_e oscillation signal events for Δm^2 = 0.01, 0.005 and 0.003 eV^2 are shown along with the expected background under three run scenarios.* $\sin^2(2\theta) = 1.0$ *for this table.*

As an illustration of the sensitivity of E889 to ν_e appearance we have calculated the numbers of signal and background events in the far detectors for the same evolutionary scenario that was discussed for the muon disappearance type of analysis (Table 12). An initial run of four months with 2.2×10^{20} POT with the D3 and D24 detectors will be followed by another four month run with 2.2×10^{20} POT and D68. The complete experiment will have 8.8×10^{20} POT or 16 months of running with all four detectors. At 68 km the ν_e oscillation signal will stay approximately the same as at 24 km while the backgrounds will fall by a factor of 8. The events are shown with no energy cut, and a cut requiring 500 photoelectrons (350 MeV for electrons) and 800 photoelectrons (560 MeV for electrons), respectively. Such a cut preferentially eliminates background from misidentified π^0s and also increases the confidence of the electron identification. We have also required that the showering particle be within an angle of 90 degrees of the neutrino beam and be within the standard fiducial volume. The initial four month run with D3 and D24 would have a signal to background of one for $\Delta m^2 = 0.005$ eV^2 at maximum mixing and enough statistics for more than a 5 standard

deviation effect.

We define the significance of the oscillation result by the equation

$$\sigma = \frac{f_c - f_p}{\sqrt{({\sigma_c}^2 + {\sigma_p}^2)}} \tag{18}$$

where f_c is the actual number of events at the far site including the effects of oscillations, backgrounds, and the cuts which have been discussed in the previous sections. f_p are the predicted number of background events extrapolated from observations in D1 and D3. σ_p and σ_c are the systematic error on the background prediction and the statistical error on the number of events at the far site, respectively. The numerator is simply proportional to $\sin^2(2\theta)$. We show the spectrum of the single ring showering events in Figure 37 at D24 and D68 after 16 months of running with oscillation parameters of $\Delta m^2 = 0.01$ eV^2 and 0.005 eV^2 at full mixing along with the expected background. The oscillation signal will be very large and unmistakable.

The 90% confidence limit is obtained by placing $\sigma = 1.64$ and calculating the value of Δm^2 and $\sin^2(2\theta)$ that produce such an effect at each of the far sites including D3. Figure 38 shows the Δm^2 versus $\sin^2 2\theta$ 90% confidence level plot for the three run scenarios. An initial four month run with detectors at D3 and D24 would produce a Δm^2 limit of 0.0025 eV^2 at maximal mixing. The limit in mixing angle from this initial run would be $\sin^2 2\theta > 0.01$ for $\Delta m^2 > 0.05$ eV^2. The 16 month run with the full detector should set a limit in Δm^2 of 0.001 eV^2 with maximal mixing. The limit in $\sin^2 2\theta$ will be less than 0.001 for large Δm^2 which can be obtained by using D3 as the far detector and D1 as the near detector.

V.6 CONCLUSION

In this chapter we calculated the sensitivity of the experiment with a complete Monte Carlo simulation of the neutrino beam and the detector. The calculation was performed for three analysis channels (1) direct ν_μ disappearance, (2) $QE(\mu)/NC(\pi^0)$ ratio, and (3) ν_e appearance. For each analysis channel we have included the statistical and systematic errors expected at both D24 and D68. The event counts in D24 will be large enough that the ultimate sensitivity will be obtained by careful control of the systematic errors using the two near detectors. On the other hand, the oscillation signal at D68 will be large so that even with smaller statistics we will extend the sensitivity to small values of Δm^2. If a signal is found in the direct muon disappearance mode then it will be confirmed by the comparison of the ratio $QE(\mu)/NC(\pi^0)$ in the near and far detectors.

The direct muon disappearance method will be sensitive down to $\Delta m^2 = 0.003$ eV^2 at full mixing and to $\sin^2(2\theta) = 0.015$ at high Δm^2 at 90% confidence level (Figure 33). The $QE(\mu)/NC(\pi^0)$ ratio method will be sensitive down to $\Delta m^2 = 0.004$ eV^2 at full mixing and $\sin^2(2\theta) = 0.03$ at high Δm^2 (Figure 35). This method will be an independent check on the direct muon disappearance method. The electron appearance method will have an extraordinary reach down to $\Delta m^2 = 0.001$ eV^2 at full mixing and $\sin^2(2\theta) = 0.001$ at high Δm^2 (Figure 38). If an oscillation signal is observed the combination of all three methods will unambiguously determine the actual oscillation channel between $\nu_\mu \rightarrow \nu_\tau$, $\nu_\mu \rightarrow \nu_e$, or $\nu_\mu \rightarrow \nu_s$ where ν_s is a sterile neutrino.

We have designed the experiment to develop over time and explore the oscillation parameter space with increasing sensitivity. Figures 33, 35, and 38 show the complete sensitivity of the experiment and also the sensitivity in the initial runs of the experiment. The experiment will establish or rule out the Kamioka atmospheric anomaly in the very first run of 4 months duration with only half the number of detector tanks. The complete experiment will not only irrefutably establish the signal, but will measure Δm^2 with an error of 10-20% (Figure 34).

The analysis in this chapter was based on various conservative assumptions. The most conservative assumptions are the fiducial volume and the AGS intensity. There will be almost twice as many events in the entire detector as the nominal fiducial volume of 6.5 m radius and 13 m height. We will certainly use all of these events for analysis, although some of them might be poorly measured. In particular the non-contained events will be from higher energy neutrinos; therefore comparison of the ratio of contained to non-contained events in the near and far detectors could be another independent method of analysis. The AGS has now started to deliver 6×10^{13} protons per pulse, much more than our assumption of 4×10^{13} protons per pulse. We have shown the sensitivity using a simple counting and extrapolation scheme. Further analysis of the energy spectrum and vertex distributions in each of the tanks will no doubt increase the sensitivity of the experiment.

REFERENCES

1. C. H. Llewellyn Smith, Phy. Rep. **3**, no. 5 (1972) 261.
2. S. J. Barish, et al., Phys. Rev. D**16** (1977) 3103.
3. L. A. Ahrens, et al., Phys. Rev. D**34** (1986) 75; ibid **35** (1987) 785.
4. M. Nakahata, et al., J. Phys. Soc. Japan **55** (1986) 3786.
5. Dieter Rein and Lalit Sehgal, Annals of Physics **133** (1981) 79.
6. Review of Particle Properties, Physical Review D **50** (1994) 1173.
7. Private communication, Howard Nicholson, Mount Holyoke college.
8. W.N. Hess, et al., Physical Review **116** (1959) 445.
9. W.N. Hess, E.H. Canfield, R.E. Lingenfelter, J. Geophys. Res. **66** (1961) 665.
10. S. Hayakawa, 'Cosmic Ray Physics; nuclear and astrophysical aspects,' Wiley-Interscience, New York (1969).
11. D. Rein and Lalit M. Sehgal, Nuclear Physics B**223** (1983) 29.
12. 'Proposal to Participate in the Super-Kamiokande Project,' C.B. Bratton, et al., The US Kamikande collaboration, December 23, 1992.
13. FLUKA92, A.Fassò, A.Ferrari, J.Ranft, P.R.Sala, G.R.Stevenson and J.M.Zazula, Proceedings of the Workshop on Simulating Accelerator Radiation Environments, Santa Fe, USA. 11-15 January, 1993.
14. H.C. Fesefeldt, Simulation of hadronic showers, physics and applications. Technical Report PITHA 85-02, III Physikalisches Institut, RWTH Aachen Physikzentrum, 5100 Aachen, Germany, September 1985.
15. Y. Fukuda, et al., Physics Letters **B** (1994) 237.
16. B. Achkar, et al., Nuclear Physics B **434** (1995) 503. G. Zacek, et al., Phys. Rev. D **34** (1986) 2621. G. S. Vidyakin, et al., JETP Lett. **59** (1994) 364.
17. R.I.Steinberg, DUHEP-9306001, Jun 1993. Presented at Int. Workshop on Neutrino Telescopes, Venice, Italy, Mar. 1993.

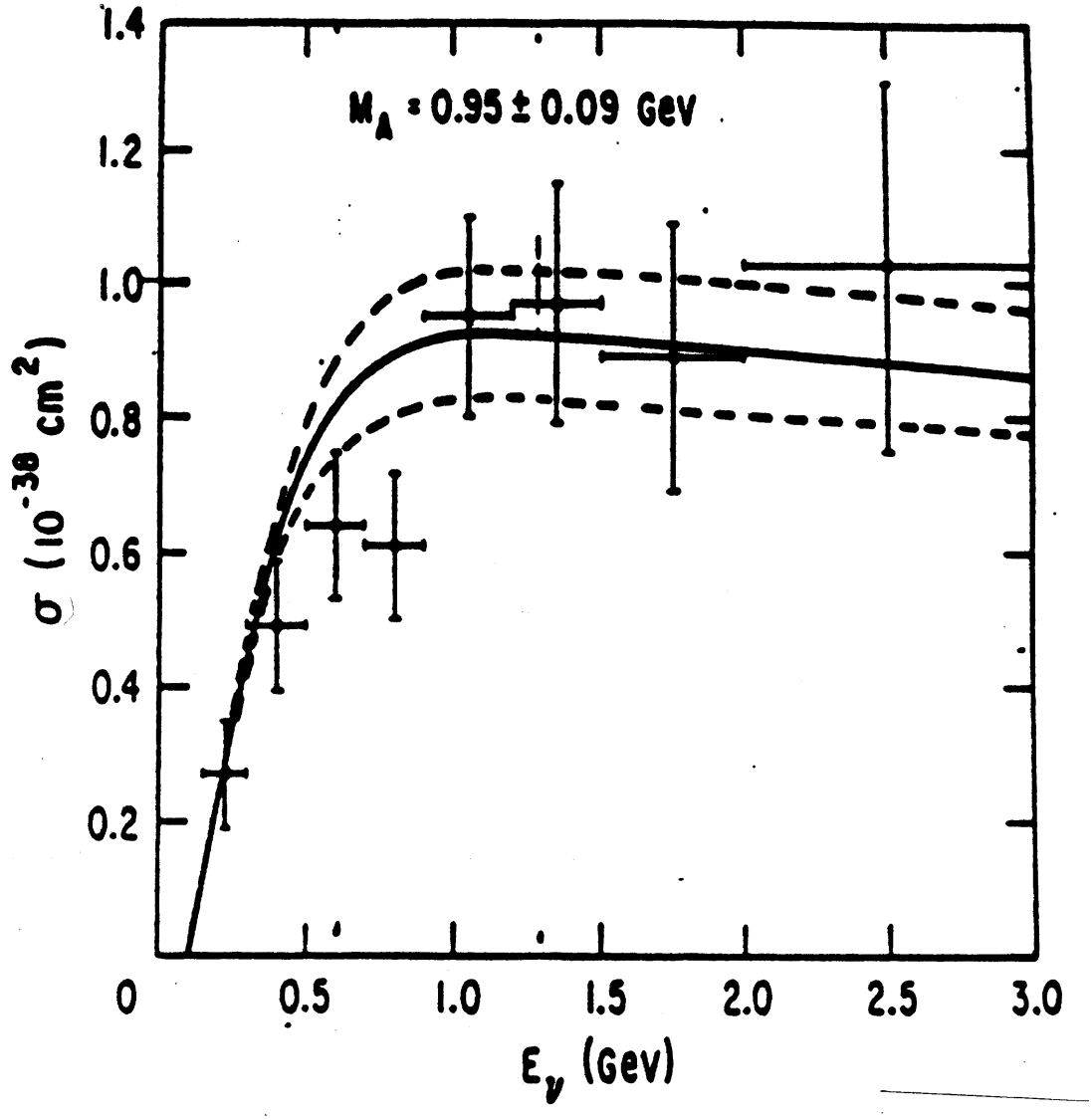

Figure 1: *Total cross section for $\nu_\mu n \to \mu^- p$ as a function of neutrino energy. The dashed curve shows the theoretical error.*

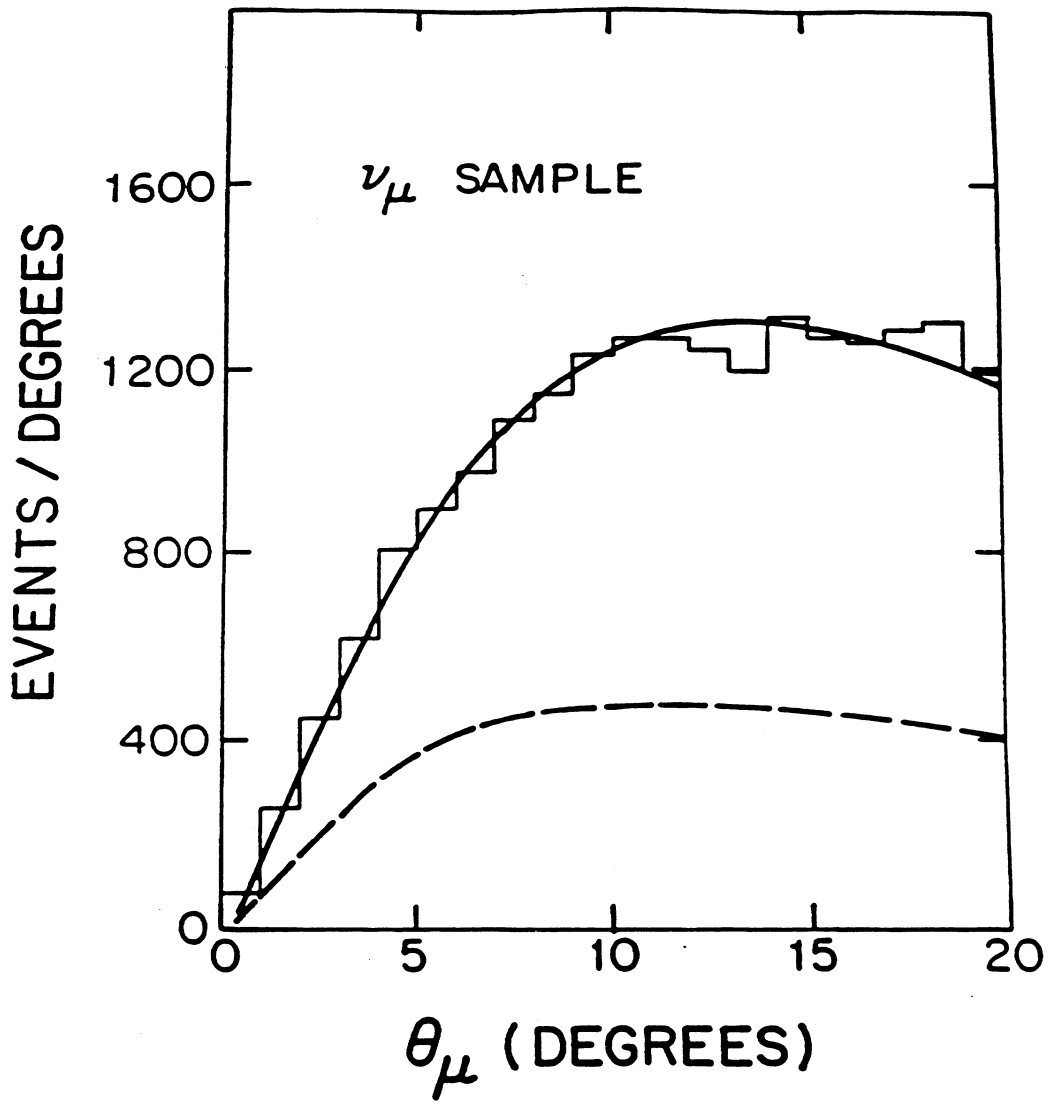

Figure 2: *Quasi-elastic muon events versus the angle of the muon as measured in E734 at the BNL-AGS. The histogram is the data, the solid curve is a Monte Carlo calculation of the spectrum of all muon-like events, and the dashed curve is a calculation of the background from charged and neutral current pion production events.*

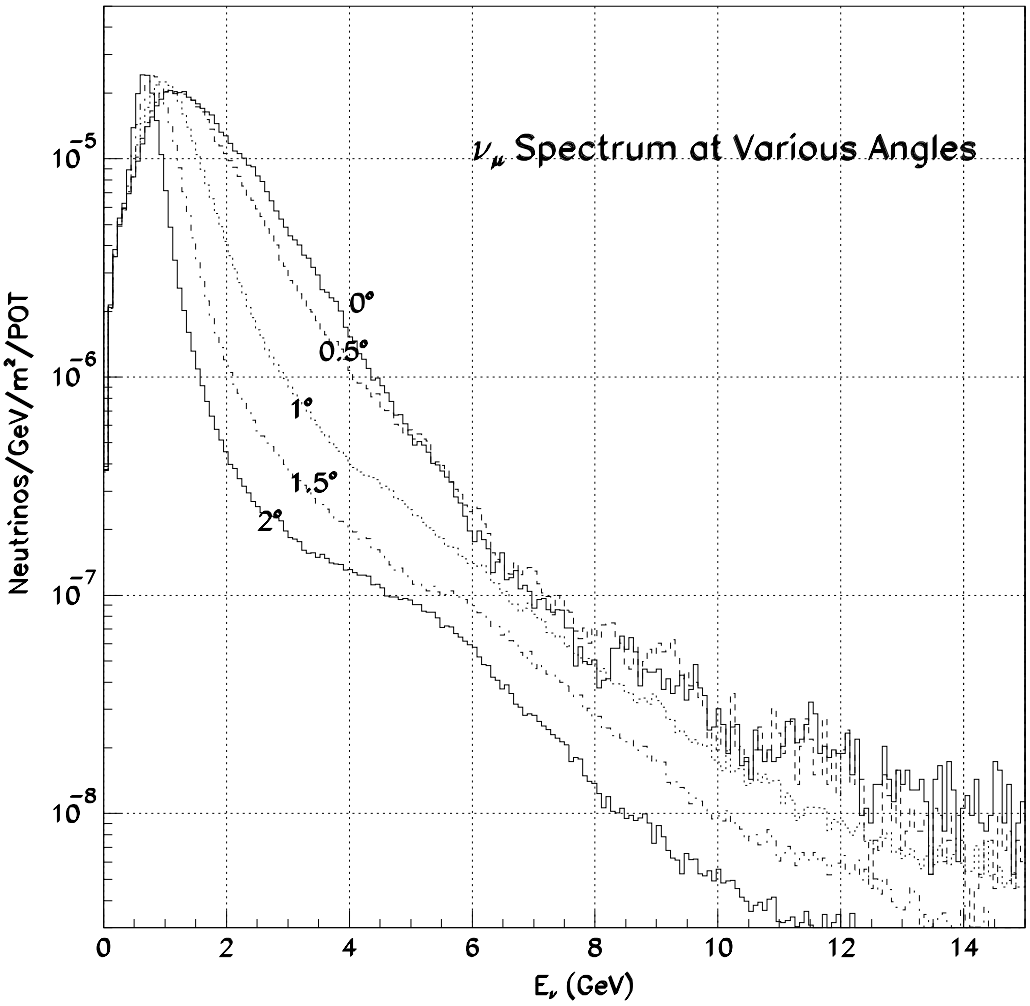

Figure 3: *Spectrum of neutrinos at 1 km at various angles with respect to the decay tunnel axis. The 1.5 degree spectrum was used for calculating the total event rates, however the event simulations in the detectors were performed using the full energy-angle correlation on an event by event basis.*

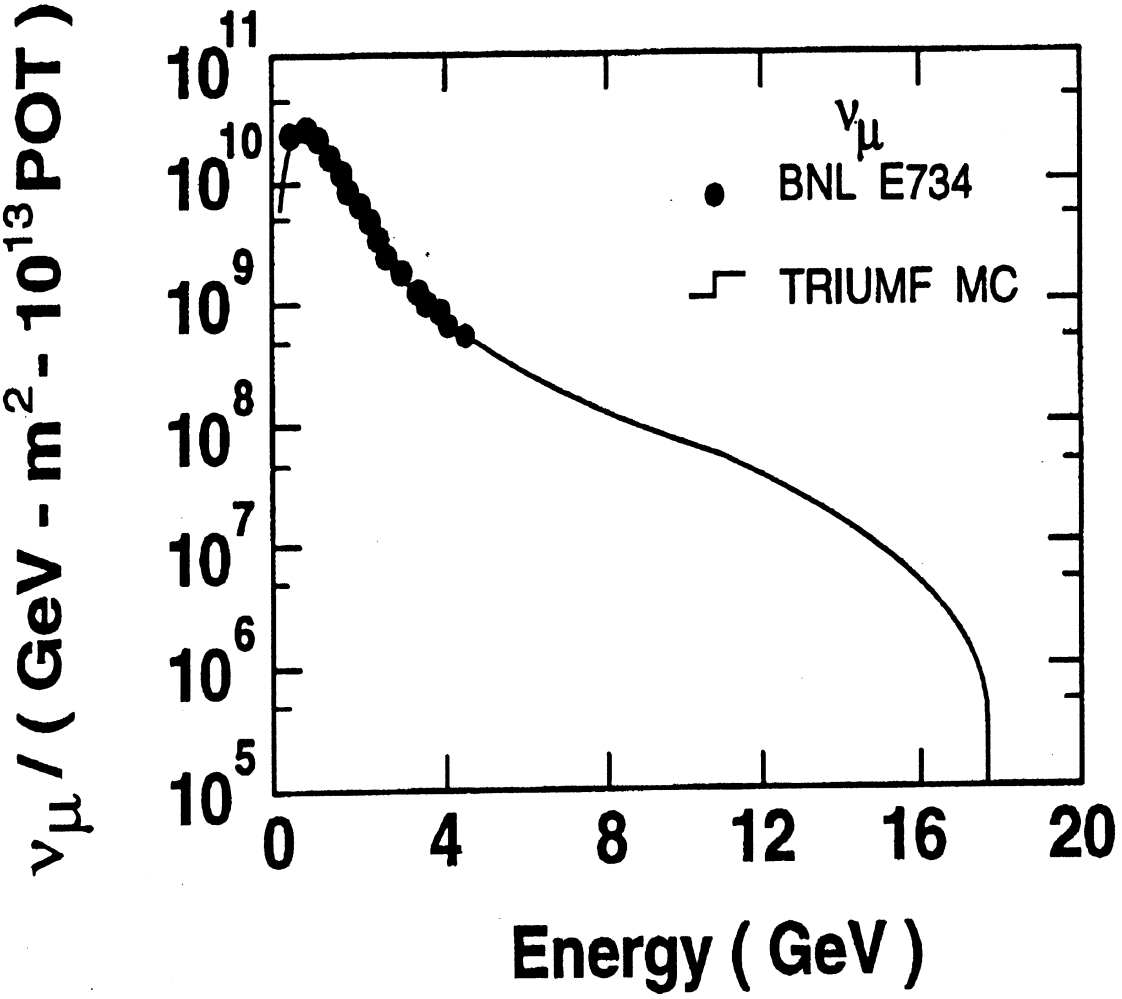

Figure 4: *Neutrino spectrum measured in E734 compared to the Monte Carlo calculation used for this proposal.*

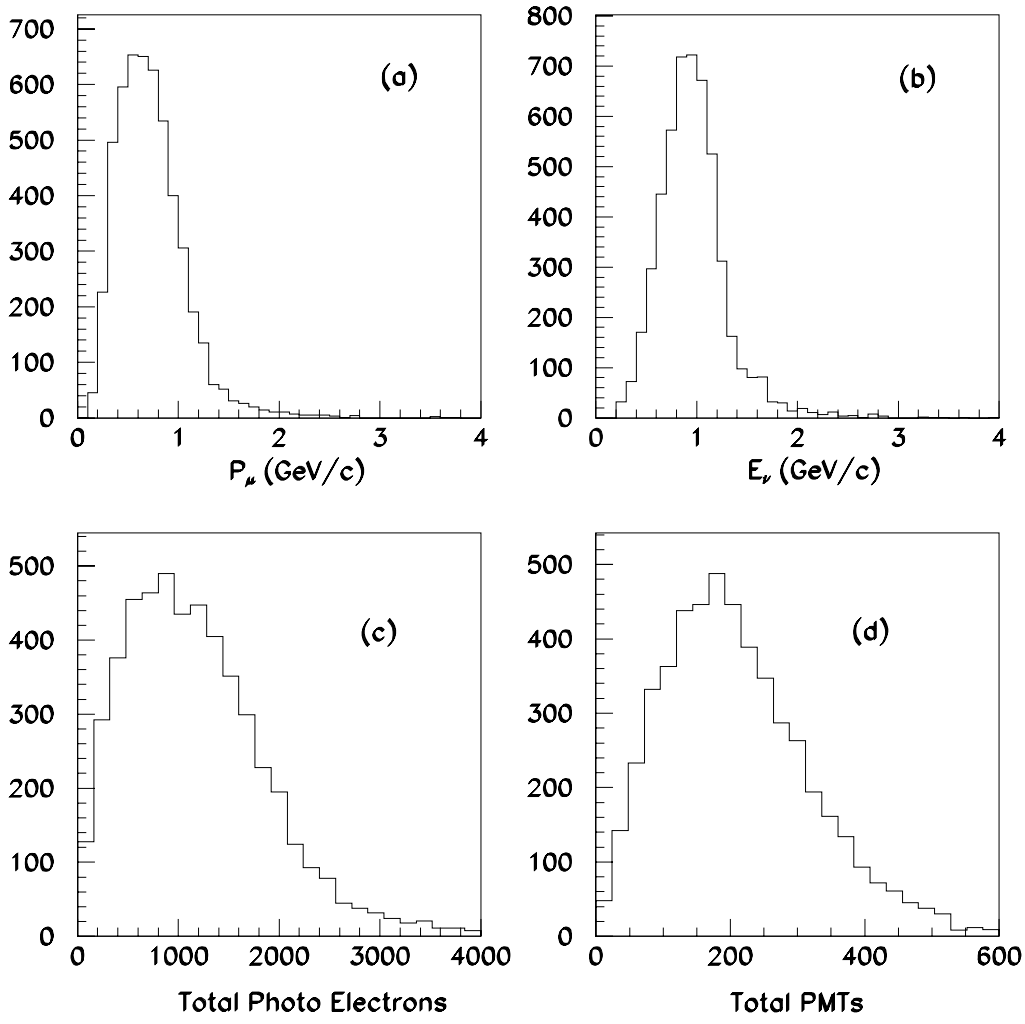

Figure 5: *Spectrum of contained muons (a) from quasielatic interactions of neutrinos with spectrum (b). The number of photoelectrons and the number of photomultipliers are also shown in (c) and (d), respectively. The simulation was for 5000 events with vertices in the fiducial volume and contained muons.*

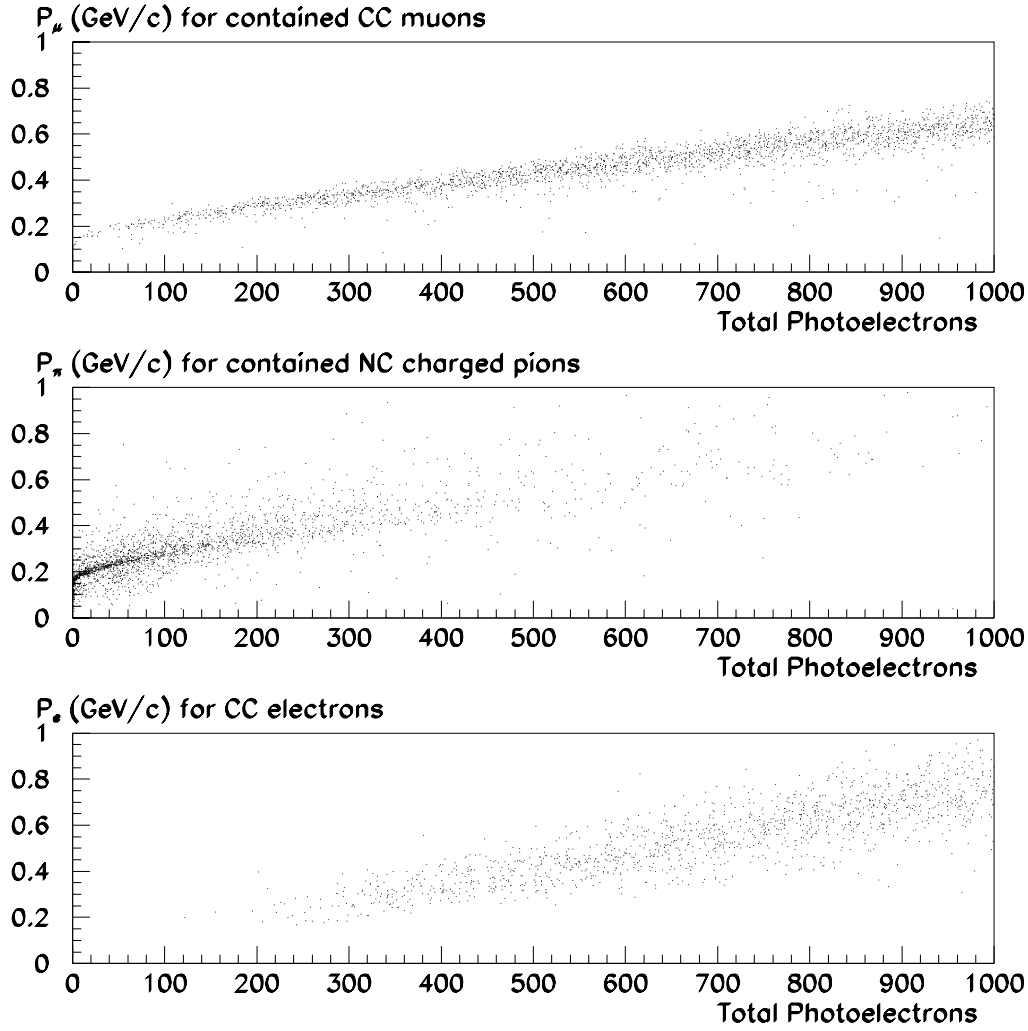

Figure 6: *The response in total number of photoelectrons of the water Cherenkov detector for muons, charged pions, and electrons as a function of momentum.*

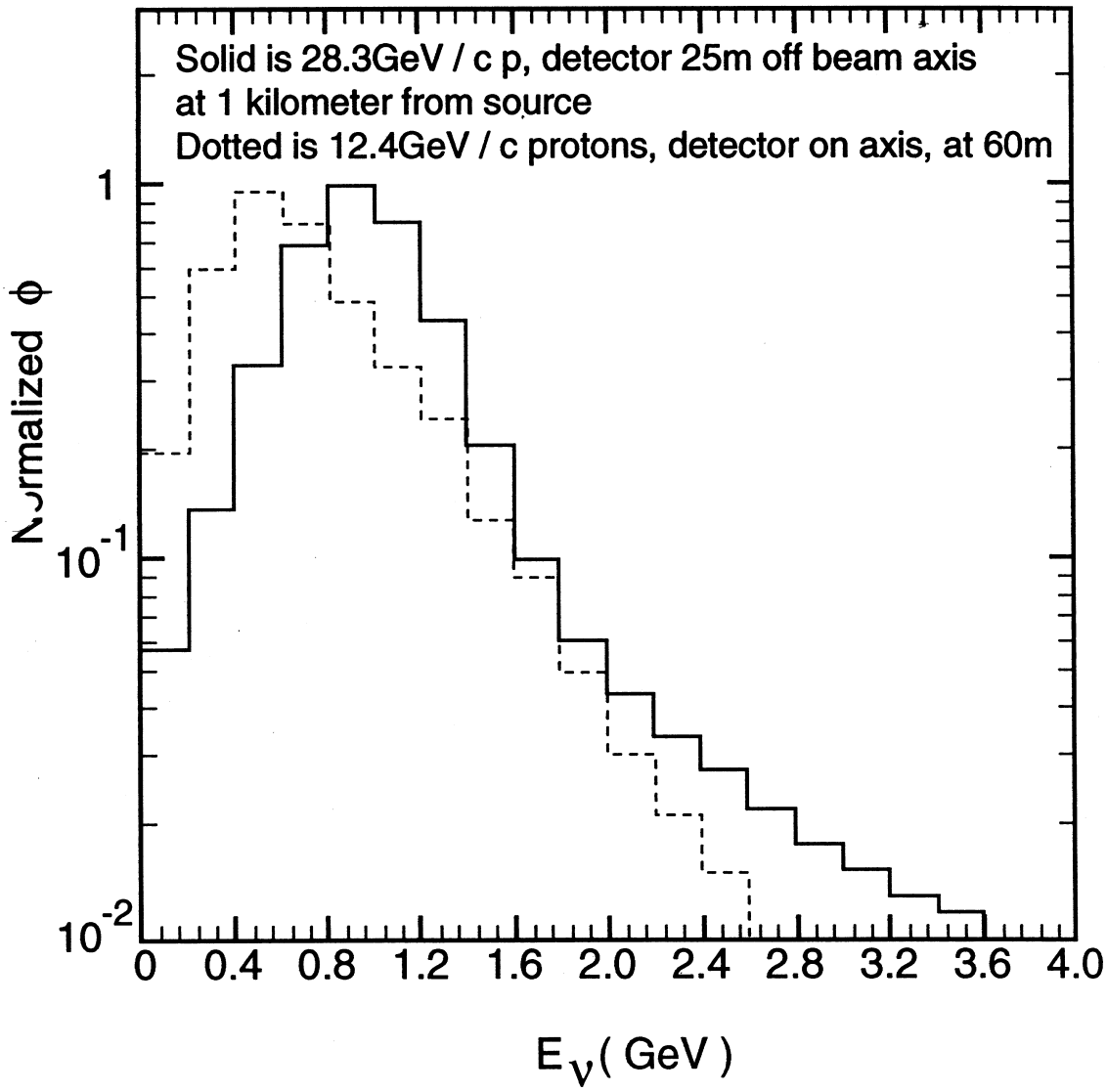

Figure 7: *Spectrum of neutrinos at the Argonne National Laboratory ZGS accelerator (dotted, 12.4 GeV) compared to the BNL-AGS neutrino spectrum (solid) at 1.5 degrees or 25 m off beam axis at 1 km.*

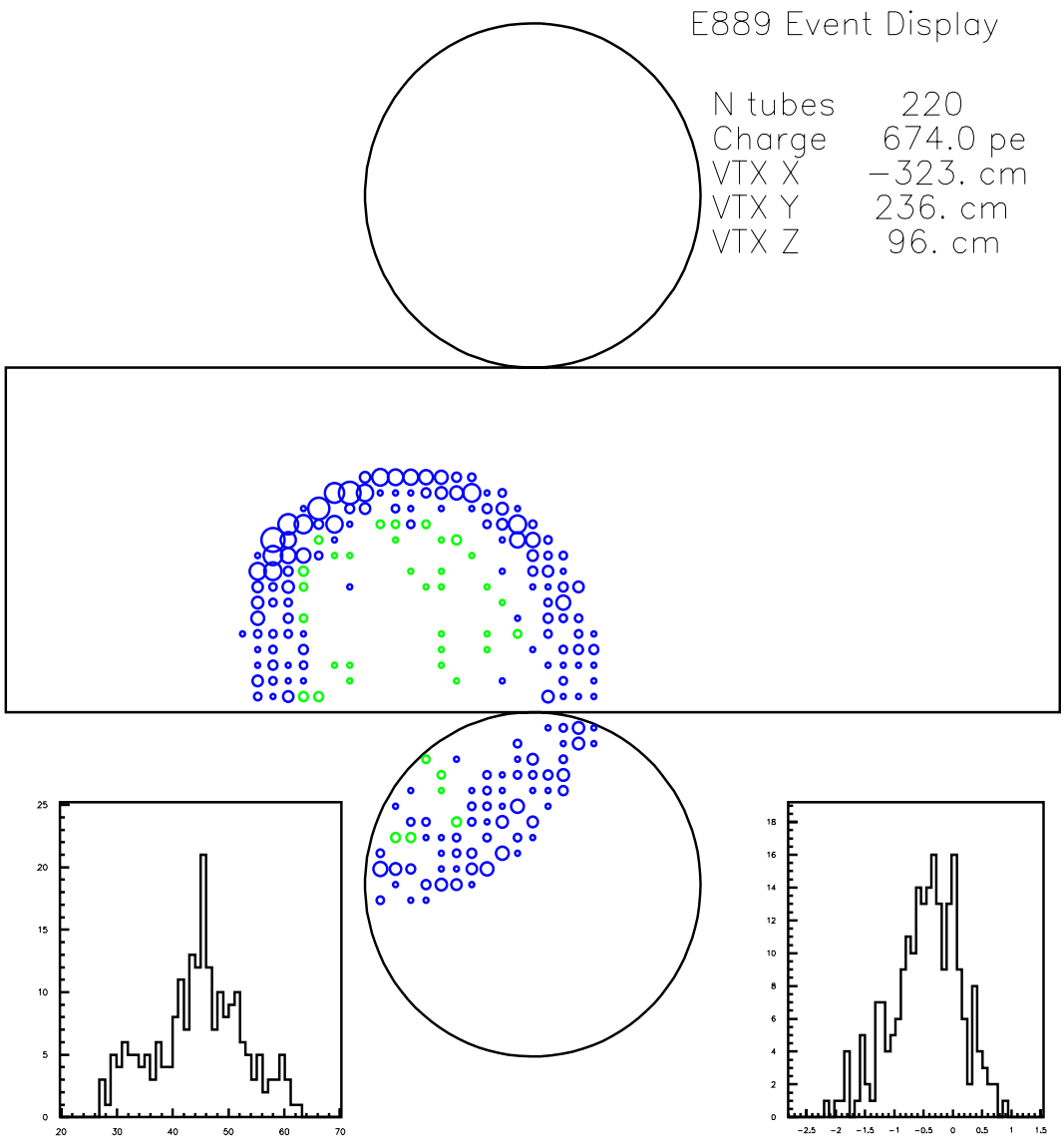

Figure 8: *Typical $QE(\mu^-)$ event in the fiducial volume. The size of the circles indicates the pulse-height in each PMT. The histogram on the left is of the raw time (ns) of the PMT hits with the event time set to 0. The histogram on the right is of the corrected time (ns) which is the raw time minus the flight time to the vertex.*

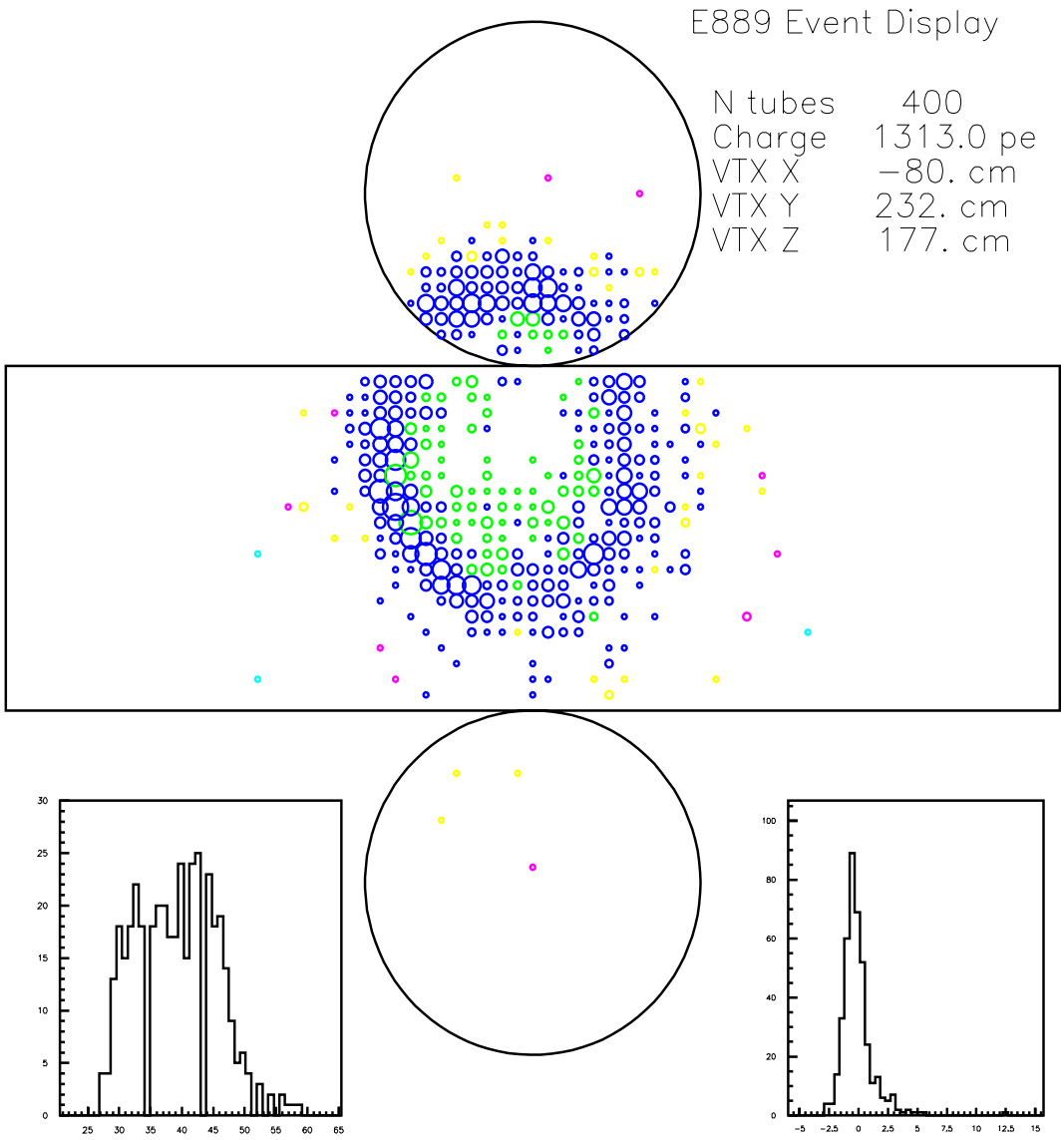

Figure 9: *Typical $QE(e)$ event in the fiducial volume. See the caption of Figure 8 for the description.*

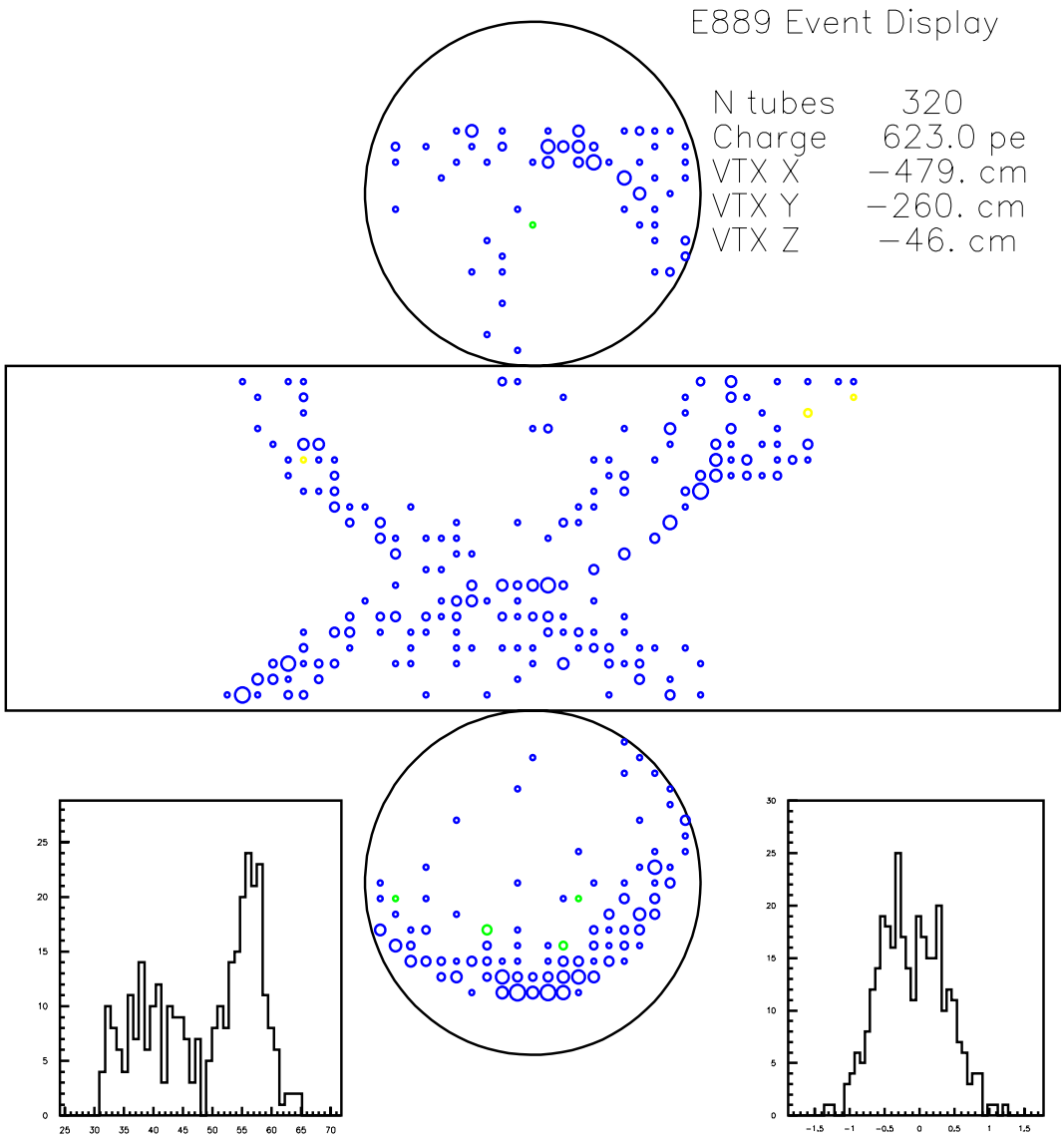

Figure 10: *Typical multi-ring pion event in the fiducial volume. See the caption of Figure 8 for the description.*

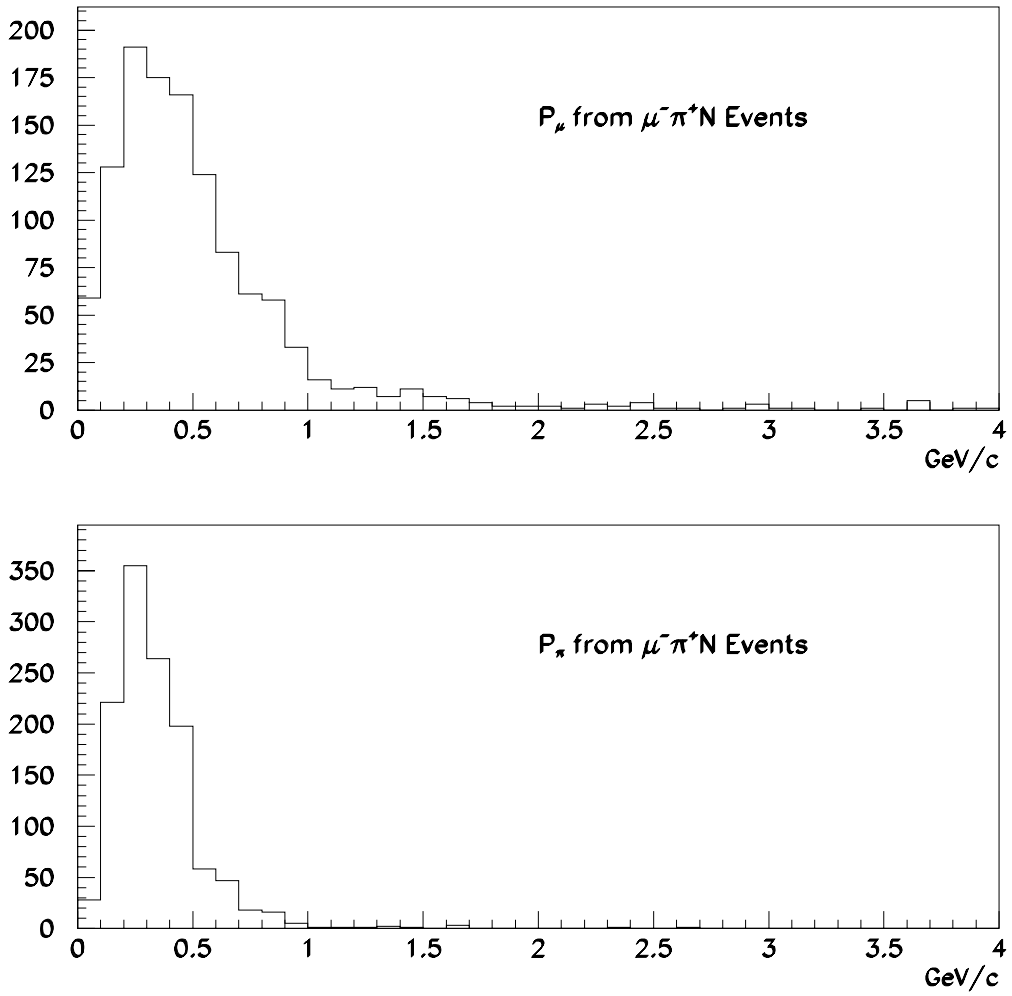

Figure 11: *Momentum distribution of muons (top) and pions (bottom) in charged current single pion production events.*

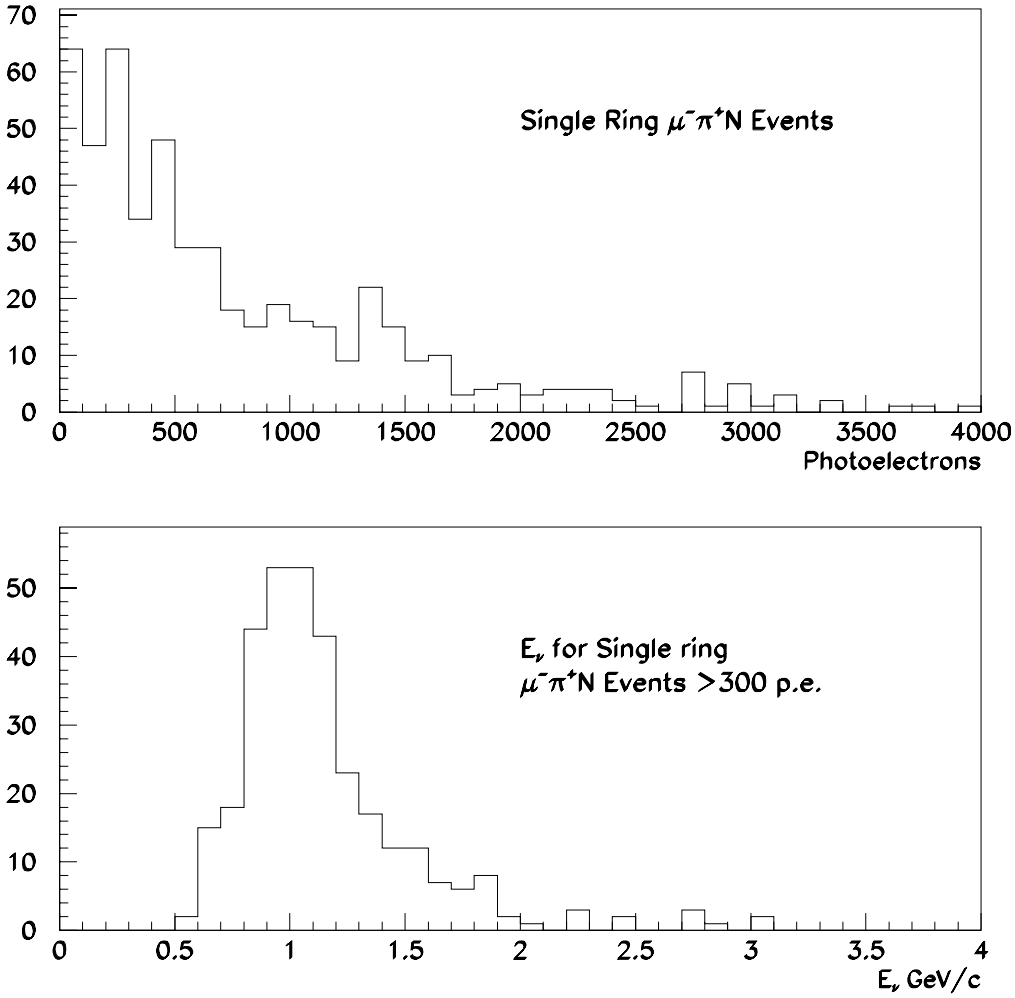

Figure 12: *Photoelectron distribution of single ring charged current single pion production events (top) and the spectrum of the neutrinos (bottom) that produce the events above 300 photoelectrons.*

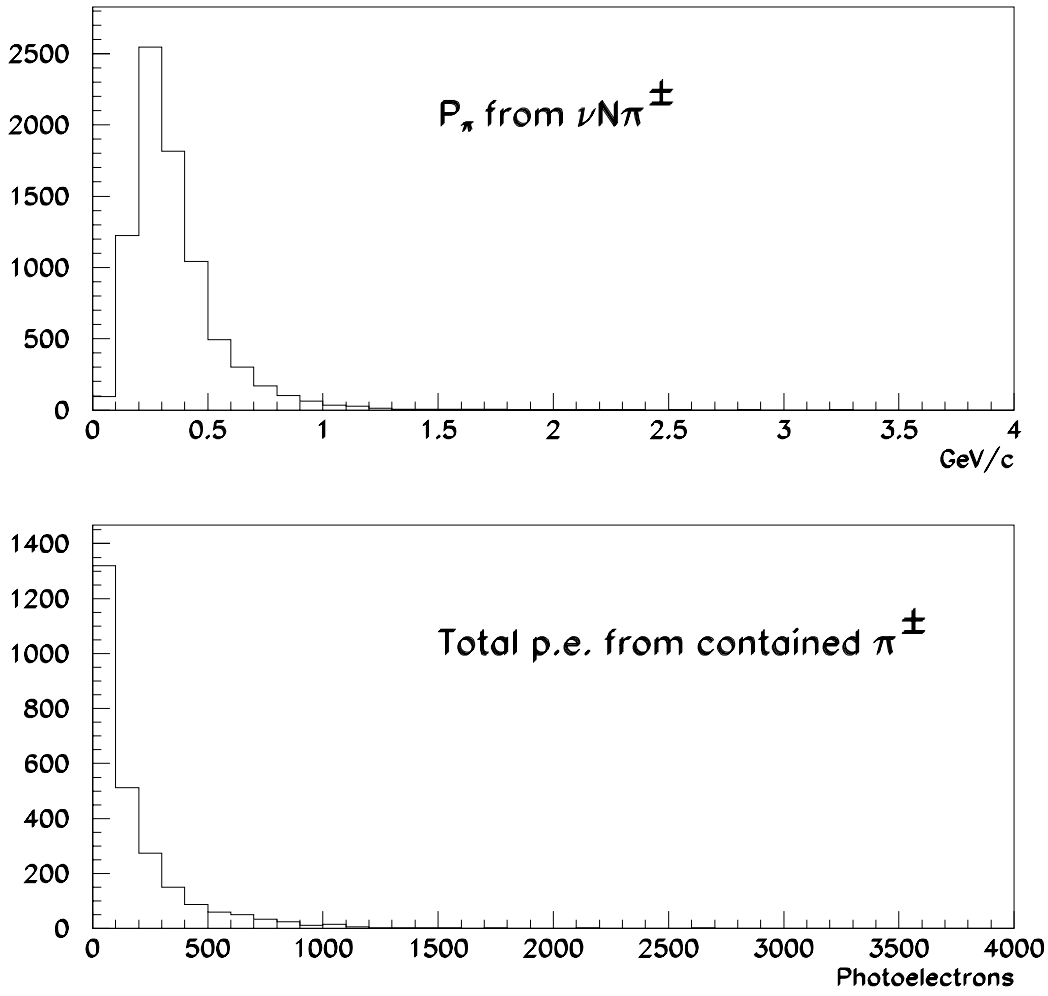

Figure 13: *Momentum and photoelectron spectrum of charged pions from neutral current single charged pion events.*

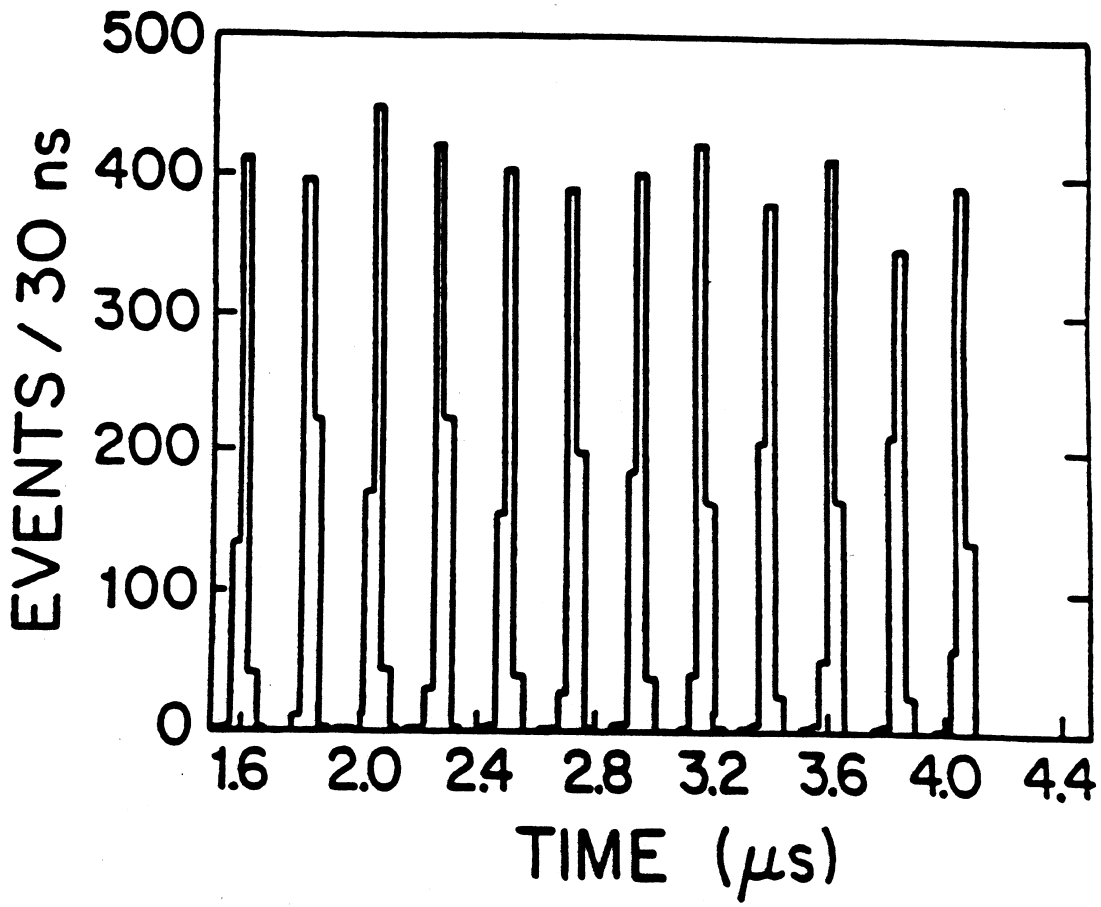

Figure 14: *The bucket structure of the AGS neutrino beam reconstructed in the E734 detector from neutrino events. The AGS beam for E734 had 12 buckets of 22 ns width and 220 ns apart.*

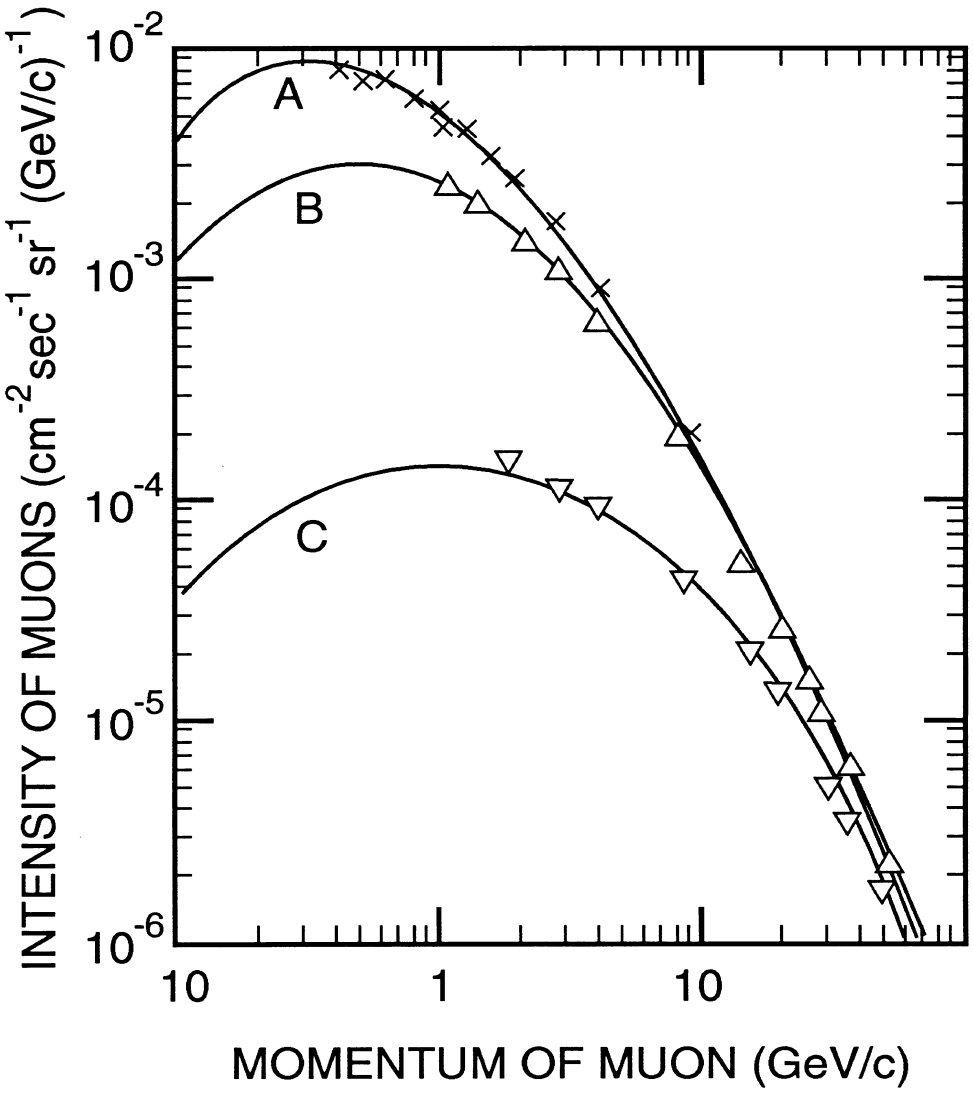

Figure 15: *The cosmic ray muon spectrum at sea level and at a mountain top from Ref. 10. (A) vertical flux at 3200 m, (B) vertical at sea level, (C) 68° at sea level.*

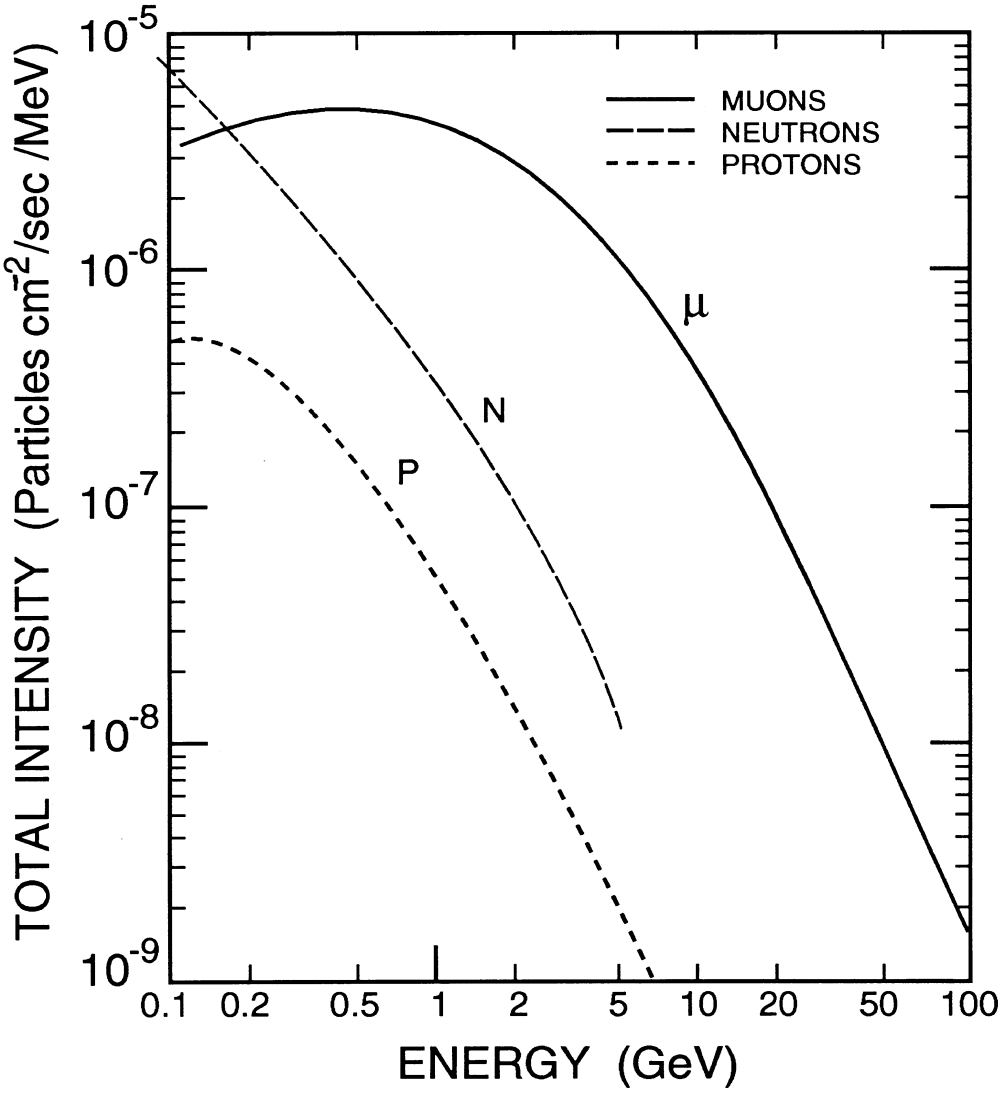

Figure 16: *The cosmic ray spectra for muons, neutrons, and protons from Ref. 7. Also see Ref. 8 and 9.*

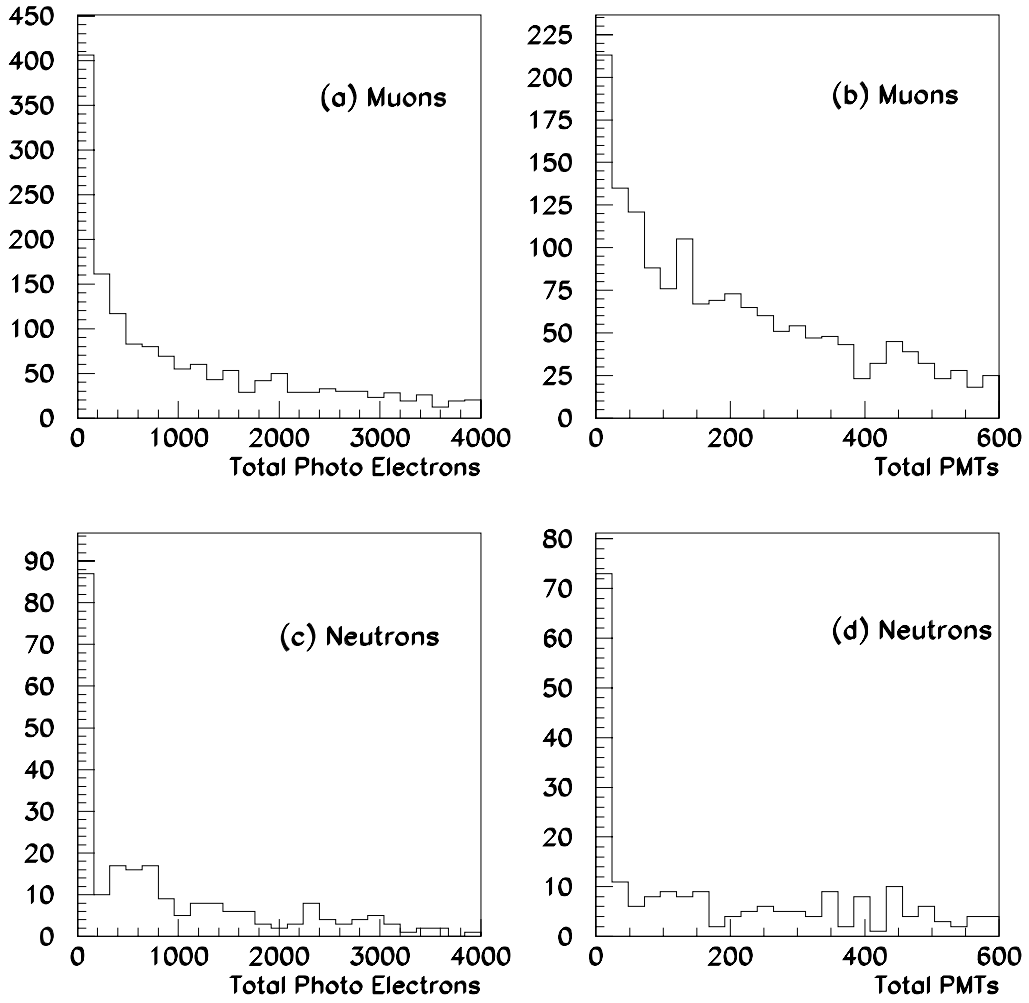

Figure 17: *The spectra of photoelectrons and the number of PMTs from cosmic ray muon and neutron events. Comparing to Figure 5, simple cuts on the pulse height should be very effective in removing large part of the background.*

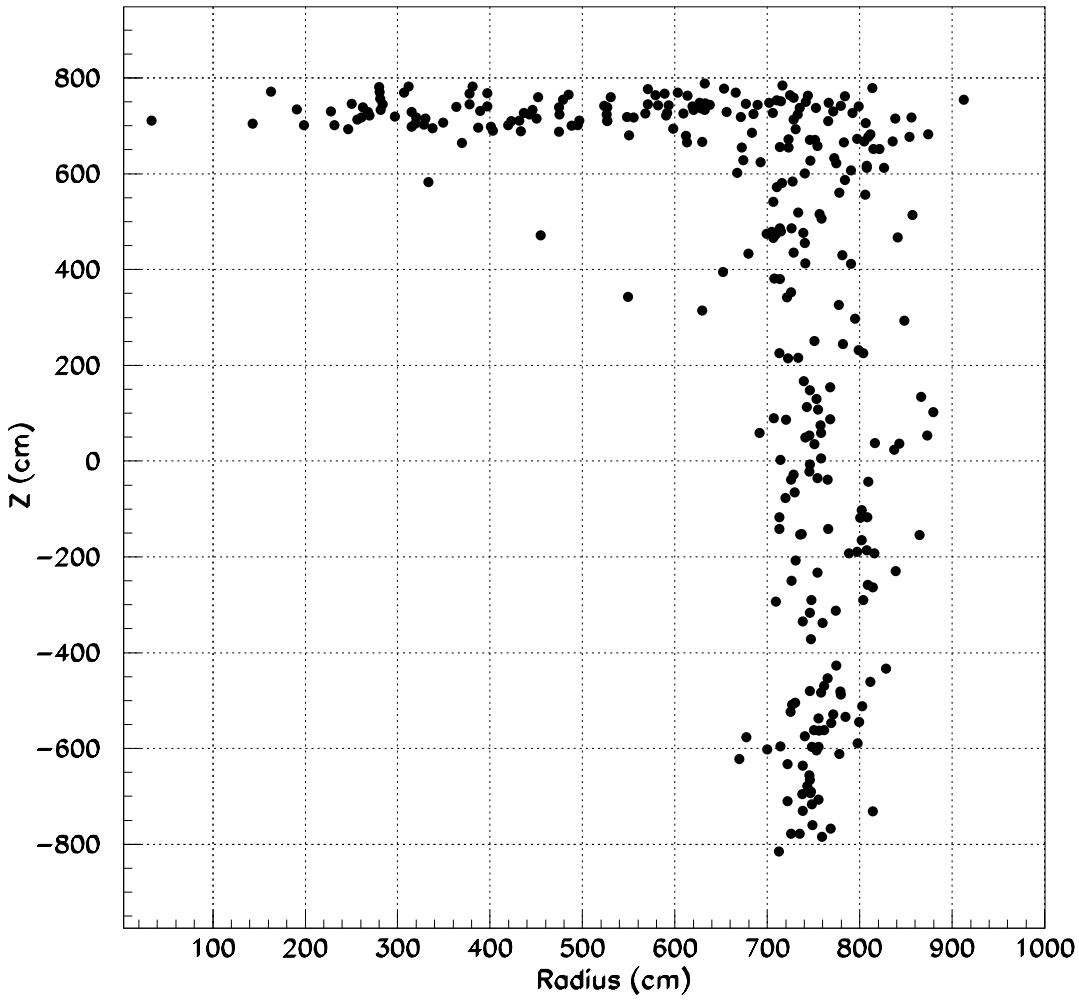

Figure 18: *The reconstructed vertex positions (radius versus Z, co-ordinate along the tank cylinder axis) of a cosmic ray muon entering the inner detector. The vertex resolution is different for the two orthogonal coordinates, in the direction of the muon and perpendicular to it.*

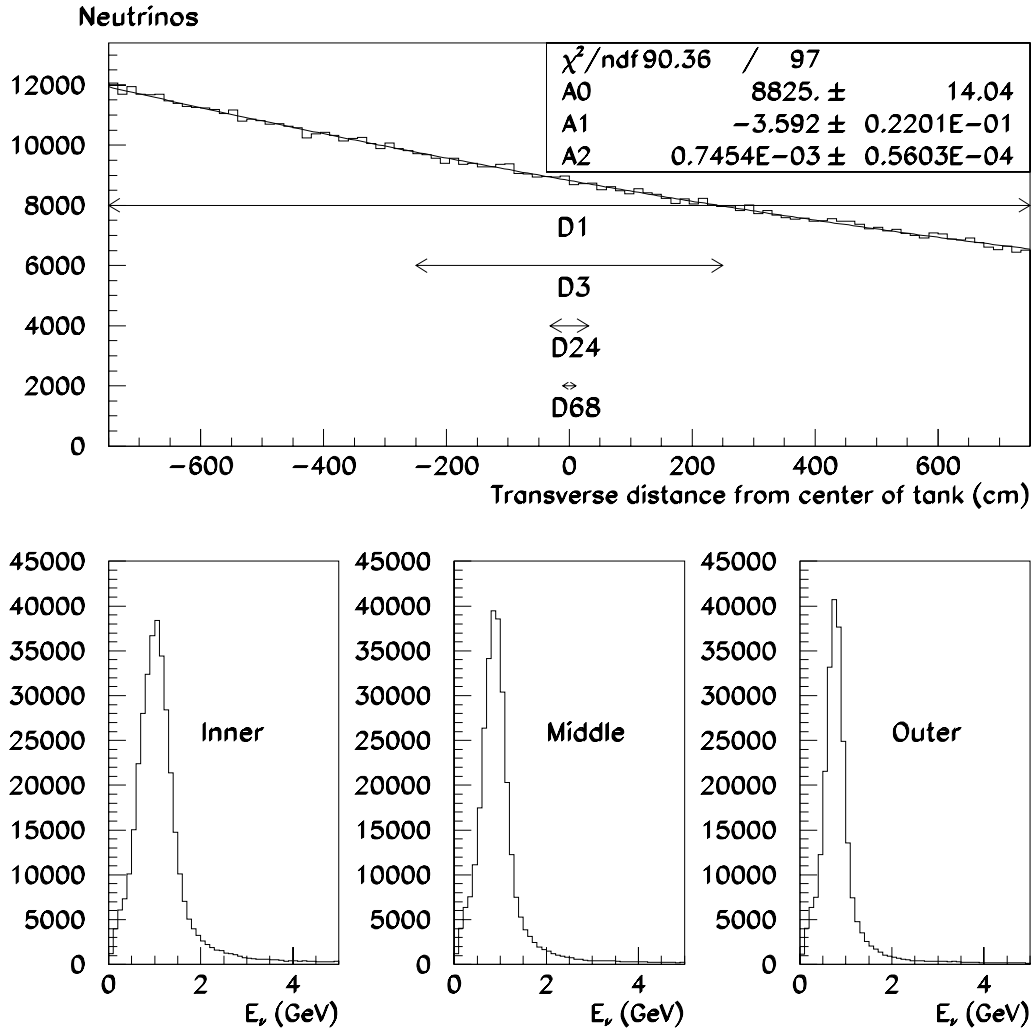

Figure 19: *Distribution of neutrinos incident on a flat square offset by* 1.5^o *from the beam axis. The fall of neutrino intensity is well fit by a function* $A_0 + A_1 x + A_2 x^2$ *where* x *is the distance transverse to the beam axis from the center of the tank. The neutrino spectra for the inner 1/3 (-7.5 m to -2.5 m), the middle 1/3 (*$\pm$*2.5 m), and the outer 1/3 (2.5 m to 7.5 m) are shown at the bottom.*

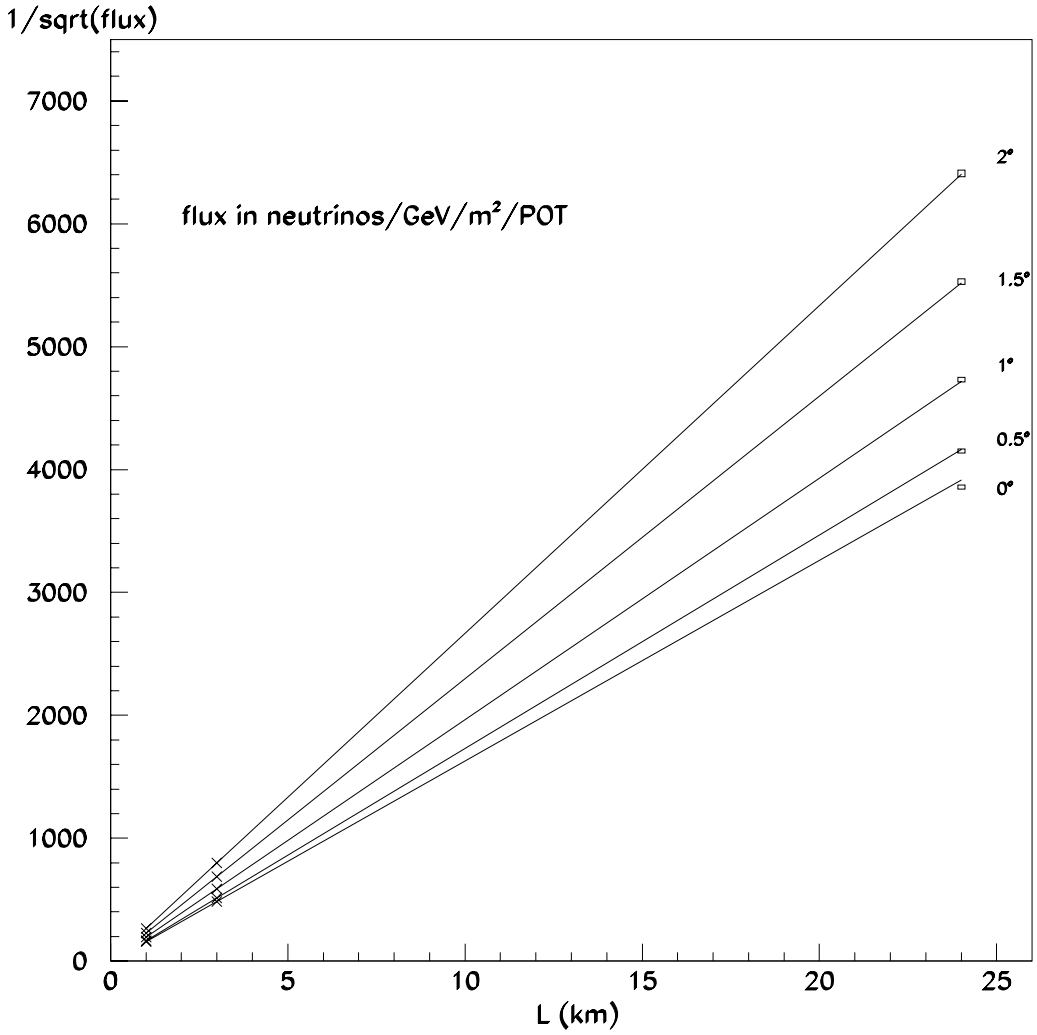

Figure 20: $1/\sqrt{flux}$ *versus distance from a GEANT Monte Carlo simulation. A line drawn through the points at 1 and 3 km predicts the flux at the 24 km site. The* $1/(r-r_0)^2$ *behavior does not depend on the angle, and it is better at 1.5 degrees than at 0 degrees. The Monte Carlo calculated flux at the 24 km is indicated by a box, the vertical size is the statistical error achieved after 16 months of running E889. The results are similar for the 68 km site.*

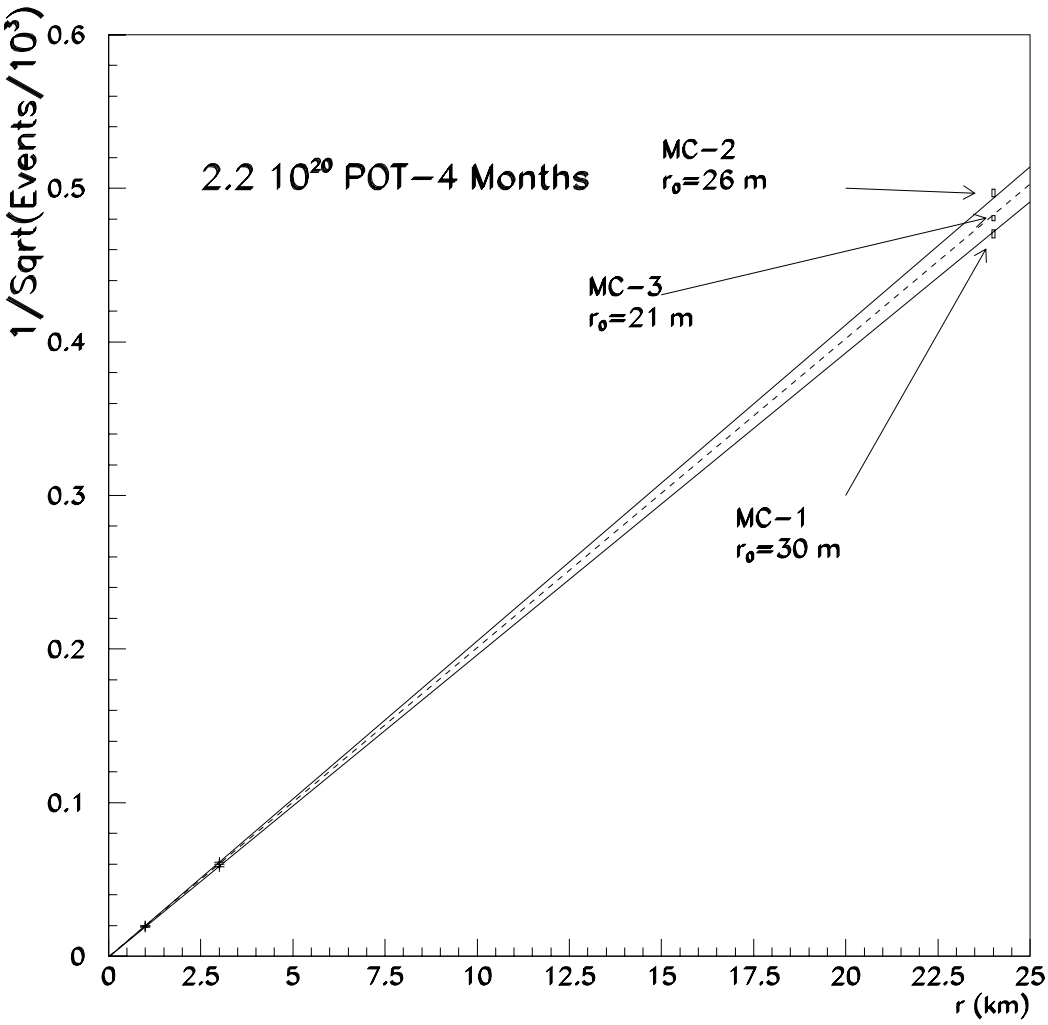

Figure 21: *The count rates of quasi-elastic muon events in 4 months, displaying the* $1/(r - r_0)^2$ *law. Though Monte Carlo variations alter both the overall normalization and* r_0*, the* $1/(r - r_0)^2$ *behavior does not change. The effects of path-length and cross section in the detectors are included using three different Monte Carlo calculations (Table 6). The Monte Carlo statistical error is shown as a box at 24 km. The 68 km results are similar.*

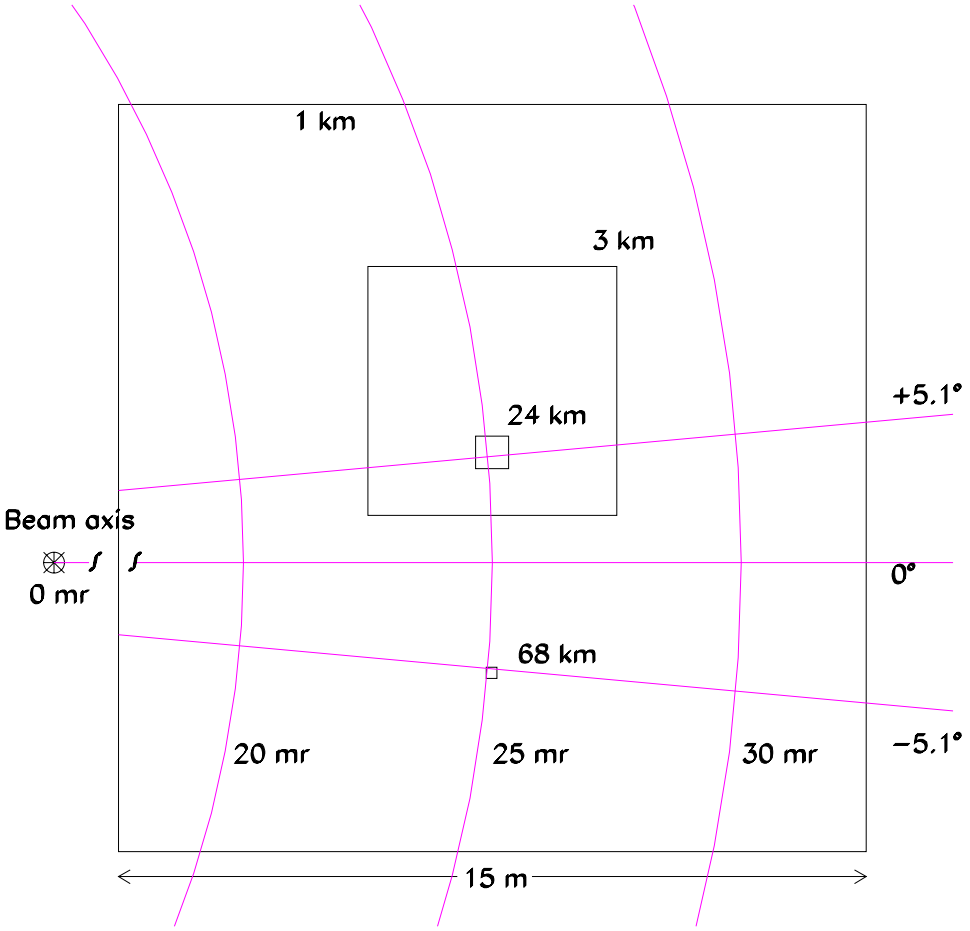

Figure 22: *The detectors as viewed from the production target in polar (in mr) and azimuthal (in degrees) angle with respect to the beam axis. The largest square is the area of D1, the smaller square is the area and location of D3, etc. The beam axis is oriented so that both Northville and Plum Island locations are at the same polar angle, but separated only by* 10.2^o *in azimuth. All detectors and the beam are assumed to be on the ground except for the 1 km detector, D1, which is below current ground level by 4 m.*

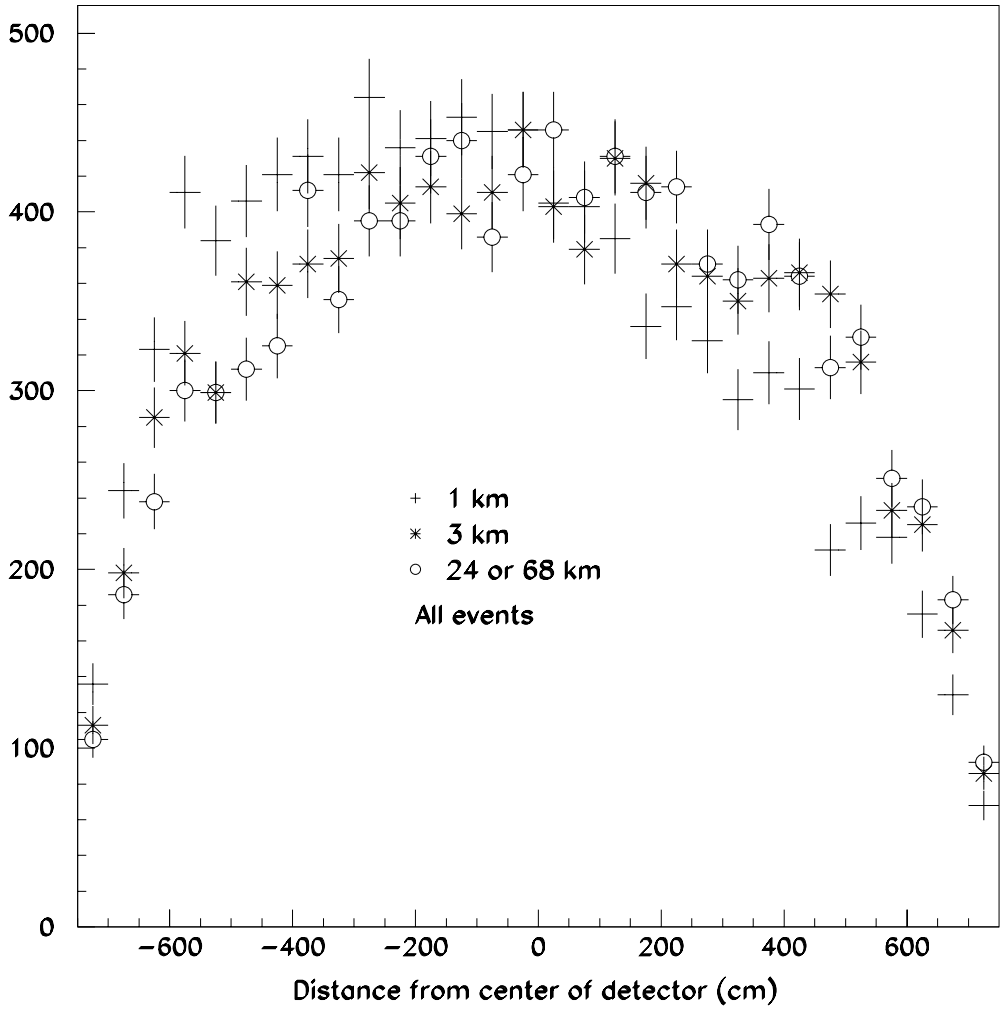

Figure 23: *Distribution of the quasi-elastic event vertices inside the entire inner volume of cylindrical tanks located at 1, 3, 24, and 68 km. The same number of events were generated for all detectors. The statistical errors on the simulation are also shown.*

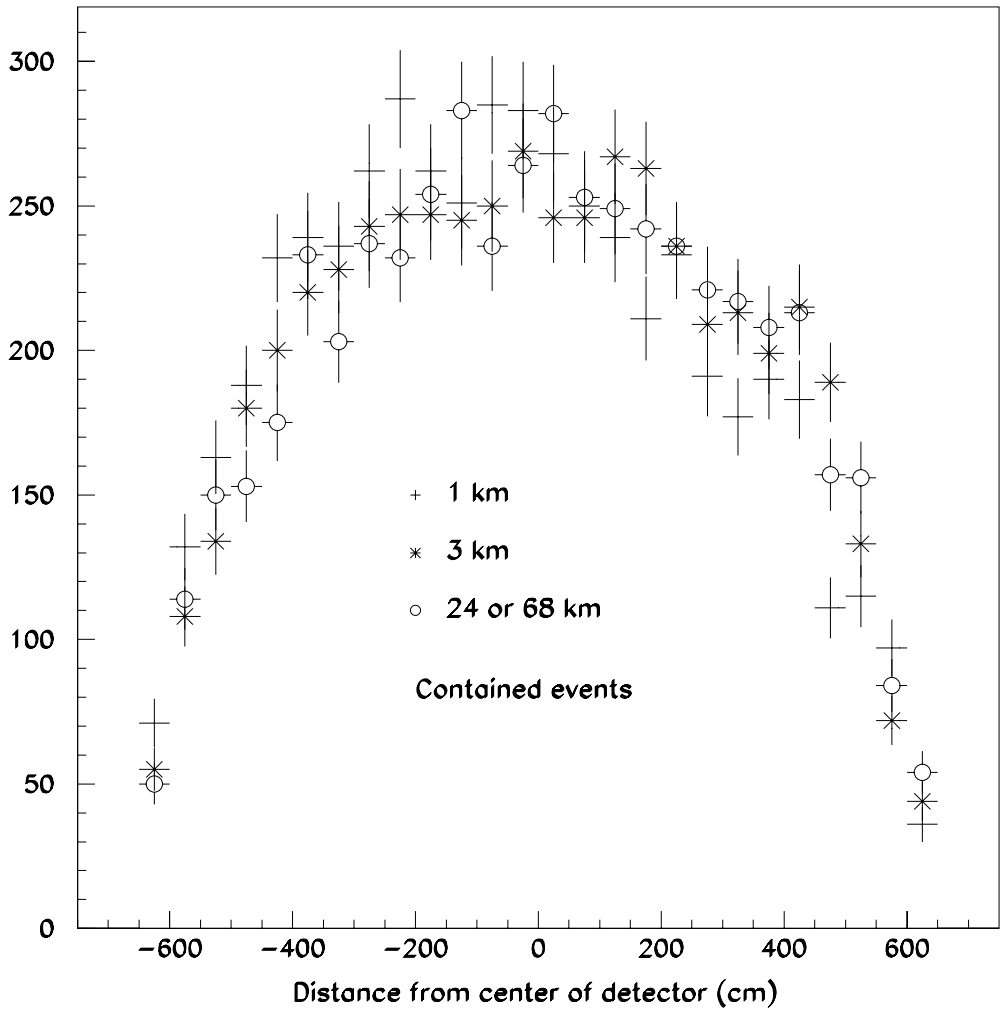

Figure 24: *Distribution of the contained quasi-elastic event vertices inside the fiducial volume of cylindrical tanks located at 1, 3, 24, and 68 km. The fiducial and containment cuts were applied to the events shown in Figure 23.*

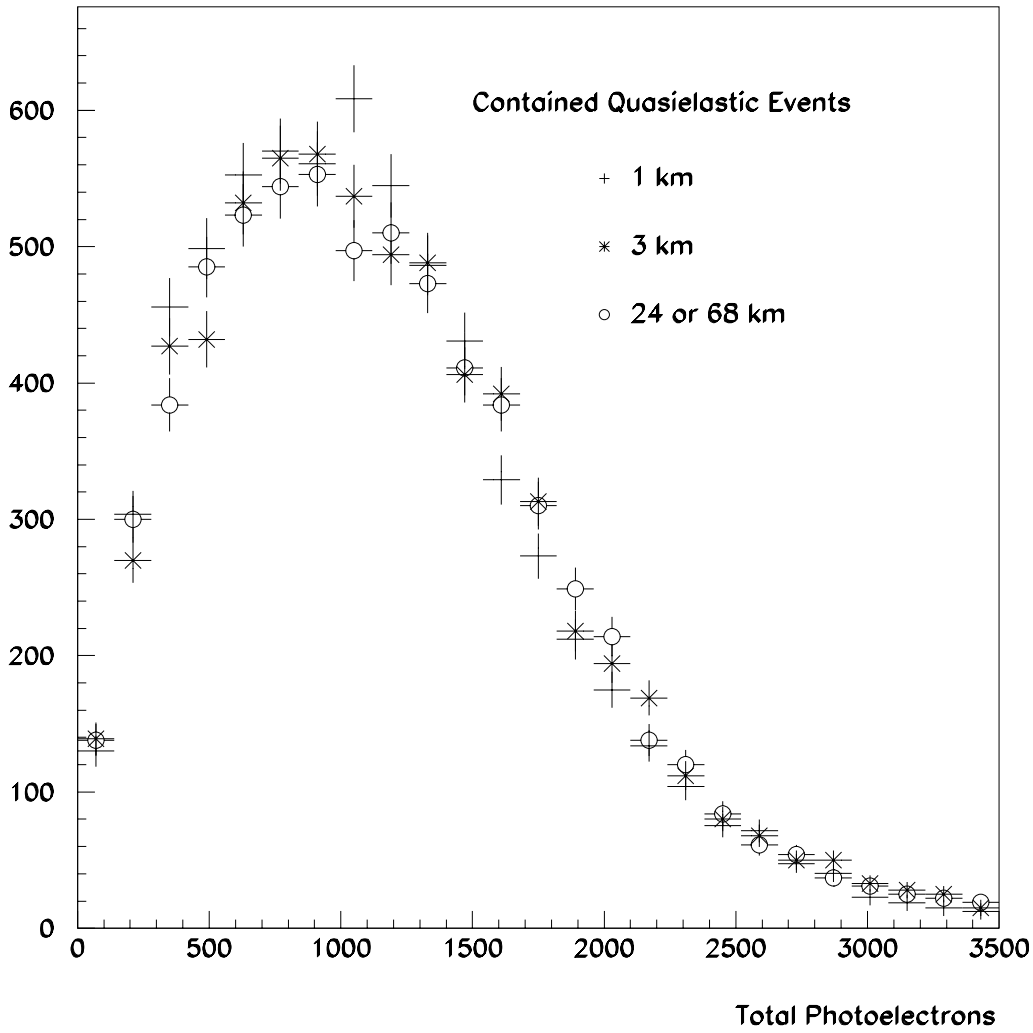

Figure 25: *Photoelectron spectrum of quasi-elastic events with the fiducial and containment cuts. The same number of events were generated for each detector location. The error bars are from Monte Carlo statistics. 750 photoelectrons corresponds to about 550 MeV/c muon momentum.*

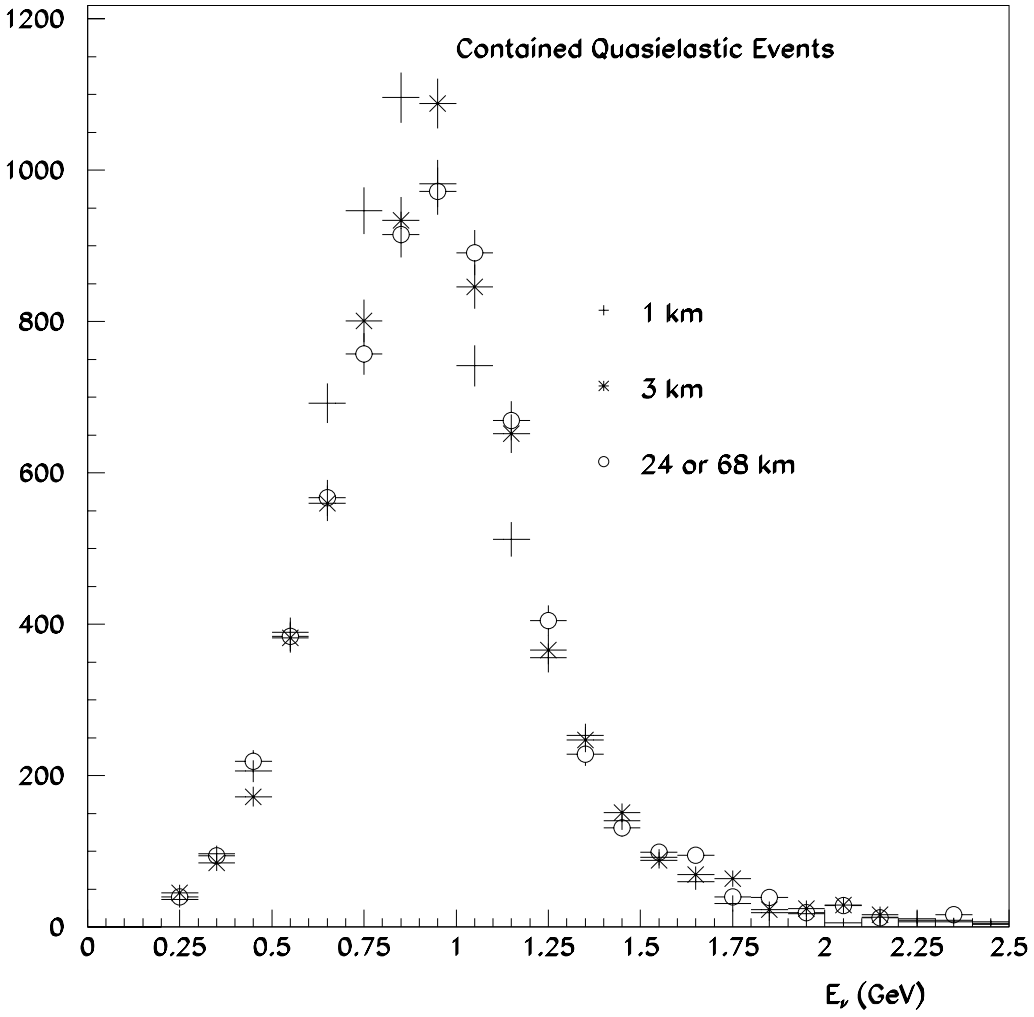

Figure 26: *Spectrum of neutrinos that produce quasi-elastic events in Figure 25. The same number of events were generated for each detector location. The error bars are from Monte Carlo statistics.*

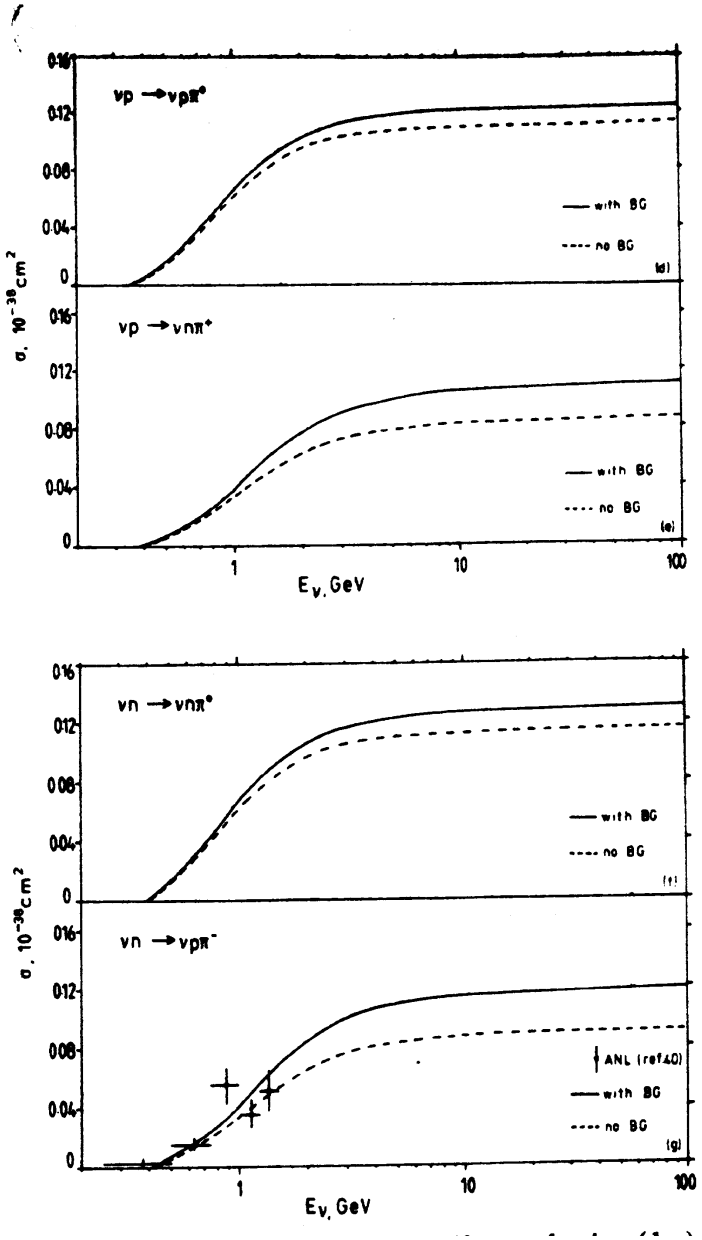

Figure 27: *Cross sections for various neutral current pion production channels from Ref. 5. Calculations are for a pure resonant model (dashed) and a model with both resonant and incoherent nonresonant production (solid).* $m_A = 0.95\ GeV/c^2$ *and* $\sin^2\theta_W = 0.22$ *for these calculations.*

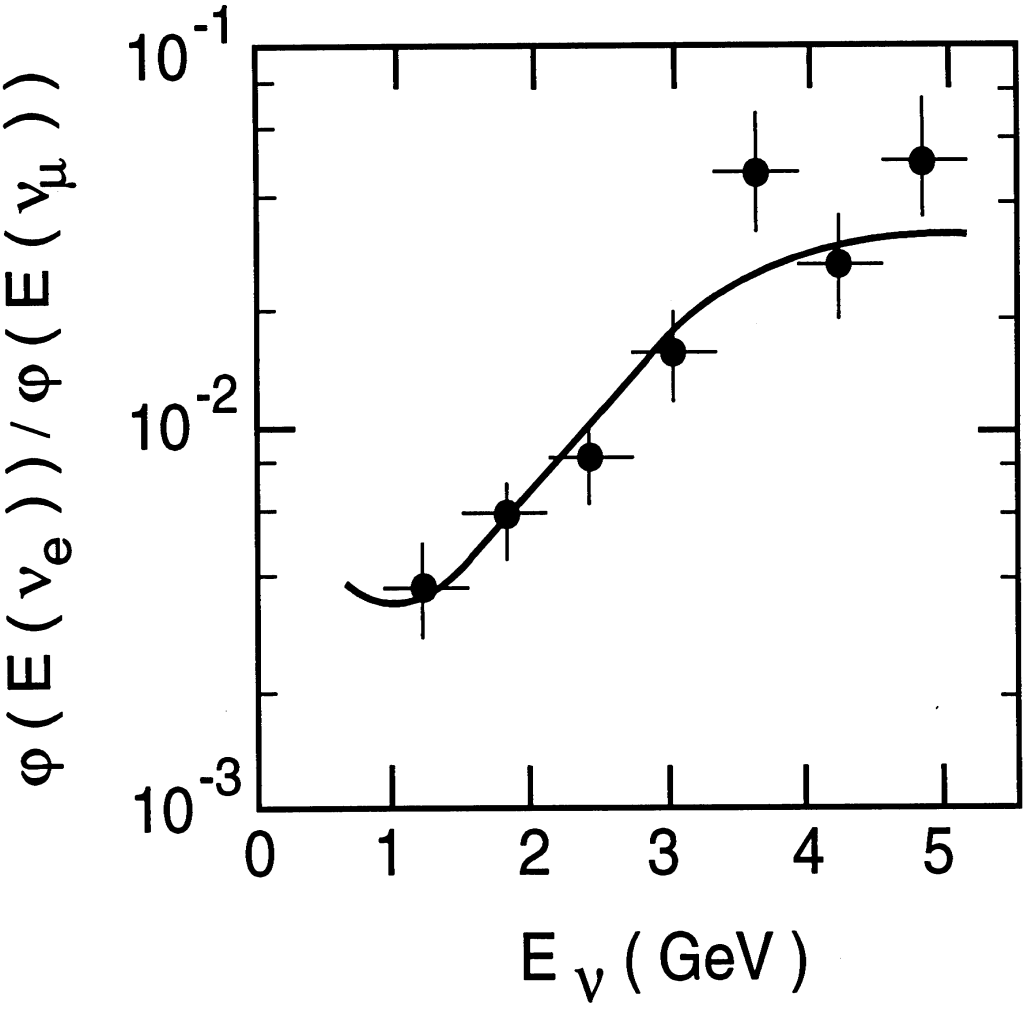

Figure 28: *Measurement of the ratio* $\frac{\Phi(\nu_e)}{\Phi(\nu_\mu)}$ *as a function of energy in experiment BNL-E734.*

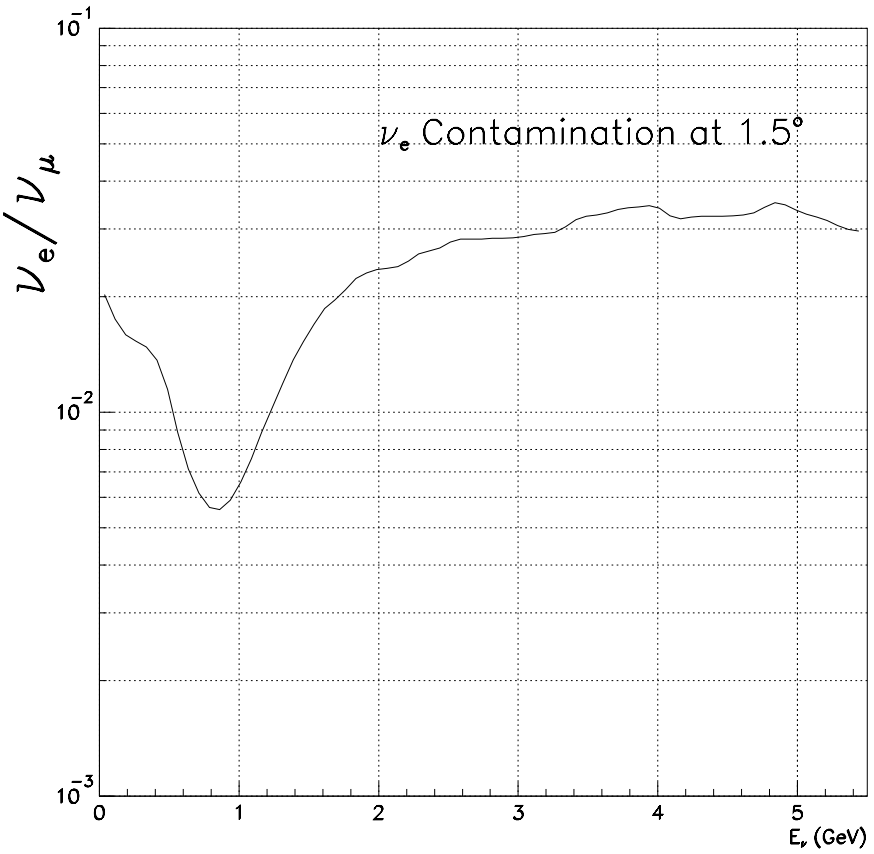

Figure 29: *Calculation of the ratio* $\frac{\Phi(\nu_e)}{\Phi(\nu_\mu)}$ *as a function of energy at* 1.5^o *from the beam axis.*

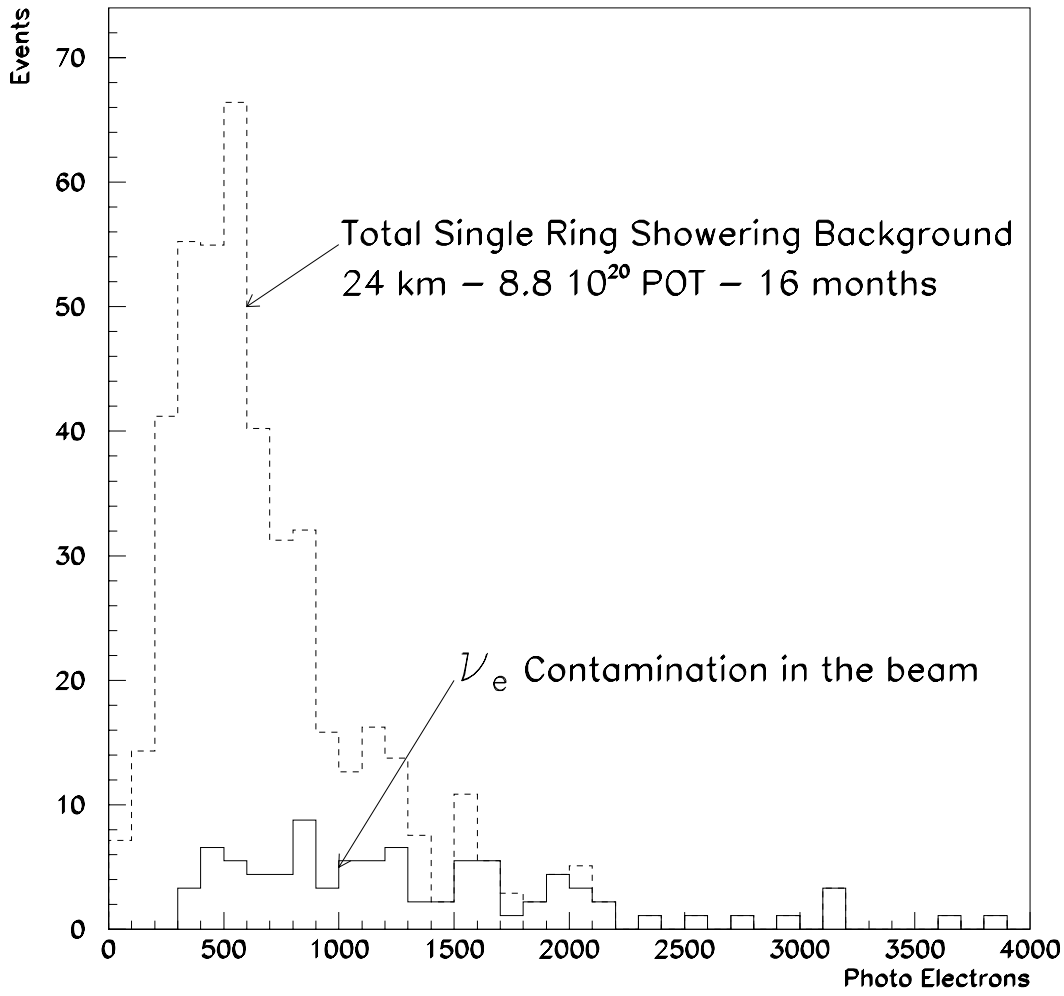

Figure 30: *The expected photoelectron spectrum from background single ring showering events at detector D24 after* 8.8×10^{20} *POT or 16 months of running. The spectrum will be the same at D68, but the number of events will be about 1/8. The solid distribution is from the* ν_e *component in the beam and total (dashed) includes misidentified* π^0*s from neutral current events. The fraction of events due to* ν_e*'s is 1/4, but about 20% are above 4000 photoelectrons.*

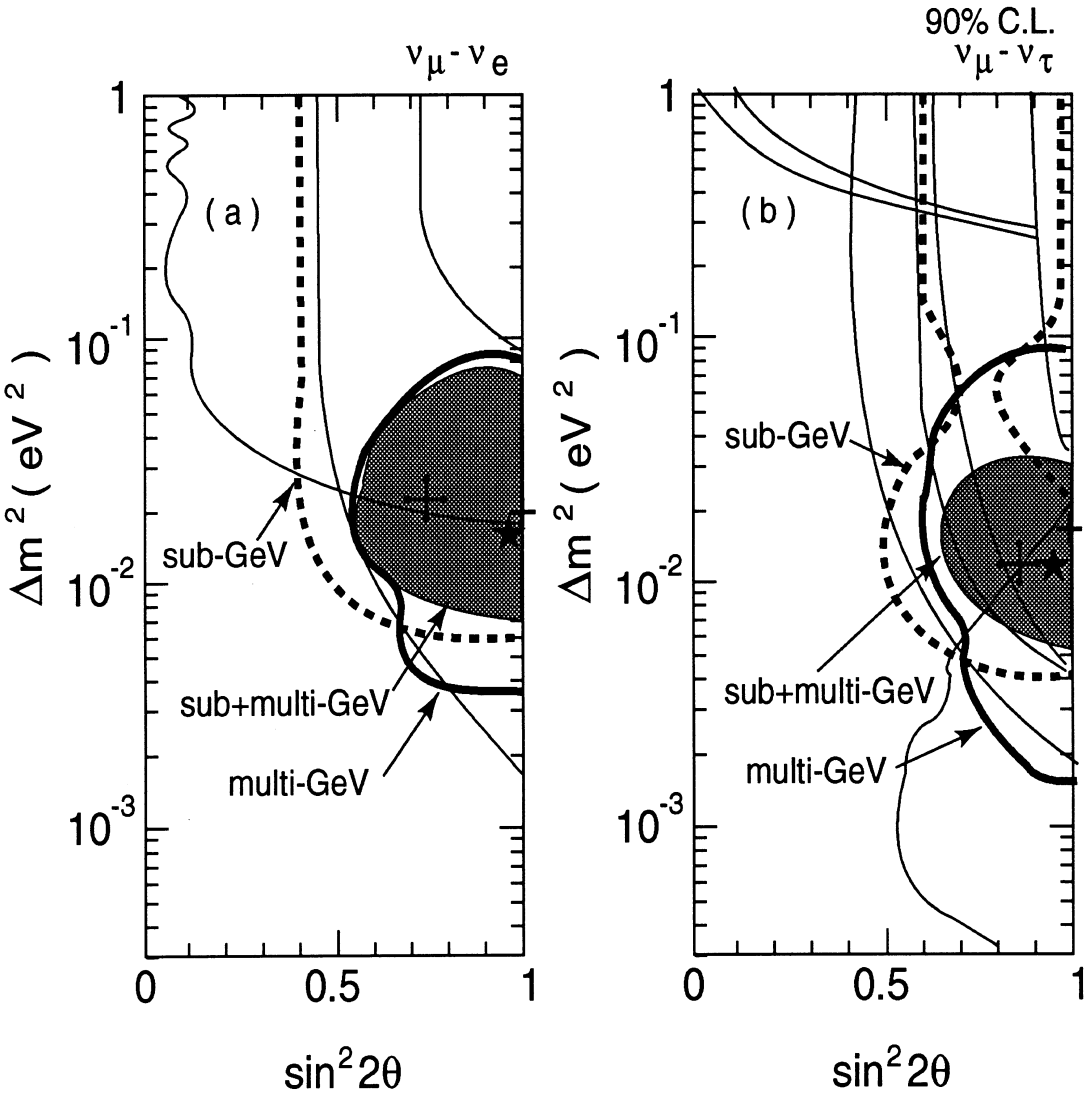

Figure 31: *Allowed region in* Δm^2 *and* $\sin^2(2\theta)$ *from the atmospheric neutrino results in Kamioka from Ref. 15.*

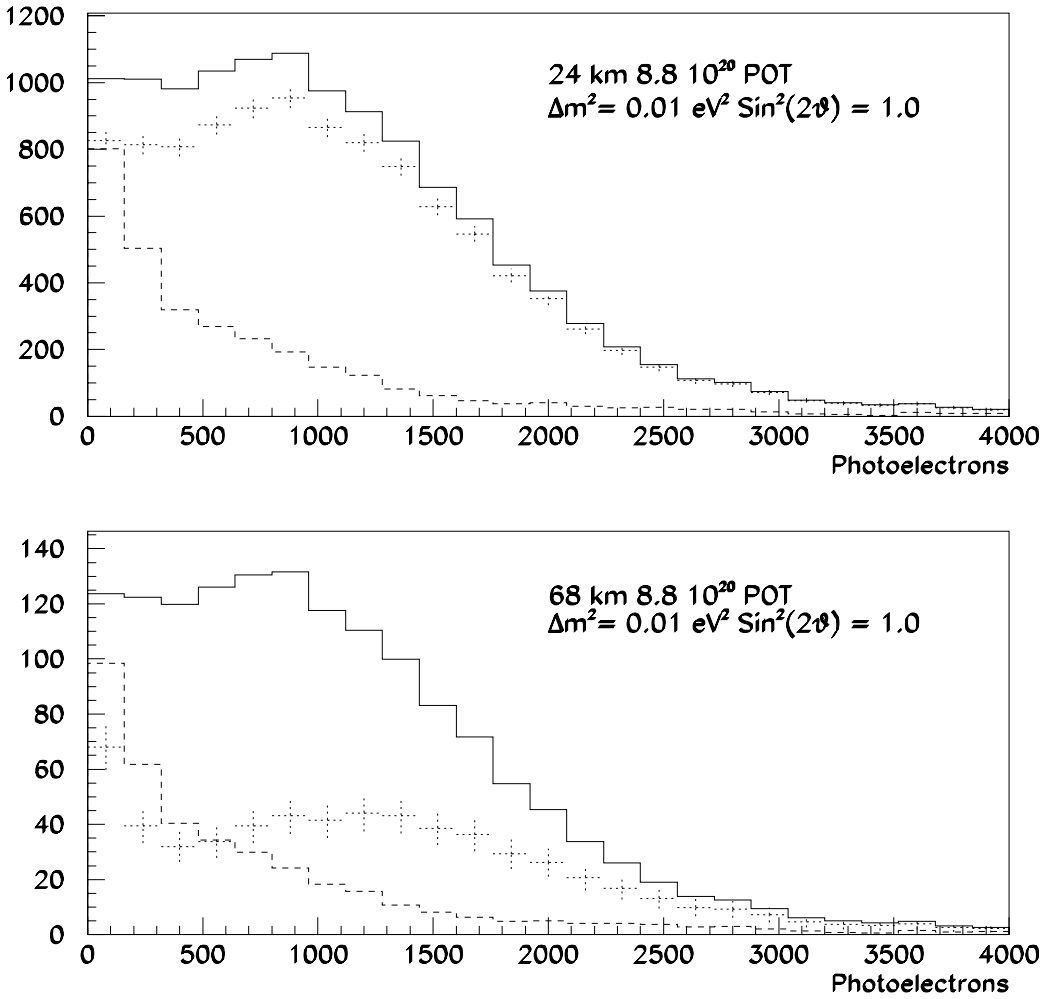

Figure 32: *Top: Spectrum of single ring muon like events in units of the number of total photoelectrons without (the solid histogram) and with (error bars) oscillations* ($\Delta m^2 = 0.01\ eV^2$, $\sin^2(2\theta) = 1.0$) *at the 24 km site. Bottom: Same at the 68 km site. The shape and normalization of the spectrum without oscillations will be predicted from measurements in D1 and D3. The systematic errors on this prediction is included in the error bars. The background from all sources for no oscillations is shown as the dashed histogram. The running time is for* 8.8×10^{20} *POT or 16 months.*

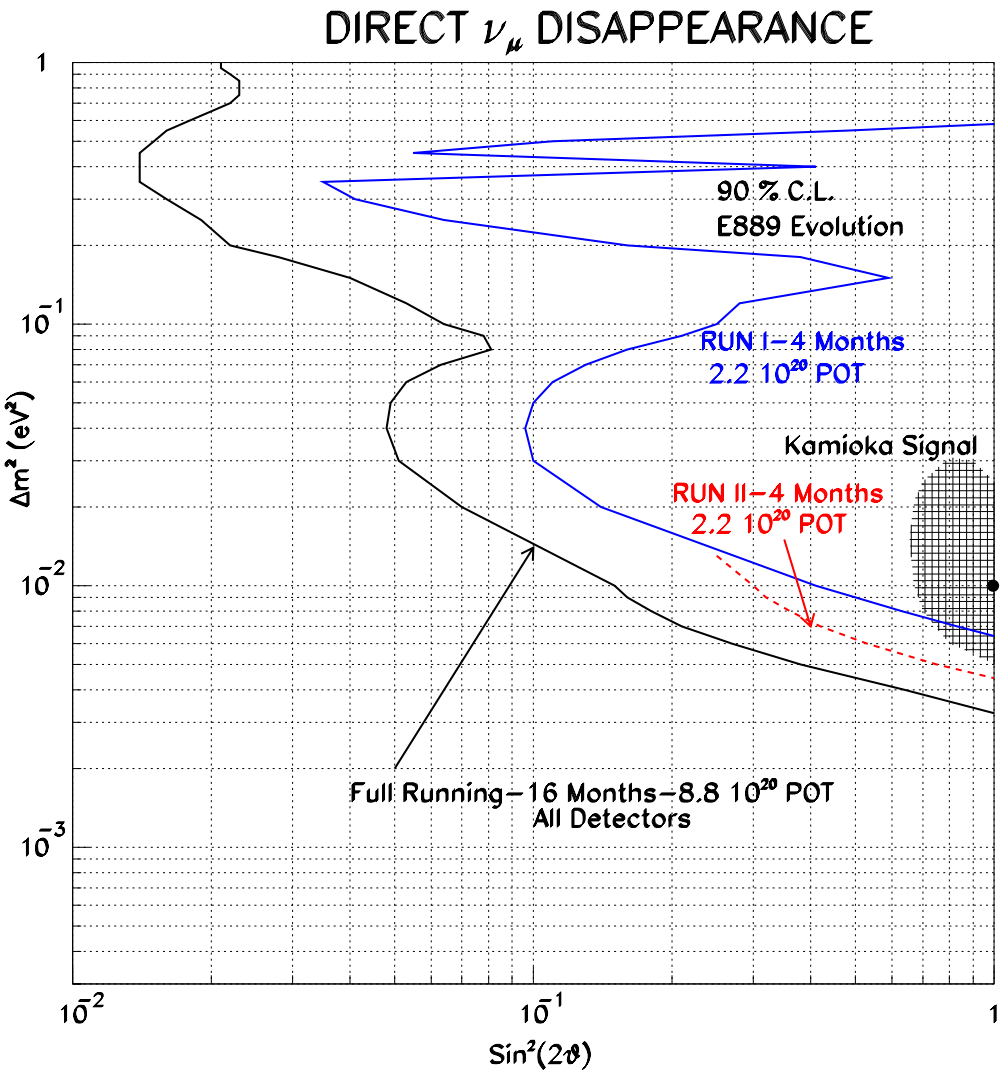

Figure 33: *The 90% confidence limit obtained with the quasi-elastic muon disappearance analysis as the experiment evolves. The first run will be with detectors at 3 and 24 km. The second run will occur after adding a third detector at 68 km, and the complete running will include a fourth detector at 1 km and* 8.8×10^{20} *POT.*

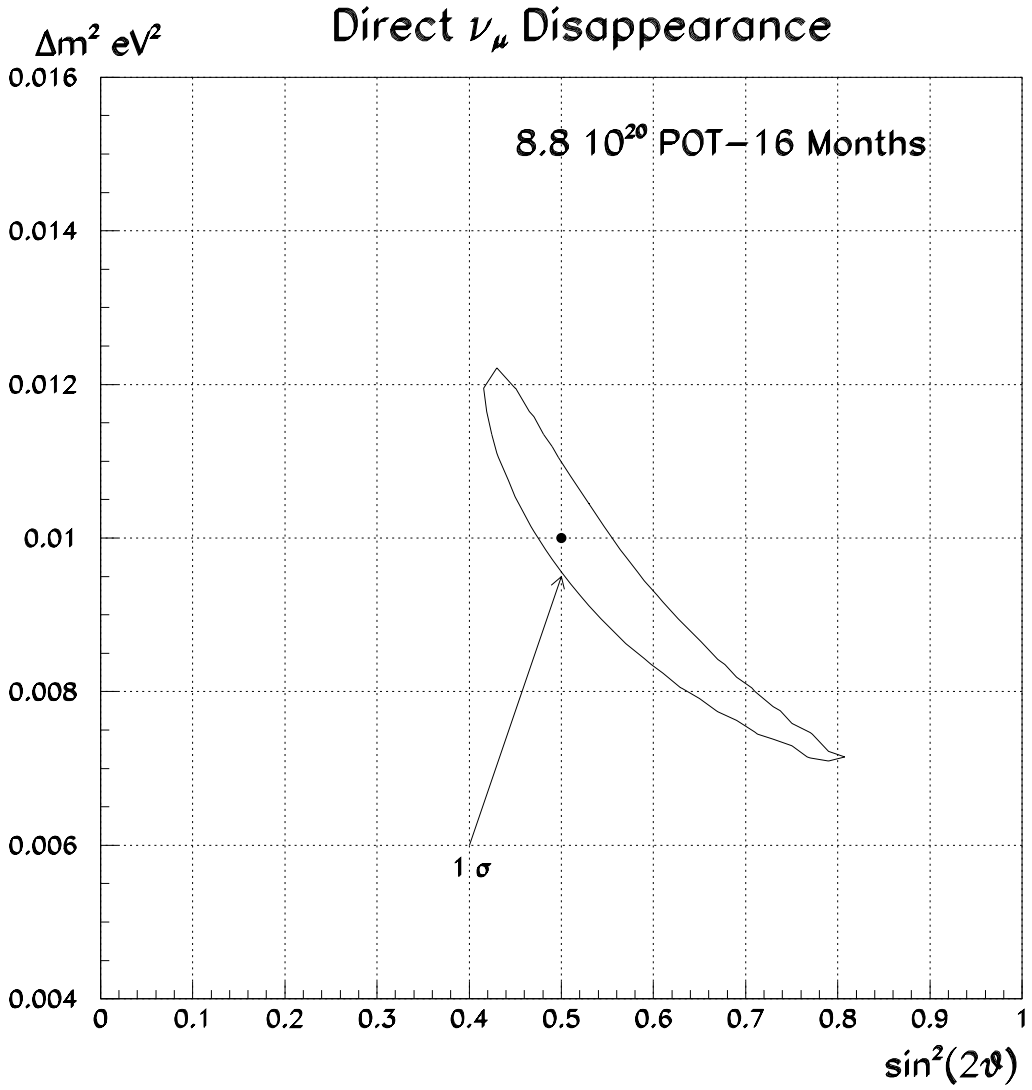

Figure 34: *1 σ confidence level coutour from measurements at D24 and D68 assuming oscillations with $\Delta m^2 = 0.01\ eV^2$ and $\sin^2(2\theta) = 0.5$.*

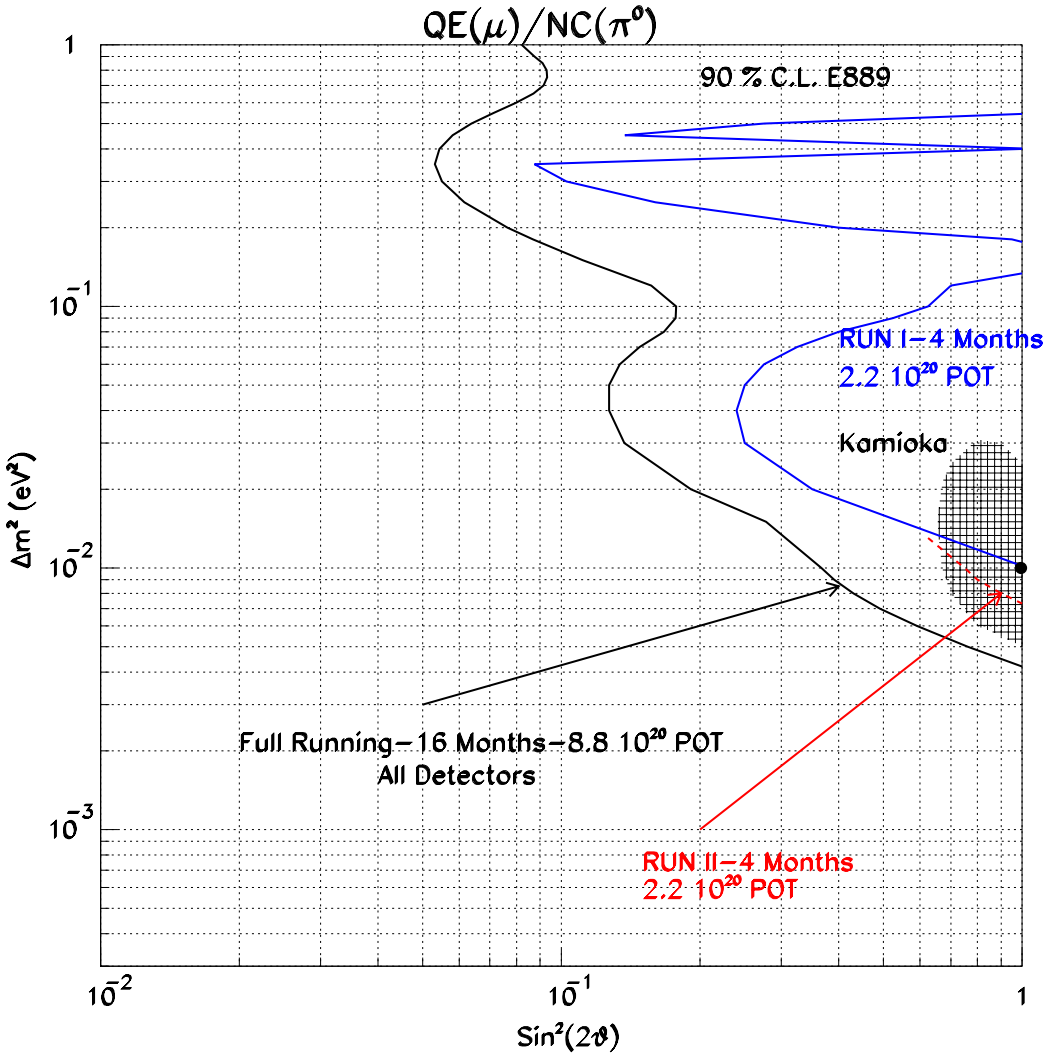

Figure 35: *90% confidence level exclusion contours for* Δm^2 *and* $\sin^2 2\theta$ *for a* ν_μ *disappearance signature when the muon counts in each detector are normalized to the number of reconstructed neutral current* π^0 *events. The sensitivity for the complete experiment and the initial runs is shown.*

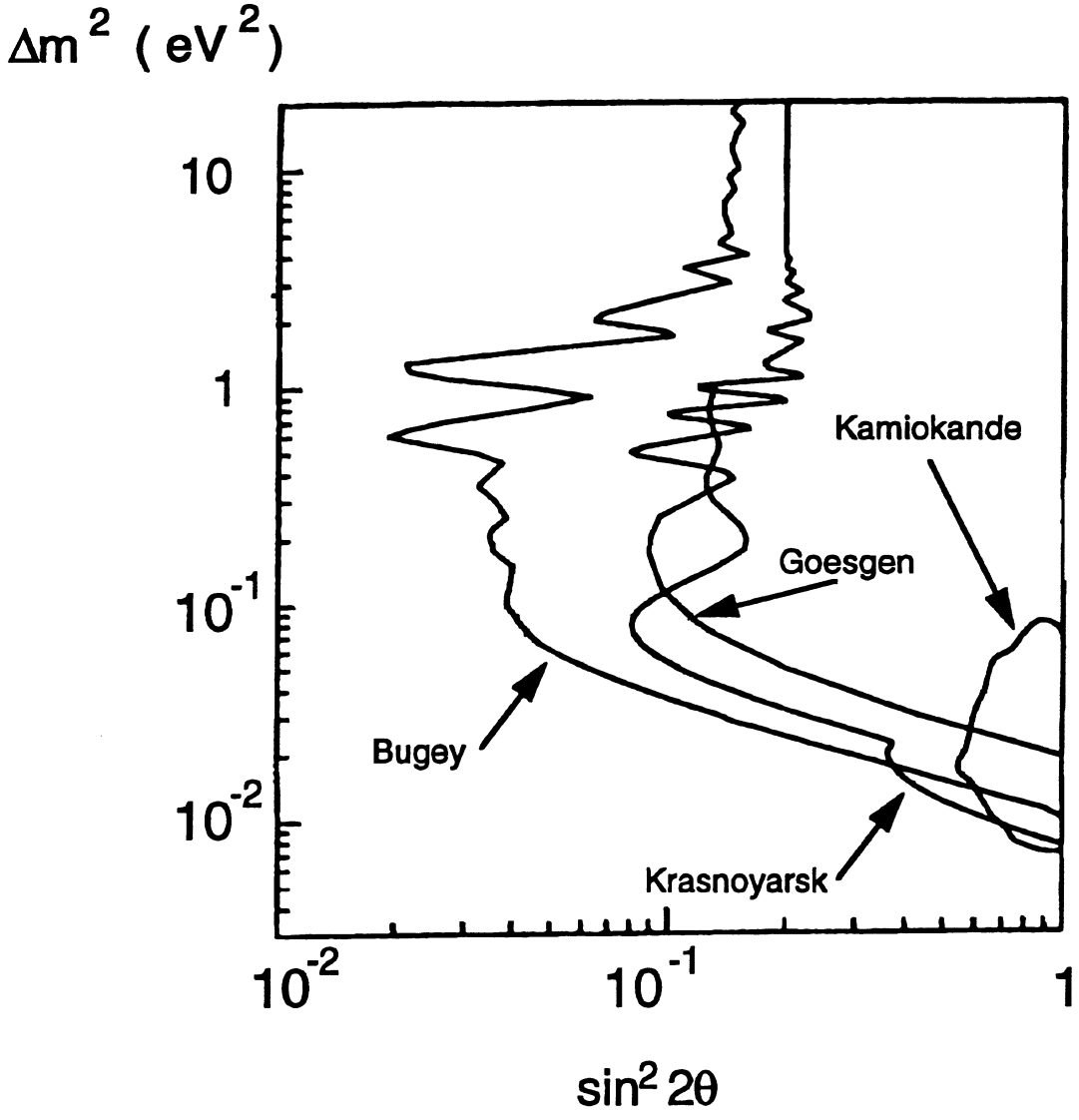

Figure 36: *Limits on anti-electron neutrino disppearance from reactor experiments and the allowed region if the Kamioka result is interpreted as* $\nu_\mu \rightarrow \nu_e$ *oscillations.*

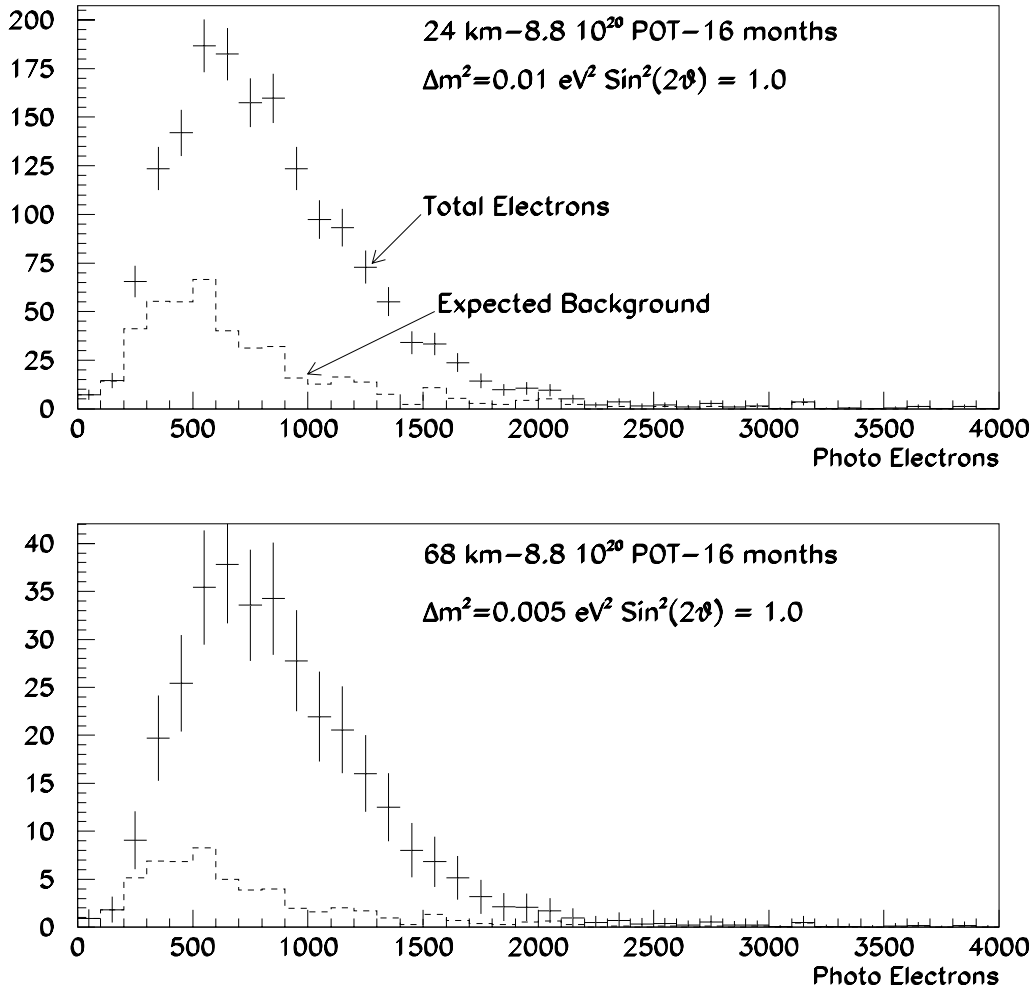

Figure 37: *The photoelectron spectrum of single ring showering electron-like events in the presence of* $\nu_\mu \rightarrow \nu_e$ *oscillations.*

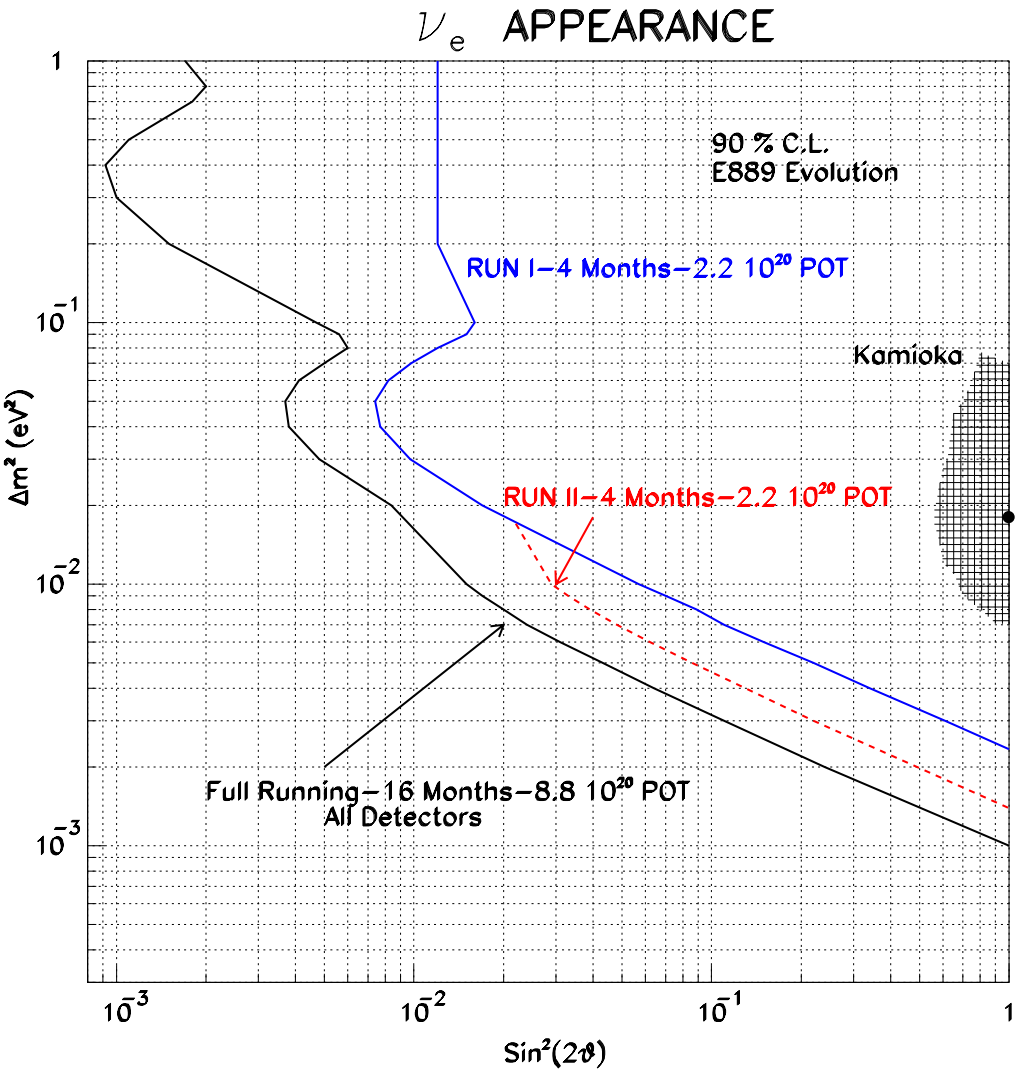

Figure 38: *90% confidence level exclusion contours for* Δm^2 *and* $\sin^2 2\theta$ *for a* ν_e *appearance signature for the complete experiment and for the initial runs.*